NICOTIANAMINE BIOSYNTHESIS IN PLANTS

A DISSERTATION SUBMITTED TO THE GRADUATE DIVISION OF THE UNIVERSITY OF HAWAIʻI AT MĀNOA

DOCTOR OF PHILOSOPHY

MOLECULAR BIOSCIENCES AND BIOENGINEERING

by James Thomas Carrillo

Dissertation Committee:

Dulal Borthakur, advisor

Joseph Jarrett

Pratibha Nerurkar

Zhiyan Du

Michael Muszynski

DEDICATION

To my mother and my sister

Dr. Kabi Neupane and Dr. Mike Melzer for introducing the field of molecular biology to ambitious undergraduate students

Dr. Dulal Borthakur, your passionate lecturing style and appreciation for science is an inspiration. Thank you for your mentorship, patience and dedication to science and education

Alexandra Elbayak and everybody keeping Sci-hub open

ACKNOWLEDGEMENTS

All my family and friends, thank you for your moral support. My wife Kehau and children Aili, Gene, Alia and Rowan. My uncles and aunties that have been there for me always: Jill, Wally & Claudia, Roy & Ann, Gino & Linda and my cousins. Sandra and Tina, thank you.

My committee members and faculty of Mānoa and Leeward campuses. I've known such great teachers, in STEM fields but also many great teachers in general. Your work is greatly appreciated, thank you Dulal Borthakur, Joseph Jarrett, Pratibha Nerurkar, Zhiyan Du, Michael Muszynski, Kabi Neupane, Mike Melzer, Jon-Paul Bingham, Qing X. Li, David Christopher, Gernot Presting, Philip Williams, Sladjana Prisic, Floyd Reed, From Leeward C.C., Michael Reese, Jiajia Garcia, Siu Roger Kwok.

My current and former lab mates. I am so grateful that my lab has not been fraught with tension. Instead, I've only known kind-hearted and genuine people. Thank you especially, Michael Honda, Ahmed Bageel, and Kazue Ishihara. My thanks and best wishes to the many other student researchers in lab 418.

FUNDING AND SUPPORT

This work was supported by the USDA NIFA McIntire-Stennis Grant, managed by the College of Tropical Agriculture and Human Resources (CTAHR)

To the donors of the Sachiyuki Masumoto Scholarship, the Sylvia H.L. Yuen and Harold S. Masumoto Fellowship. Thank you.

~~~~~~~~~ TABLE OF CONTENTS ~~~~~~~~~

Chapter ~~~~~~ page number

List of Tables and Figures 4

Abbreviations 6

Literature Review 7

Abstract 41

Introduction 44

Research Objectives 54

Methodology 55

Part I: ***SAM-synthetase from giant leucaena*** 55

Part II: ***SAM-synthetase from Acacia koa and mutagenesis experiments*** 60

Part III: ***5'-methylthioadenosine nucleosidase from giant leucaena*** 67

Part IV: ***nicotianamine synthase from giant leucaena*** 70

Part V: ***Gene expression analysis following iron fertilization of giant leucaena seedlings*** 78

Results 83

Part I: ***SAM-synthetase from giant leucaena*** 83

Part II: ***SAM-synthetase from Acacia koa and mutagenesis experiments*** 90

Part III: ***5'-methylthioadenosine nucleosidase from giant leucaena*** 107

Part IV: ***nicotianamine synthase from giant leucaena*** 110

Part V: ***Gene expression analysis following iron fertilization of giant leucaena seedlings*** 120

Concluding Statements 125

References 133

Literature Review

Figure 1: A model showing the effect of endotransglucosylase... 14

Figure 2: Sequence alignment of various plant metallothionein... 16

Figure 3: Metallothioneins are structurally diverse... 17

Table 1: Brief collection of recent plant metallothionein studies from 2012... 19-20

Figure 4: Amino acid subunits which form glutathione... 22

Figure 5: (A) Chemical structure of NA... 26

Figure 6: Fe uptake strategies of graminaceous species... 28

Figure 7: Net charge of $Fe3+$ complexes of nicotianamine... 30

Figure 8: Chemical structure of 8HQ... 37

Figure 9: Chemical structure of mimosine... 39

List of Tables ~~~~~~~~~~~~~~~~~~~~~~~~~~~~~~~~~~~~~ page number

Table 1: List of primers using for amplification of the giant leucaena SAM-synthetase... 56

Table 2: List of primers using for amplification of the A. koa SAM-synthetase... 62

Table 3: Complete details for the nineteen genes... 82

Table 4: Real-time PCR conditions and reaction details... 82

Table 5: Kinetic constants and total SAM production... 102

Table 6: The rate of nicotianamine production... 117

List of Figures ~~~~~~~~~~~~~~~~~~~~~~~~~~~~~~~~~~~~ page number

Figure 1: Methionine pathways in plants... 46

Figure 2: Biosynthetic pathway for nicotianamine... 51

Figure 3: HPLC chromatograms depicting the retention times... 65

Figure 4: Composition of fifteen refolding buffers from... 74

Figure 5: (A) Homodimeric assembly shown with cyan-colored... 85

Figure 6: Multienzyme sequence alignment of select plant... 86

Figure 7: Phylogenetic tree based on protein sequences... 87

Figure 8: SDS-PAGE analysis of recombinant giant leucaena... 88

Figure 9: (A) LSAMS activity at different concentrations of NaCl... 89

Figure 10: The effect of temperature and pH on SAM degradation... 90

Figure 11: Lineweaver-Burke plot depicting LSAMS kinetics... 91

Figure 12: Key residues (I310, Y65, I193, and A104)... 93

Figure 13: (A) 3d modelling of the A. koa SAM-synthetase... 96

Figure 14: Multiple sequence alignment showing conserved regions... 96

Figure 15: SDS-PAGE analysis of KSAMS expression by E. coli... 97

Figure 16: Optimal conditions for KSAMS: (A) pH, (B) temperature... 98

Figure 17: The activity of KSAMS in the presence of... 99

Figure 18: (A) Lineweaver-Burke plot depicting KSAMS kinetics... 100

Figure 19: The sites of mutagenesis, relevant residues and distances... 104

Figure 20: Coulombic electrostatic potential of SAM-synthetases... 105

Figure 21: Optimal pH **(A)** and temperature **(B)** for MTA hydrolysis... 108

Figure 22: HPLC chromatograms indicating MTA degradation by DsbA-**LMTAN**... 109

Figure 23: Monomeric giant leucaena nicotianamine synthase... 110

Figure 24: Multiple sequence alignment of plant NA-synthases... 112

Figure 25: SDS-PAGE analysis of LNAS purified from 1 L... 113

Figure 26: SDS-PAGE analysis of expression, purification... 114

Figure 27: Relative efficiency of 15 solutions in their ability... 115

Figure 28: The starting concentration of SAM in... 116

Figure 29: Optimal NA production in three enzyme assays... 119

Figure 30: Relative fold change of select genes from root... 122

Figure 31: Relevant chemical structures and pathways involving NA... 130

Figure 32: Hypothetical intermediate compounds and order... 131

Abbreviations~~~~~~

Nicotianamine (**NA**)

S-adenosylmethionine (**SAM**)

5'-methylthioadenosine (**MTA**)

RNA Ligase-Mediated-Rapid Amplification of cDNA Ends (**5'-RLM-RACE**)

Giant leucaena SAM-synthetase (**LSAMS**)

Giant leucaena nicotianamine synthase (**LNAS**)

Acacia koa SAM-synthetase (**KSAMS**)

3-hydroxy-4-pyridone (**3H4P**)

E. coli SAM-synthetase (**EcMAT**)

~~~~~~~~~ LITERATURE REVIEW ~~~~~~~~~

The following literature review is a comprehensive overview of plant metal homeostasis, specifically for distinguishing between the many methods of metal chelation. Throughout this dissertation the in vitro biosynthesis of nicotianamine is a primary focus, however the utility of this compound in plant tissues should be noted. Although there are many strategies available for plants, as described in this literature review, nicotianamine is shown to be the only specialized compound for metal solubilization, stabilization and transport.

Metal uptake, transport and storage in plants depend on specialized ligands with closely related functions. Individual studies differing by species, nutrient availability, tissue type, etc. are not comprehensive enough to understand plant metal homeostasis in its entirety. A thorough review is required which distinguishes the role of ligands directly involved in chelation from the myriad of plant responses to general stress. Distinguishing between the functions of metal chelating compounds is the primary focus of this review; reactive oxygen species mediation and other aspects of metal homeostasis are also discussed. High molecular weight ligands (polysaccharides, phytochelatin, metallothionein), low molecular weight ligands (nicotianamine, histidine, secondary metabolites) and select studies which demonstrate the complex nature of plant metal homeostasis are explored.

As sessile organisms, plants are often subject to unideal conditions and must develop diverse methods to manage micronutrients. Essential metals, such as iron (Fe), copper (Cu), manganese (Mn) and magnesium (Mg), are highly important in plants as they facilitate the capture and transfer of light energy within chloroplasts (Shcolnick and Keren, 2006; Zhang et al., 2018), although molybdenum (Mb), zinc (Zn), cobalt (Co) and nickel (Ni) are also recognized as essential as they serve as required enzyme cofactors (Castillo-González et al., 2018; Gericó et al., 2020). Elements that do not serve a biological function are often referred to as non-essential or toxic metals, some of which are cadmium (Cd), lead (Pb), mercury (Hg) and arsenic (As). Their damaging effects in plants are due to the displacement of essential metals, reactive oxygen species (ROS) production and ultimately impact plant growth by reducing efficiency of photosynthesis (Lysenko et al., 2020; Solti et al., 2016). High levels of essential metals will result in similar toxic effects, such as increased production of antioxidant enzymes superoxide dismutase and catalase (Tadaisky et al., 2020). It is worth noting that superoxide dismutase and catalase require a metal cofactor and thus are themselves subject to metal availability and oxidative stress (Shahpiri and Deljoonia, 2018; Ulusu et al., 2017). Metal chelating ligands are of paramount importance as they reduce the reactivity of metallic ions, thus reducing ROS production, however the function and properties of these compounds should be clearly distinguished from other biological roles. Understanding the individual function of any one ligand in maintaining metal homeostasis is difficult for four reasons.

1) Individual studies may consider the production or regulation of one or a few ligands only.
2) Different metallic ions do not trigger the same plant response.
3) Distinguishing genuine trends in plant metal homeostasis is difficult; certain species (hyperaccumulators/hypertolerant varieties) have overdeveloped methods to deal with toxicity that do not accurately reflect how most plants cope with stress.
4) The entire plant body is involved in metal homeostasis and many strategies are active simultaneously in metal uptake and transport.

For the above reasons it is important to understand the specific role of metal-chelating ligands and how they are implemented by plants. This review considers metal chelating ligands as either high molecular weight (HMW), or low molecular weight (LMW) compounds. HMW compounds are formed in polymerization reactions, are more variable in size and structure and are associated more often with the chelation/sequestration of non-essential metals. LMW compounds describe a diverse group of metabolites with metal chelating properties. Whereas HMW compounds tend to sequester metals, LMW compounds generally promote mobility throughout plant tissue.

Due to the numerous strategies available to plants it can be difficult to rank ligands by effectiveness or infer reason as to why one strategy develops over another. For example, in pea plants Cd is localized to the cytosol, whereas in maize Cd is observed mostly in the cell wall (Lozano-Rodriguez et al., 1997). While Cd localization in maize may be clearly observed it is complex to explain why. Although cell wall polysaccharides may sequester toxic metals and serve as an effective barrier, a variety of metal uptake methods have been observed in plants. Monocot species, such as maize, secrete mugineic acid (MA) phytosiderophores while dicot species do not. MA secretion has been shown to enhance the uptake of Fe and Zn (Zhang et al., 1991) however, it remains unclear how non-essential metals compare in inducing MA secretion, MA chelation or in uptake efficiency. Fe deficiency strongly induces MA secretion and the production of various metal transporters, resulting in the increased uptake of available metallic ions. In Fe-deficient wheat the uptake of Zn, Cu and Mn is increased, however this is not observed for Cd (Shenker et al., 2001). The effect of MA compounds in root development and uptake/transport of non-essential metal chelates have not been investigated thoroughly. Furthermore, seemingly inconsequential differences in plant growth media influencing root cell wall development may affect Cd uptake. Root structure and the development of apoplastic barriers affect Cd uptake, shown by a 79% greater Cd uptake in hydroponic grown maize compared to aeroponically grown (Redjala et al., 2011). Root cell walls of aeroponically grown maize resemble that of soil grown plants, while hydroponic conditions result in delayed maturation of root exodermis at growth tips thus facilitating metal uptake. Comparing multiple studies on plant metal uptake becomes incredibly complex if media type, environmental conditions, nutrient composition and plant species must be considered. Although many of these factors may not be explicitly detailed in studies they can greatly influence metal uptake.

Plant metal tolerance is a common measure used in studies, based on metal accumulation or the production of metal chelating ligands. Hyperaccumulators provide unique insights into plant metal homeostasis and function very differently than most plant species. Upregulation of histidine synthesis is observed in *Alyssum lesbiacum* as a response to subtoxic concentrations of nickel (Ni); a remarkable 36-fold increase of free histidine was measured in the xylem (Krämer et al., 1996). Contrary to this, the Ni-hyperaccumulator *Thlaspi goesingense* exhibits no change in histidine synthesis in response to Ni (Persans et al., 1999). Tolerance is instead attributed by a 1.6-fold higher glutathione content and a two-fold increase of glutathione reductase activity (Freeman et al., 2004). Studies of the biomolecular mechanisms and evolution of Ni-hyperaccumulator *T. goesingense* demonstrate the complexity of plant metal homeostasis. Roughly half of cellular Ni in *T. goesingense* was shown to be cytosolic with no significant Ni-S coordination shown by X-ray absorption spectroscopy (Krämer et al., 2000); thus hypertolerance/hyperaccumulation is directly due to highly active antioxidant mediation by glutathione and not to chelation by metal ligands. Furthermore, metal hyperaccumulation by *T. goesingense* may have developed tangentially to irregular hormone regulation. Compared to non-accumulators, *T. goesingense* exhibits constitutive high production of salicylic acid, unaffected by metal availability or infection (Freeman et al., 2005). Typically plant pathogens and infection elicit increased salicylic acid production by the host, thus regulating genes for resistance. The hormonal state of *T. goesingense* is that of perpetual pathogen stress, however if Ni is not abundantly available the plant becomes susceptible to infection by powdery mildew (Freeman et al., 2005). For *T. goesingense*, metal hyperaccumulation may have evolved to compensate for defects in the typical plant response to infection. In short, high salicylic acid promotes glutathione synthesis and creates a high tolerance for oxidative stress. An increased capacity and uptake of Ni then serves as a defense against plant pathogens.

Distinguishing the function of metal chelating ligands is essential when describing plant metal homeostasis but rarely is this possible when considering metal chelating properties alone. Many compounds are produced in plants containing carboxylic acid or thiol groups which have been shown to have metal chelating properties, however they are not discussed in detail in this review. Select aspects of metal homeostasis must be considered, such as ROS management, and many ligands serve multiple functions. The objective of this review is to elucidate the roles of important metal chelating ligands within the overwhelming topic of plant homeostasis in general.

1. High molecular weight ligands

1.1. Polysaccharides

Thickening of the cell wall and modification of polysaccharides are typical responses to non-essential metals and metal toxicity. Early diverging plants, such as charophytes (algae) and bryophytes (mosses and liverworts), are convenient model organisms for cell wall studies. Moss protonemata growth is like pollen tube growth and root tip growth of angiosperms during metal-induced stress (Krzesłowska et al., 2009).

The cell wall matrix provides a useful barrier for toxic metals and is highly relied upon in early diverging plants.

In addition to providing structural support, cellulose, hemicellulose and pectin of the cell wall chelate various metals thus effecting their uptake and translocation. The rice mutant *bc13* has impaired cellulose synthase activity affecting the physical strength of vascular bundles and sclerenchyma cells (Song et al., 2013). The *bc13* mutant, while morphologically indistinguishable from the wildtype, contains 22% less cellulose and exhibits a higher tolerance to Cd. Translocation of Cd from the root system to the leaves is reduced by 40-50% in *bc13*, however Cd tolerance is achieved at the expense of structural strength. Compared to the wild type, approximately one-third of the force is required to break *bc13* stalks due to its reduced cellulose content.

Cell wall thickening due to increased pectin content is often observed during metal toxicity. Adsorption experiments reveal a strong affinity for Pb, Cu, Co and an extremely poor affinity for Cd and Zn by pectin (Kartel et al., 1999). Similar effects on the cell wall have been observed by a variety of metals, such as Cu accumulation in *Scopelophila cataractae* (Konno et al., 2010), Pb accumulation in *Funaria hygrometrica* (Krzesłowska et al., 2009), and aluminum (Al) accumulation in *Nicotiana tabacum* (Chang et al., 1999). Metallic ions are chelated to acidic pectic polymers, specifically at sites of de-esterified homogalacturonan and rhamnogalacturonan units (Konno et al., 2010). Cross-linking between pectin polymers by calcium (Ca) ions or esterification is necessary for controlling cell wall rigidity and extensivity. Metals which are sequestered in plant roots, such as Cd and Al, are localized to cell wall components and displace Ca ions, thus disrupting pectin cross-linking and inhibiting root growth (Iwai et al., 2019; Webster and Gadd, 1996). Xyloglucan endotransglucosylase (XET) shuffles xyloglucan bonds between strands of hemicellulose that allows for gradual expansion to occur (Fig. 1). Al toxicity induced transcriptional down regulation of XET causing decreased cell wall extensivity (Yang et al., 2011). Transgenic tobacco overexpressing XET contained 25-27% less xyloglucan, resulting in half the accumulation of Cd in the root compared to wildtype and restoring root growth (Han et al., 2014).

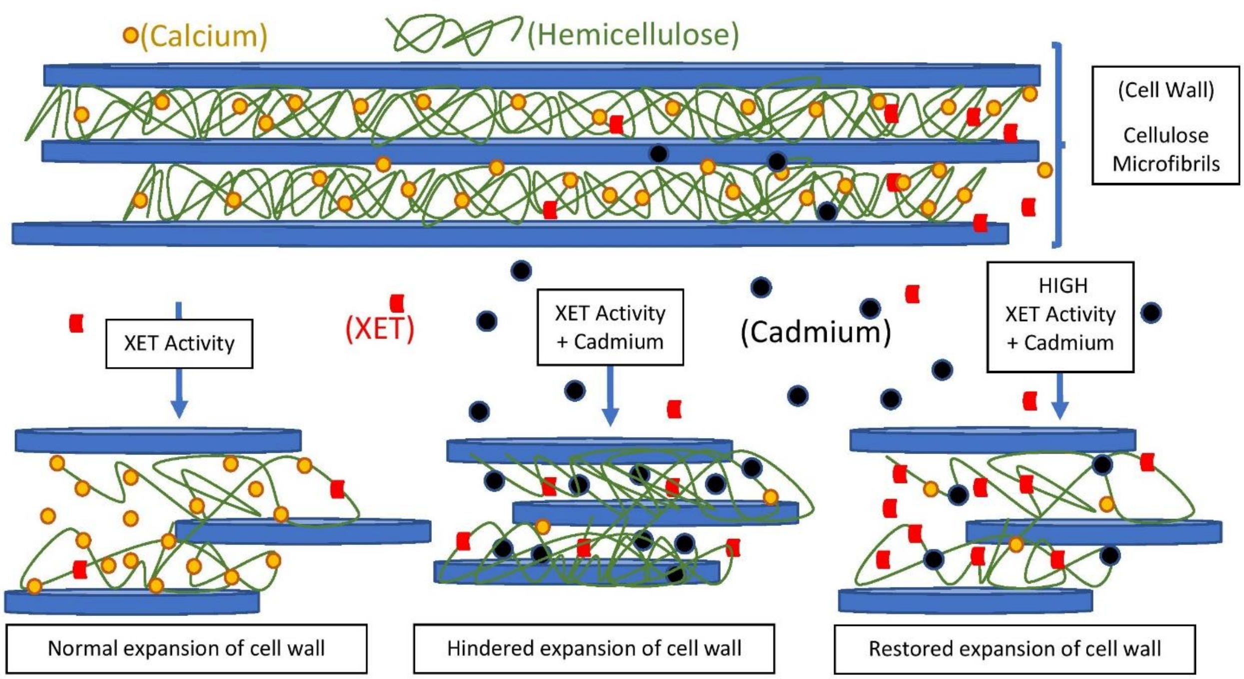

Figure 1: A model showing the effect of endotransglucosylase (XET) activity on cell wall extensivity. XET activity influences cell wall extensivity and the number of available binding sites for metal ions. Ca ions form bridges between acidic functional groups of hemicellulose, which are displaced by cadmium, resulting in reduced XET activity. The shuffling of hemicellulose cross-linking by XET allows for gradual cell wall expansion and root elongation, which is restored in transgenic plants overexpressing XET. High XET activity reduces total xyloglucan content of the cell wall, thus reducing binding sites for cadmium and increased flexibility between cellulose microfibrils. It would suggest, although undetermined, that structural integrity and calcium content of the cell wall may be compromised.

1.2. Metallothioneins

Plant metallothioneins control several physiological responses in plants, specifically for the mobilization of metallic ions in seed germination (Hanley-Bowdoin and Lane, 1983), leaf senescence (Buchanan-Wollaston, 1994; Guo et al., 2003), as well as in response to toxic metals (Zimeri et al., 2005). Plant MT studies tend to focus on host metal accumulation and tolerance, however it should be clearly stated that MTs do not primarily serve to deal with metal toxicity. The protein structure of plant MTs (4-8 kD) is characterized by having an hourglass shape containing a linker region of variable length that connects two-cysteine rich metal binding domains (Fig. 2). They contain mainly small amino acids that lend little structural stability, thus requiring metal chelation for proper folding. These thiol-rich binding domains are capable of chelating various essential and non-essential metals. Plant MTs are classified into four types based primarily on their amino acid sequence due to highly identical MT isoforms exhibiting differences in regulation, expression and metal affinity (Fig. 3). The consensus is that type I MTs are expressed primarily in root, type II in leaf and type III are associated with fruit ripening. Type IV MTs were the first of this family to be discovered and are referred to as E_c, meaning “early cysteine” proteins. Hanley-Bowdoin and Lane (1983) observed that radiolabeled cysteine was incorporated into an “early cysteine” protein by mRNA within dried wheat embryos, however not by mRNA from germinated embryos. Nearly 25% of the supplied cysteine was incorporated into a Zn-MT, however E_c protein synthesis drastically declined after 5 h of germination, demonstrating its timely importance during the earliest stage of growth.

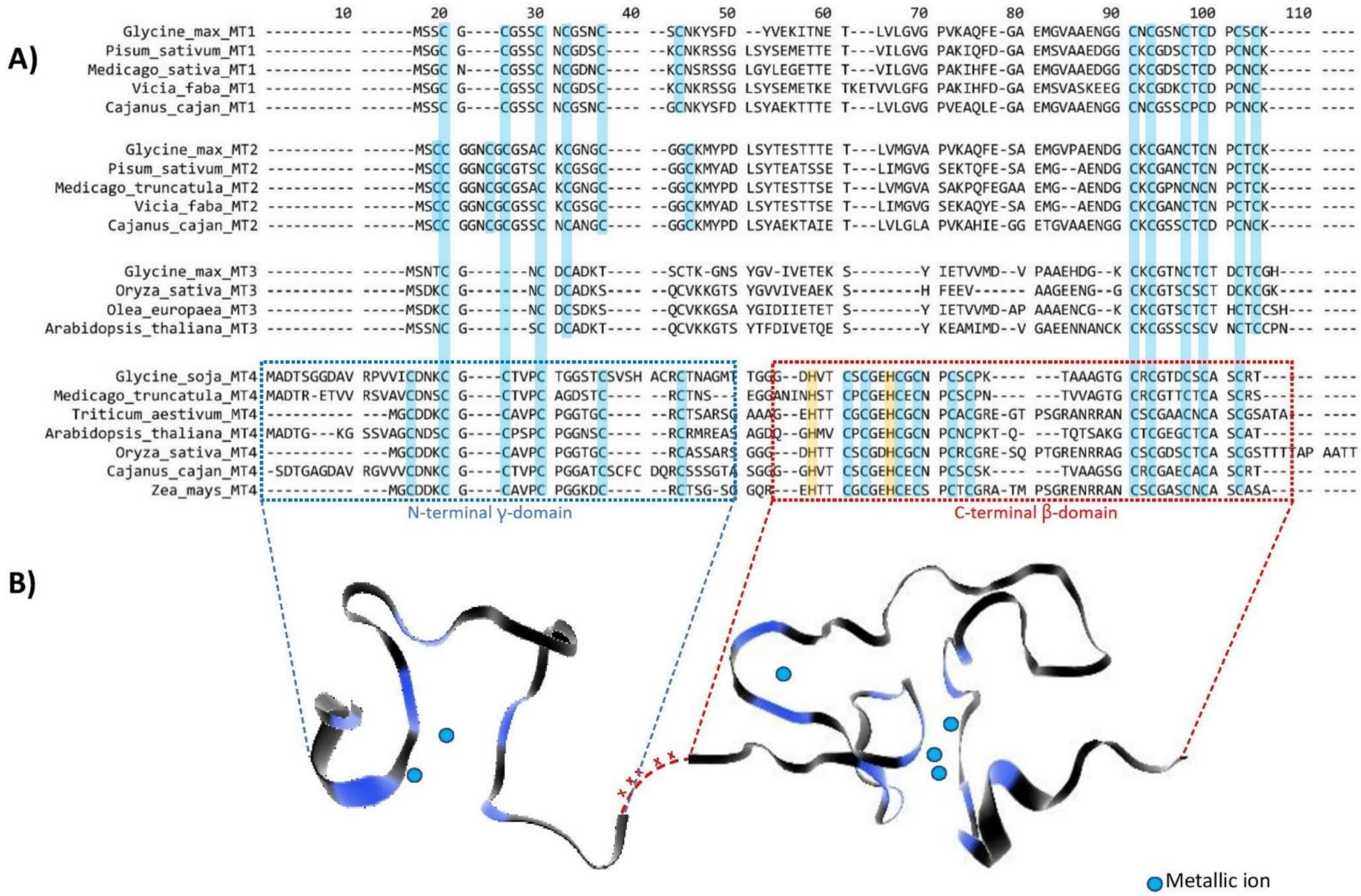

Figure 2: Sequence alignment of various plant metallothionein types 1-4 reveal conserved cysteine and histidine residues involved in metal chelation (A). Differences between metallothionein types can be observed in the arrangement and number of conserved cysteine residues (blue columns) and histidine (yellow columns). Structural information of plant metallothioneins is limited but an example is provided based on separately determined structures of the metal binding domains of wheat E_c metallothionein (B). This hypothetical structure of the full-length type-4 plant metallothionein is shown with the linker region (red dashed line) and conserved cysteine residues (blue). The true structure may be drastically different as the flexible linker region may allow for interactions between metal binding domains and different conformations may be possible.

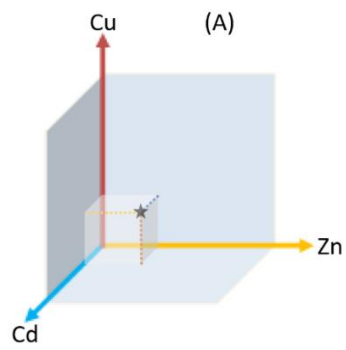

Figure 3: Metallothioneins are structurally diverse and thus exhibit a specialized preference for metallic ions. A 3-coordinate graph with each axis representing metal species affinity visually depicts this selective nature. A hypothetical metallothionein with equal affinity for Cu, Zn or Cd would be represented by the star in (A). Similarly, a type-4 plant metallothionein with Zn-preference (B) or a type-1 exhibiting high Cu-preference (C) are depicted.

Deciphering plant MT function is challenging as most studies focus on either in vitro binding characteristics or altered metal tolerance. The diversity of structure and regulation observed by plant MTs suggests a diversity of function as well. There are three important questions to address MT function: *Which metals take precedent in binding? How do MT structural variants differ in binding affinity and metal species preference? How is gene regulation affected by MT chelation of metal?*

Type I and type II generally affect Cu accumulation, type III and type IV preferentially bind to Zn (Freisinger, 2008; Guo et al., 2008; Mir et al., 2004; Murphy, 1997). Atypical preferences, such as for Ni (Ferraz et al., 2012), or uncharacteristic MTs are not uncommon. A type II MT, presumably a Cu-MT, is highly induced by the addition of Zn to grow media (Huang et al., 2009). The rice MT *OsMTI-1b* lacks the ability for binding Cu despite being classified as a type I, an expected Cu-MT (Nezhad et al., 2013). Characterizing MTs by their metal chelating properties is a challenge due to degradation by proteases during purification. A type IV MT from pea has been purified with some success from host tissue as well as from heterologous expression by *E. coli* (Kille et al., 1991).

Strong evidence suggests that conserved histidine residues in type IV plant MTs allows for selection of Zn over Cu/Cd. Site-directed mutagenesis of wheat E_c (Leszczyszyn and Blindauer, 2010) and a type IV His→Cys mutant isoform in soybean (Pagani et al., 2012) support the role of conserved histidine sites for allowing Zn preference. Stage of development, tissue type and external factors such as stress and metal availability influence MT synthesis. Three *Brassica rapa* MT genes, *BrMT1* (type I), *BrMT2* (type II) and *BrMT3* (type III) exhibit completely different responses to plant hormones, heavy metals and abiotic stresses (Ahn et al., 2012). Plant MT gene regulation is not clear as multiple sources have identified variable and lengthy 3'untranslated regions (Moisyadi and Stiles, 1995). MT genes contain at least one conserved intron; two introns were identified in type I MT genes of cotton and rice (Che et al., 1998; Hudspeth et al., 1996). The *rgMT-1* intron, a type I MT in rice, was demonstrated by GUS assay to enhance MT expression in rice cell culture (Hsieh and Huang, 1998). Alternative splicing of pre-mRNA was observed in rice MT type I gene *OsMT-I-Id* in response to abiotic stress (Gautam et al., 2012). Determining the regulation and expression of MT genes in plants is relatively unexplored compared to in vitro experiments (Table 1).

Table 1: Brief collection of recent plant metallothionein studies from 2012 to date. Protein structure determination, affinity for various metals and a well-defined role in metal homeostasis remain important topics.

Species	Gene	Type	Metals	Brief Summary	Reference
Brassica rapa	*BrMT1, BrMT2, BrMT3*	I, II, III	Cu, Zn, Mn, Fe	RT-PCR analysis of metallothionein gene expression effected by various abiotic stresses. Highly differential regulation was observed between the three metallothionein genes studied.	Ahn et al., 2012
Arabidopsis thaliana/ Oryza sativa	N/A	N/A	N/A	In silica analysis of metallothionein promoter sequences, most often detected are metal response elements and general stress response elements.	Dąbrowska, 2012
Noccaea caerulescerns	*NcMT3*	III	Cu, Zn, Cd, Pb	Heterologous expression in *E.coli* and purification. Binding capacity investigated and lack of secondary structure observed.	Fernandez et al., 2012
Nicotiana tabacum	*CUP1*	I	Cd	Heterologous expression of yeast metallothionein in *N. tabacum* confers Cd tolerance.	Krystofova et al., 2012
Oryza sativa	*OsMT1e-P*	I	Cu, Zn	Transgenic tobacco expressing OsMT1e-P showed higher tolerance to various abiotic stresses. RT-PCR analysis shows developmental and salt stress differential regulation of *OsMT1e-P*.	Kumar et al., 2012
Elsholtzia haichowensis	*EhMT1*	I	Cu	Cu-tolerance conferred in *E. coli* expressing EhMT1. RT-PCR show high expression in roots and strong induction by copper and heat-shock.	Xia et al., 2012
Cicer arietinum	*cicMT2*	II	Zn, Cd	Larger Cd-thiolate clusters are formed by metallothioneins in the presence of sulfide. The variable linker-region of plant metallothioneins is suspected to allow larger metal cluster formation compared to mammalian metallothioneins.	Huber and Freisinger, 2013
Jatropha curcas L.	*JcMT2a*	II	Cu, Cd	Heterologous expression in *E. coli* and metal-sensitive yeast mutants conferred metal tolerance. Transcript analysis by RT-PCR indicate highest expression of JcMT2a in leaf tissue induced by Cu.	Mudalkar et al., 2014
Arabidopsis thaliana	*mt1a, mt2a, mt2b, mt3*	I, II, III	Cu, Zn, Cd	Arabidopsis mutants deficient in numerous metallothionein isoforms did not differ in Cu or Zn tolerance, Cd tolerance affected slightly. Redistribution of Cu from senescing leaves was most affected in lines lacking metallothioneins.	Benatti et al., 2014
Ziziphus jujuba	*ZjMT*	I	Cd	Transgenic *A. thaliana* lines were demonstrated to have higher NaCl and Cd tolerance than wildtype.	Yang et al., 2015
Glycine max	*GmMT1, GmMT2, GmMT3, GmMT4*	I, II, III, IV	Zn	Raman spectroscopy on four metallothionein isoforms of soybean. Structural differences and protein donor groups contributing to zinc chelation.	Tomas et al., 2016
Solanum lycopersicum	*MT1, MT2, MT3, MT4*	I, II, III, IV	Cd	Gene expression of each metallothionine (types I, II, III, IV) in different tissue types. Mineral content of Ca, Mg, Mn, Fe, and Zn are affected by cadmium.	Kisa et al., 2016
Halostachys caspica	*HcMT*	II	Cu, Zn, Cd	Expression of HcMT fusion protein in *E. coli* enhanced tolerance to Cu, Zn, and Cd. Gene expression of HcMT is increased in plant in response to Cu, Zn and Cd.	Liu et al., 2016

Table 1: (Continued)

Species	Gene	Type	Metals	Brief Summary	Reference
Cucumis sativus	*CsMTL2*	II	Zn, Cd	Metal accumulation in *E. coli* expressing CsMTL2 was highest compared to other cell lines expressing CsMTL2m (CcMTL2 with removed spacer region), human metallothionein-like protein 1 and phytochelatin-like protein.	Pan et al., 2016
Oryza sativa	*N/A*	N/A	N/A	Intermediate filament like (OsIFL) protein of rice shown to interact with a metallothionine in the nucleus. Either OsIFL and OsMT were fused to a fluorescent protein counterpart to detect their interaction, also observed as induced by NaCl stress.	Soda et al., 2016
Coffea arabica	*CaMT21*	II	Zn	Four metallothionine genes were identified in plant, gene expression analysis revealed a positive correlation between Zn application and CaMT21.	Barbosa et al., 2017
Oryza sativa	---	I	---	In silico docking analysis of multiple rice metallothioneins. Lead nitrate is predicted to have the highest affinity for type I rice metallothioneins.	Devvret et al., 2017
Oryza sativa	*OsMTI-1b*	I	Ni, Zn, Cd	Recombinant fusion protein containing the N-terminal of OsMT1-1b confirms that efficient metal chelation is possible without the complete metallothionine protein.	Malekzadeh and Shahpiri, 2017
Sedum plumbizincicola	*SpMTL*	?	Cd	A novel plant metallothionein resembling type I, although containing additional cysteine residues and a high capacity for sequestering cadmium.	Peng et al., 2017
Oryza sativa	*ricMT*	II	Cu, Cd	Overexpression of ricMT conferred a greater tolerance to H_2O_2 generated by toxic Cu/Cd concentrations. Cu shown to be more toxic than an equal concentration of Cd due to a greater H_2O_2 generated by Cu.	Zhang et al., 2017
Musa acuminata	*musMT3*	III	Zn, Cd	Order and coordination of metal ion binding by a type III metallothionein.	Cabral et al., 2018
Zea mays	*ZmMT1*	I	Cd, Pb, Zn	Heterologous expression in *E. coli* binding capacity is measured in various solutions. Capacity for chelating Pb is high.	Duan et al., 2018
Oryza sativa	*OsMT1, OsMT2, OsMT3, OsMT4*	I, II, III, IV	Hg	Heterologous expression in *E.coli* of four rice metallothionine isoforms was investigated for their ability to remove mercury from solution. Type I proved the most effective.	Shahpiri and Mohammadzadeh, 2018
Coptis japonica	*CjMT2*	II	Cd	In silico analysis of binding capacity, stability, and protein structure.	Singh et al., 2019
Physcomitrella patens	*PpMT2*	II	Cu, Cd	Heterologous expression in yeast and Arabidopsis increased Cu and Cd accumulation and improved tolerance to metal stress.	Liu et al., 2020
Pisum sativum	*PsMT1 / PsMT2*	I / II	Cd	Nodule formation by transgenic *Rhizobium* lines expressing PsMT1 and PsMT2 enhanced tolerance to Cd in a Cd-accumulating strain of *P. sativum*.	Tsyganov et al., 2020

Plant MTs are unique ligands in metal homeostasis because they are both structurally and functionally diverse and strictly regulated. Their functions are so strictly conserved that functional similarities exist between plant and mammalian variants. Many studies of mammalian MT reveal increased expression during early embryonic growth and in damaged tissue (Coyle et al., 2002; Kimura et al., 2000). Non-plant MT studies tend to focus primarily on the transcriptome changes, not in measuring metal tolerance or metal uptake of the host. Zn-dependent transcription factors and redox-regulated transcription are affected in neonatal mice with altered MT activity (Kimura et al., 2000). Equivalent changes in gene regulation by MTs have yet to be shown in plants. Despite the conservation of MTs in plants and other forms of life, Benatti et al. (2014) demonstrated that *Arabidopsis* mutants containing multiple knockouts of MT genes grew with minimal differences compared to wildtype. Detecting transcriptome-wide changes in plants with altered MT expression may reveal their regulatory roles or at least clearly demonstrate their importance in metal homeostasis and development in the future.

1.3. Phytochelatin

Phytochelatin (PC) is produced as a response to non-essential metals, especially by Cd, for the purpose of chelating and ultimately sequestering within the cell vacuole. PC is produced from units of glutathione by phytochelatin synthase, yielding oligomers of (γ-Glu-Cys)n-Gly (n = 2-11) (Fig. 4). Glutathione is an essential antioxidant and serves many roles in detoxification however phytochelatin synthesis has been adopted by all higher plants in response to non-essential metallic ions. Precursor compounds of PC, namely glutathione, γ-Glu-Cys and cysteine, have metal chelating properties however determining their in vivo role as a ligand is challenging (Delalande et al., 2010). PC synthetase is constitutively expressed and immediately depletes cytoplasmic glutathione upon exposure to Cd (Grill et al., 1985). Knockdown Arabidopsis studies using mutants with impaired glutathione (*cad2-1*) or PC synthesis (*cad1-3*) suggest that PC chelates are less mobile and restricted more efficiently to plant roots (Sobrino-Plata et al., 2020; Wang et al., 2018). Overexpression of PC synthase results in Cd-hypersensitivity as glutathione serves as an initial defense against ROS (Lee et al., 2003). Superoxide dismutase, catalase and ascorbate production become dominant methods for neutralizing ROS after 24 hours as glutathione production becomes dedicated to PC synthesis (Jozefczak et al., 2014).

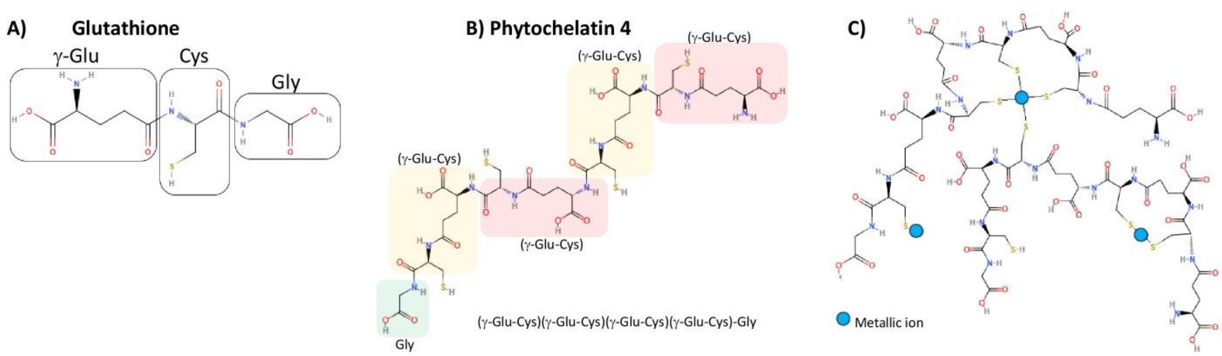

Figure 4: Amino acid subunits which form glutathione are outlined (A). Similarly, prepolymer units of phytochelatin 4 are identified by colored boxes (B). In the presence of metallic ions, a variety of chelate complexes may form between thiol groups of the same phytochelatin molecule or multiple molecules (C).

PC synthase is activated in the presence of heavy metals; the strength of activation was determined as Cd, Pb, Zn, antimony (Sb), silver (Ag), Hg, As, Cu, tin (Sn), silver (Au) and bismuth (Bi) in order of strongest to weakest activator (Le Faucheur et al. 2005). Only some heavy metals can form a stable complex with PC, Cd being the most observed. PC-Pb complex is not readily formed (Leopold et al., 1999), but has been observed in *Sedum alfredii* leaf (Zhang et al., 2008). Other metals, mainly Cu, Hg and As, are shown less commonly to form PC complexes in vitro (Hartley-Whitaker et al., 2001; Krupp et al., 2009; Mijovilovich et al., 2009; Salt et al., 1989; Sneller et al., 1999). In *Dunaliella tertiolecta*, Zn and Cd induced PC synthesis equally, although typically Cd is a much stronger inducer than Zn (Tsuji et al., 2002). This was shown to be due to Zn promoting glutathione synthesis more effectively and increasing the substrate pool for PC synthase. Heavy metal toxicity upregulates every pathway step leading up to PC synthesis starting from sulfur assimilation (Xue et al., 2007), cysteine biosynthesis (Domínguez-Solís et al., 2001; Fediuc et al., 2005), and glutathione synthesis (Rüegsegger et al., 1990, 1992).

While all higher plants are capable of PC synthesis, it has been reported as absent in certain bryophytes and pteridophytes (Gekeler et al., 1989; Petraglia et al., 2014). Nonvascular plants accumulate less toxic metal, produce less proteinaceous thiol-ligands, and suffer more from metal-induced oxidative damage than vascular plants (Kováčik et al., 2017). This may be due to the inability to manage toxic/excess metallic ions in the cytosol. Only short-length PC, (γ-Glu-Cys)n-Gly (n = 2-4), is produced by bryophytes and in far less quantity than found in higher plants (Gekeler et al., 1989). In contrast to metallothionein, a similar metal-chelating cysteine-rich polypeptide, the primary role of PC in plants is in detoxification and sequestering in vacuole. ATP-binding cassette transporters direct metal saturated phytochelatin or glutathione-conjugates into the vacuole for storage and recycling (Martinoia et al., 1993; Mendoza-Cózatl et al., 2010). While the name *phyto-chelatin* implies "plant chelating compound" they have been shown to be also produced in the fungi *Saccharomyces cerevisiae*, *Neurospora crassa*, *Candida glabrata* (Kneer et al., 1992) and even in the nematode *Caenorhabditis elegans* (Vatamaniuk et al., 2001).

While metal detoxification by PC is well studied, the many roles of PC synthase is intriguing. Metal detoxification is only one aspect of PC synthase, a multifunction enzyme involved in many types of threat detection and threat management. Toxic metal species trigger PC synthesis; xenobiotics trigger hydrolase activity of PC synthase, and most recently a third function of PC synthase was demonstrated in indole glucosinolate synthesis. Kühnlenz et al. (2015) generated transgenic *Arabidopsis* lines expressing nematode PC synthase (CePCS) in order to demonstrate the role of plant PC synthases in plant-pathogen response. While PC synthesis and Cd resistance were restored by heterologous expression of CePCS, those transgenic lines were susceptible to the potato pathogen *Phytophthora infestans*. It is believed that plant PC synthase acts upon a glutathione-conjugated intermediate involved in detecting bacterial pathogens (De Benedictis et al., 2018) and that CePCS was unable to restore this function. In addition to providing red-ox balance in the cytosol, glutathione functions in the presence of xenobiotics (e.g. electrophilic herbicides) by forming thiol-conjugates catalyzed by glutathione S-transferases (Beck et al., 2003; Blum et al., 2007; Dixon et al., 2002). The resulting thiol-conjugate is deglycinated by PC synthase, similarly to the repeated deglycination reactions in PC synthesis, prior to importing into the vacuole.

2. Low molecular weight ligands

2.1. Nicotianamine and Mugineic Acids

Nicotianamine (NA) is ubiquitous in plants, a strong chelator of Fe, and is essential for the internal trafficking of Mn, Fe, Co, Zn, Ni and Cu. Under the acidic conditions found in the xylem (pH 5 – 6.5), metallic ions preferentially complex with small acidic metabolites such as citrate and histidine, although Fe^{3+}-NA and other metal complexes have been demonstrated to form in vitro as low as pH 5.2 (Rellán-Álvarez et al., 2008). While metals are far less soluble in alkaline environments, as in the phloem (pH 7 – 8), they preferentially bind to NA (Fig. 5.A). In other neutral and alkaline fluids in plants, such as in symplastic and intra-organ transport, NA is crucial in the distribution of metallic ions to developing tissues. While maintaining solubility, NA also greatly reduces the reactivity of Fe through chelation. Toxic amounts of ROS can be generated by repeated cycles of reduction, either by enzymatic or chemical means, and oxidation of reactive Fe. NA is highly effective at chelating Fe and maintaining a nonreactive state, thus discouraging hydroxyl radicals from forming though Fenton and Haber-Weiss reactions. Fe^{2+} complexes formed with most chelators, such as EDTA, will always autoxidize and form Fe^{3+} under aerobic conditions. Surprisingly, autoxidation is not observed when

Fe^{2+} is complexed with NA, even during deliberate oxygenation of the solution (von Wirén et al., 1999).

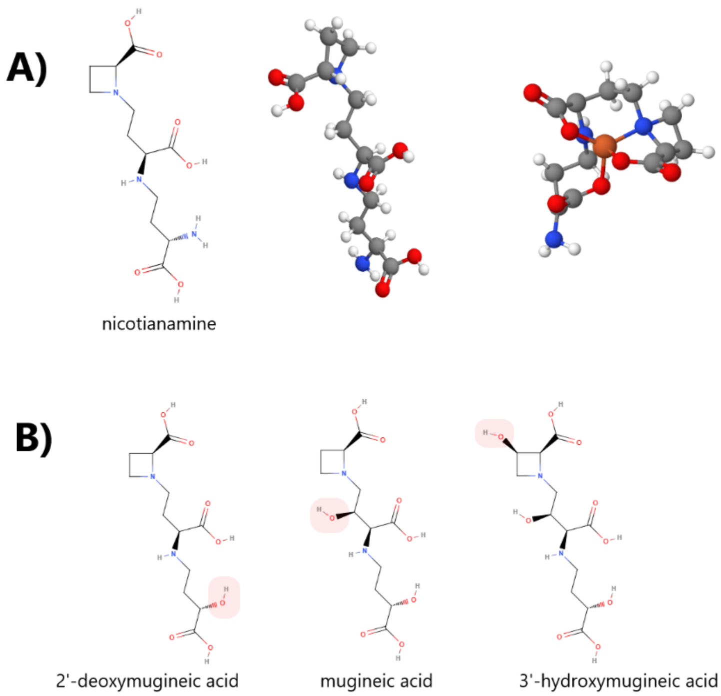

Figure 5: (A) Chemical structure of NA (left), ball-stick model (middle), and as metal chelate complex (right). **(B)** Common derivatives of NA in graminaceous species, addition of hydroxyl groups is highlighted in red. 2'-deoxymugineic acid (left), mugineic acid (middle), and 3'-hydroxymugineic acid (right). Certain species are better known for having extended pathways for mugineic acid modification, such as *Hordeum vulgare* and 3'-epihydroxymugineic acid, other species such as *Oryza spp*. will stop at 2'-deoxymugineic acid synthesis.

Unique to graminaceous species is the ability to modify NA into mugineic acid (MA) compounds (Fig. 5.B). These modifications include varying degrees of hydroxylation that increases complex stability in acidic environments (von Wirén et al., 2000). The MA family of phytosiderophores, presently consisting of eight distinct compounds (Ueno et al., 2007), originate from 2'-deoxymugineic acid (DMA) which is derived from

NA. Graminaceous species employ an enhanced method of Fe-uptake using MA compounds known as Strategy (II). MA phytosiderophores are first secreted into the rhizosphere where they solubilize and chelate Fe^{3+} (Sugiura and Nomoto, 1984). The Fe^{3+}-MA complex is transported into the root by yellow-stripe (YS) transporters. Nongraminaceous species do not synthesize MAs and achieve partial solubilization of soil Fe^{3+} by extrusion of H^{+} and organic acids into the rhizosphere (Fig. 6). Solubilized Fe^{3+} is reduced by membrane ferric-chelate reductases (FRO) and the resulting Fe^{2+} imported via iron-regulated transporter (IRT). This method describes Strategy (I) uptake of Fe. Three species are known to utilize a hybrid method and are exceptions to the Strategy (I)/(II) classification. MA phytosiderophores, specifically the compound DMA, was first discovered in rice under Fe deficient conditions (Takagi et al., 1976). Strategy (I)-related Fe^{2+} transporters OsIRT1 and OsIRT2 were later discovered in rice as well (Ishimaru et al., 2006). Tsednee et al. (2014) demonstrated a unique uptake strategy by the Zn-hyperaccumulator *Arabidopsis halleri* which utilizes NA as a secreted phytosiderophore, resembling the Strategy (II) plant secretion of MA compounds. Also, the olive tree possesses Strategy (II) methods despite being a nongraminaceous tree. The genes for DMA biosynthesis were detected by transcriptome analysis and DMA detected directly by HPLC and mass spectrometry (Suzuki et al., 2016).

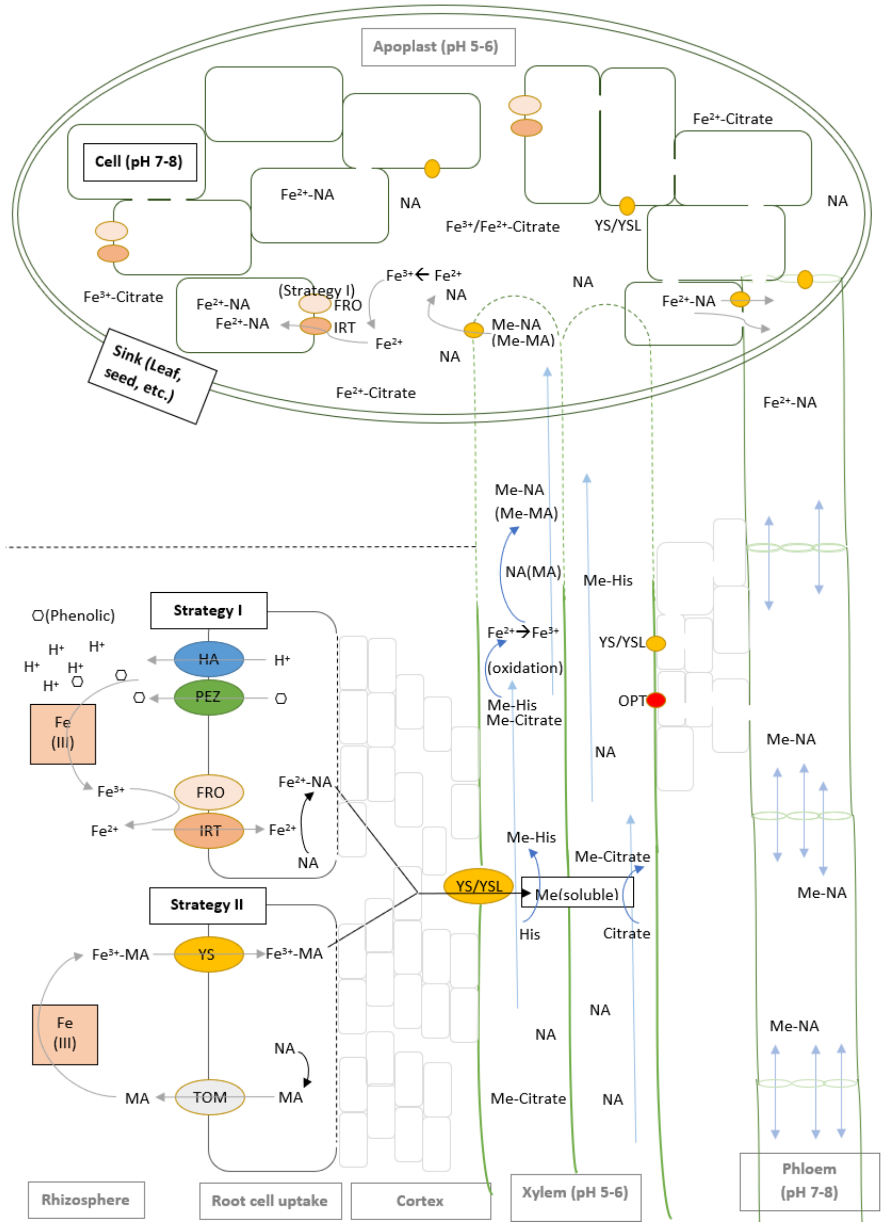

Figure 6: Fe uptake strategies of graminaceous species (strategy II: rice, barley, maize, etc) and nongraminaceous (strategy I) plants. While uptake strategies differ, internal transport is similar and achieved mainly by yellow stripe (YS; strategy II) or yellow stripe-like (YSL; strategy I) transporters. Chelation of metallic ions is required by NA and/or MA phytosiderophores to be transported by YS/YSL transporters. Other metallic ions (Me), such as Zn and Cu, may be transported as shown however YS/YSL variants vary in their selectivity for metal species. The oligopeptide transporter (OPT) family, which YS/YSL transporters belong to, are important in metal specific partitioning and xylem/phloem loading of iron. Histidine (His) and citrate predominantly bind to iron and other metals (Me) in the acidic conditions of the xylem and apoplast, although chelation by NA or MA is necessary for loading/unloading via YS/YSL transporters. Iron is specified from other metal species (Cu, Zn, Mg) to highlight that oxidation can still occur in all tissues.

Barley genes for MA synthesis were expressed in rice where only the precursor compound DMA is produced resulting in higher Fe/Zn uptake and a greater proportion of Zn moved into seeds (Masuda et al., 2008). Despite NA and MA being highly similar compounds, resulting Fe^{3+} complexes are distinguishable by host transporters, possibly due to a noticeable charge difference (Fig. 7). The Fe^{3+}-NA chelate complex is neutral while Fe^{3+}-MA carries a slight negative charge (von Wirén et al., 1999). The root transporter responsible for Fe uptake in barley (HvYS1) is highly selective for Fe^{3+}-MA chelates (Murata et al., 2006). Additionally, chimeric YS1 transporters prepared from barley and maize variants (HvYS1–ZmYS1) have identified elements of YS1 structure which permit for substrate specificity (Harada et al., 2007). Selective transport has been observed with respect to the chelated metal as well. The Arabidopsis vacuolar transporters for Zn-NA (Haydon et al., 2012) and rice yellow-stripe-like (YSL) 16-transporter for Cu-NA (Zheng et al., 2012) exhibit strong selection based on the chelated metal species. Additional studies are required to demonstrate the selective nature of YS/YSL transporters and if they allow for selective partitioning/transport of certain metals.

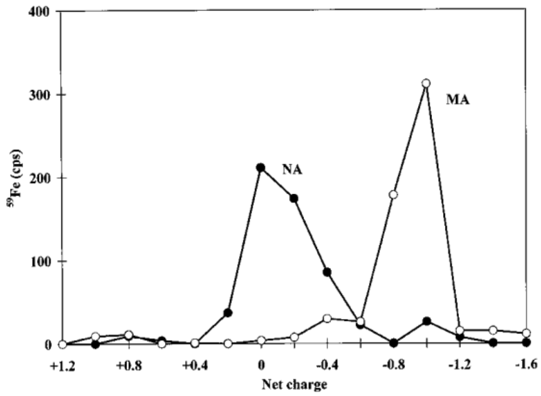

Figure 7: Net charge of Fe^{3+} complexes of nicotianamine and mugineic acid, as determined by high-voltage paper electrophoresis at pH 7.0. Figure taken from von Wirén et al., 1999.

Transgenic plant studies and hyperaccumulator species demonstrate the essential role of NA in Fe homeostasis. Engineered plants with increased NA production are highly tolerant to metals, especially for Ni (Kim et al., 2005; Pianelli et al., 2005). Zn hypertolerance in *Arabidopsis halleri* is attributed to a 73-fold higher NA synthase transcript level compared to *A. thaliana* (Weber et al., 2004). NA production is not determined by the *abundance* of metal, even though it is often associated with increased metal tolerance and uptake, rather it is determined by the bioavailability of Fe. Callahan et al. (2007) effectively demonstrated this by comparing NA production and metal uptake in seven *Thlaspi* species, some of which were hyperaccumulators of Ni. Test plants were grown in ordinary potting soil to detect preferential metal uptake capabilities and NA production in a natural unstressed state. Increased Ni uptake among the seven *Thlaspi* species agreed with increased NA production. Most notable was an inverse relationship observed between Ni and Fe content, demonstrating a preferential uptake of Ni over Fe. Constitutive high expression of metal ion transporters is common in hyperaccumulating species, as well as metal transporters with atypical preferences for Ni, Zn, or Cd (Lombi et al., 2001; Pence et al., 2000). Therefore, increased NA production is not directly due to Ni but to abnormal uptake preferences and as a response to Fe deficiency.

Transgenic plant studies where NA is produced 10-fold or more in tissues result in 2-3 fold increases in Fe content (Douchkov et al., 2005; Masuda et al., 2008; Singh et al., 2017). Commonly observed in these high-NA transgenic plants is better growth in Fe-deficient conditions and markedly increased tolerance and uptake of other metals. Increased NA production alone is not effective, although a 2-3 fold increase is significant, to result in a proportional increase in Fe uptake. Other regulatory mechanisms, affecting Fe-transporter expression or storage proteins, must determine Fe uptake activity. Most promising are multi-gene transgenic plants to increase Fe content in plants. Overexpression of ferritin, an Fe-storage protein, in rice did not affect Fe content in seeds (Drakakaki et al., 2000; Yoshihara et al., 2005), however similar studies have measured a 3-fold increase in Fe content (Goto et al., 1999). Most drastic improvement to date is a 6-fold increase in rice seed Fe content in transgenic rice lines with enhanced NA and ferritin production (Wirth et al., 2009). NA has an essential role in metal homeostasis, specifically to maintain a balanced proportion of Fe within the micronutrient pool. Engineering of multiple genes seems a promising method to significantly increase plant Fe accumulation.

2.2. Histidine

Increased histidine production is observed in the hyperaccumulation of metals, most often in Ni-hyperaccumulating plant species (Sharma and Dietz, 2006). As a free amino acid, it binds to metallic ions during xylem transport and incorporated into proteins it is essential in forming metal-binding domains and certain catalytic sites. Histidine residues in plant metallothionein types III and IV result in preference for Zn over Cu, which was confirmed by generating a His32Cys mutant (Leszczyszyn et al., 2010).

Compared to other metal ligands, histidine is of low metabolic cost as it contains no sulfur and less nitrogen than high-molecular-weight ligands. Therefore, histidine may be a preferred metal ligand if sulfur and nitrogen is scarce. Histidine and glutamate in plants closely share the same metabolic pathway, which could be a competitive junction for the synthesis of metal ligands. Glutathione, and thus also phytochelatin, synthesis relies heavily on sulfur and glutamate. Studies considering both nutrient availability and metal homeostasis are extremely scarce, the most lacking subject contained in this review. It is worth mentioning an extensive experiment by Kováčik et al. (2011) that considers changes in amino acid profile, micronutrient profile, ROS generation and secondary metabolite production in chamomile roots/shoots when subject to nitrogen deficiency and/or heavy metals. The concentration of many essential metals (Ca, Mg, Fe, and Cu) was unchanged in the shoot during nitrogen deficiency, while Cd and Ni concentrations were reduced by 46% and 33%. Limited nitrogen availability least affected phenylalanine levels (Kováčik et al., 2011), similarly observed during sulfur deficiency in *Arabidopsis thaliana* (Nikiforova et al., 2006), suggesting a high importance of phenolic derivatives and secondary compounds when nutrients are scarce. *A. thaliana* increased glutamine production during sulfur deficiency (Nikiforova et al., 2006) and although histidine was not considered in this study, glutamine is an important precursor in histidine biosynthesis.

2.3. Proline

Most abiotic stressors, heavy metal, salinity, drought, temperature and radiation cause elevated proline levels in plants (Al Khateeb et al., 2014). Allelochemical-induced toxicity causes an increase in proline synthesis (Batish et al., 2007; Chen et al., 2015). Proline-Cd (Sharma et al., 1998) and proline-Cu (Farago and Mullen, 1979) complexes have been observed in vitro, however proline-metal complexes are not stable and far less preferable in vivo. Proline accumulation between four genotypes of chickpea was in agreement with Cu tolerance and reduced lipid peroxidation (Singh et al., 2010). Cd-induced stress increased free proline concentration in plants more than any other amino acid (Kato et al., 2019; Wu et al., 2004). Often it is implied that proline is an effective ligand and although its production is highly influenced by metal toxicity it does not directly chelate metals. In a revealing study by Schat et al. (1997), increasing ambient humidity almost completely reversed metal-induced proline accumulation in *Silene vulgaris*. Leaf accumulation of Cu, Cd, or Zn were similar between plants grown at 98% and 75% relative humidity, however proline accumulation was ten times less in plants at 98%. While the direct elicitor of proline synthesis is unclear, transpiration and osmotic balance are highly influential. Proline may function primarily as an osmolyte and as an enzyme protectant (Shah and Dubey, 1997) during various high stress conditions.

2.4 Secondary Metabolites: 8-hydroxyquinoline and mimosine

The production of secondary metabolites in plants is influenced by many factors, metal induced stress/toxicity having notable effects. While the metal chelating properties of specific terpenes, phenolics, flavonoids, etc. are largely unknown, increased production is often observed under metal induced stress (Bali et al., 2019; Moghrovyan et al., 2019). The addition of Pb increased production, altered the composition and increased the allelopathic properties of *Schinus molle* essential oil (Ribeiro et al., 2019). Select crops which produce unique secondary metabolites are high value alternatives to food crops where toxic heavy metals are present in high amounts. Species of note are potential dual-function crops providing commercial value and environmental value by also removing toxic metals from soil. *Ocimum spp*. (Fattahi et al., 2019), *Mentha spp*. (Sá et al., 2015), and *Lavandula spp*. (Angelova et al., 2015) are high interest crops since harmful metallic ions are separated in the distillation of essential oils. Although plant growth may be hindered by metal induced stress, secondary metabolite production is often increased (Maleki et al., 2017).

Industrial, medicinal and experimental applications are growing which use plant secondary metabolites in the synthesis metal nanoparticles. Leaf extracts (Marslin et al., 2018; Smitha et al., 2009) exhibit shape/size-specific synthesis of nanoparticles, films, and alloys (Haverkamp et al., 2007). Many nanoparticles produced using plant extracted secondary metabolites enhance the effect of antibiotics (Jayarambabu et al., 2020; Nishanthi et al., 2019).

Secondary metabolites with exceptional metal chelating properties have been recognized as phytotoxins although they may have developed as unique phytosiderophores for the purpose of enhancing metal uptake. The evolution of allelopathic strategies is not clear because often a beneficial effect on plant growth can be observed at low concentrations of toxic compounds. This dual response to a compound is known as hormesis and is demonstrated by many modern drugs which have beneficial effects only within a specified concentration. Dosage alone determines a compounds as either “toxin” or as “medicine”. Exposure to high concentrations of many phytotoxins inhibit growth and seed germination of neighboring plants however low concentrations of the same toxin may stimulate growth. This phenomenon can be observed also by low concentrations of toxic metals resulting in stimulating root growth (Hörger et al. 2013).

The evolutionary origin of such allelopathic compounds may have initially emerged as improved means to acquire micronutrients. Many phytotoxins with metal chelating properties are not toxic as a metal-chelate, undergo degradation and are not present in high concentrations (Tharayil, 2009), thus calling into question their efficacy in nature. The elemental defense hypothesis (Boyd, 1998) attributes metal hyperaccumulation as an evolved trait for deterring herbivores and pathogens. Strong evidence against the elemental defense hypothesis states that high metal tolerance must preclude the ability for hyperaccumulation in plants, thus calling into question how metal hyperaccumulation is developed as a defense strategy. Identical is the case for evolution of phytotoxins. Toxicity alone is not enough evidence to infer the evolutionary purpose of a secondary metabolite and tolerance within the host organism must also be considered. Two examples of unique secondary metabolites are described which have unclear roles in metal uptake and may serve as novel phytosiderophores.

8-hydroxyquinoline

The phytotoxin 8-hydroxyquinoline (8HQ) is produced by *Centaurea diffusa* and exuded from the root system into the surrounding soil, thus putting neighboring plant species at a competitive disadvantage. Evidence strongly suggests that 8HQ disrupts normal cell activity by chelating divalent metallic ions, although a toxic mechanism or molecular target has not been identified (Fraser and Creanor, 1974; Jones, 1963). Plants treated with a Fe^{3+}-8HQ chelate do not exhibit growth inhibition compared to plants treated with 8HQ alone. Furthermore, Fe^{3+}-8HQ was able to restore Fe-uptake in the maize *ys1* knockout mutant (Tharayil et al., 2009). It was proposed that Fe^{3+}-8HQ is capable of free diffusion across cell membranes as Fe^{3+} and polar groups of 8HQ are buried within the complex (Fig. 8). In this case, if considered as a phytotoxin, 8HQ may result in Fe loss from the roots of competing plant species. Further studies are required to confirm the free diffusion hypothesis, as the larger oligopeptide transporter family is not well characterized except for the YS/YSL transporter subfamily.

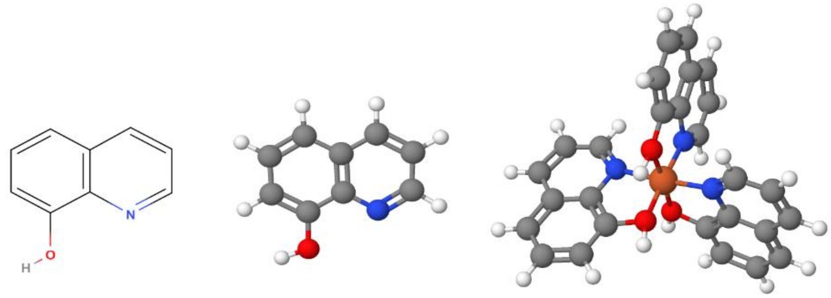

Figure 8: Chemical structure of 8HQ (left), ball-stick model (middle), and 1:3 (Fe:8HQ) chelate (right). A 1:3 best demonstrates the hydrophobic property suspected for allowing free diffusion across cell membranes, although a complex of 1:2 or 1:1 (Fe:8HQ) may also be possible.

The primary function of 8HQ may best be described as phytosiderophore, not phytotoxin. Species other than *C. diffusa* uptake the Fe^{3+}-8HQ complex and utilize the Fe, however the metabolic fate and in vitro stability of the 8HQ is unknown. Secretion of 8HQ from *C. diffusa* roots is strongly induced by Fe-deficiency and light exposure (Tharayil et al., 2009), resembling the secretion pattern of MA phytosiderophores. More research into 8HQ, both as a phytotoxin and a phytosiderophore, is required to understand this compound's unique properties.

Mimosine

Leucaena leucocephala is a woody tree legume that produces the toxic secondary metabolite mimosine. Fe chelating properties of mimosine have shown to inhibit the activity of ribonucleotide reductase, interfere with dNTP metabolism and to inhibit DNA elongation at the G1/S phase transition in the cell cycle (Dai et al., 1994). Inhibitory effects are reversed and DNA synthesis restored upon addition of excess Fe to mimosine treated cell cultures, thus confirming the relationship between chelation and growth inhibition (Gilbert et al., 1995). This toxic effect is not limited to herbivores as mimosine was shown to arrest the plant cell cycle in *Petunia hybrida* mesophyll protoplasts and tobacco BY-2 cells (Planchais et al., 2000). The Fe-chelating properties of mimosine have been long associated with toxicity, however the role of mimosine as a phytosiderophore has only recently been investigated.

Mimosine is present throughout leucaena tissue up to 5% of the plant dry weight and has been detected in the root exudate (Honda and Borthakur, 2020; Soedarjo and Borthakur,1998). Specific transporters facilitating the root uptake of a Fe-mimosine complex have not been shown, nor the identification of mimosine transporters, yet phytosiderophore properties have been demonstrated in Fe uptake experiments. Mimosine was detected in aerial tissue of tomato and bean plants grown in the presence of mimosine, along with increased Fe uptake (Honda and Borthakur, 2020).

It is possible that a Fe-mimosine chelate, either 1:1 or 1:2 complex, is transported by YSL transporters. Members of the oligopeptide transporter family may transport a Fe-mimosine chelate due to similarities to peptide or glutathione chelation complexes (Fig. 9).

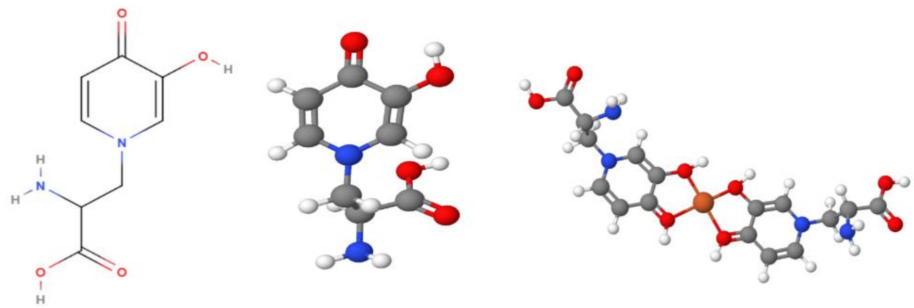

Figure 9: Chemical structure of mimosine (left), ball-stick model (middle), and 1:2 (Fe:mimosine) chelate. Different chelate ratios may form, such as 1:1 or 1:3 complex, demonstrated by competitive metal binding assay and absorption spectrophotometry (Honda and Borthakur, 2020).

Concluding remarks

Metal homeostasis is a complicated process in plants, consisting of overlapping pathways and regulation. Plants have developed various methods to maintain a balanced variety of essential metals differing in their necessity, binding capability and reactivity. The role of metal chelating ligands is extremely complex in this sense as some serve multiple functions, such as solubilizers, antioxidants, metabolites, etc., while simultaneously having crucial and specific roles as primary metabolites. Conferring metal tolerance is demonstrated often by overproduction of a single metal ligand, thus challenging future studies to consider synergistic effects between different ligands, transporters, metallic ions, etc. Plant metal homeostasis studies need to carefully consider abiotic factors and numerous metal chelating ligands that collectively determine metal uptake and stress mediation.

The bioavailability of essential metals has a significant impact on the growth and health of plants. Metals such as Fe, Zn, and Cu serve as cofactors that facilitate many necessary cellular functions. In the case of food crops, essential metals dictate the quality and nutritional value of the product. Improving nutritional content is complicated due to differences between crops, methods/resources available and various soil conditions that influence bioavailability. Investigating plant metal acquisition and metal hyperaccumulation has implications beyond food and nutrition. Hypertolerant plant varieties of non-essential metals are necessary in urban environments and for the bioremediation of contaminated soil. Addressing environmental pollution and heavy metal contamination in the future will likely require a natural approach. Phytoextraction of toxic metals from wastewater and soil is promising, however plant varieties and methods should continue to be developed and improved.

~~~~~~~~~~~~~~~ ABSTRACT ~~~~~~~~~~~~~~~

Plants rely upon a small chemical ligand, nicotianamine (NA), to chelate metallic ions during transport throughout tissues and across cell membranes. The production of this essential compound is achieved by three enzymes: S-adenosylmethionine (SAM) synthetase, NA synthase and 5'-methylthioadenosine (MTA) nucleosidase. The characterization of each of these enzymes from any plant species is lacking or absent, therefore the coding sequence for these genes were isolated from local hardwood species and characterized in vitro.

The cDNA encoding for SAM-synthetase, NA synthase and MTA nucleosidase was isolated from giant leucaena (*Leucaena leucocephala* subsp. *glabrata*) root tissue mRNA. Transcriptome data and/or 5'-RLM-RACE were used to obtain the full transcript sequence. The complete coding sequences were cloned into a T_7-expression vector and expressed in *Escherichia coli*. The giant leucaena SAM-synthetase displayed optimal enzyme activity at pH 10.0, 55 ^oC, and 200 mM KCl. In addition to thermophilic activity, giant leucaena SAM-synthetase remains highly active in solutions containing up to 4 M KCl and accepts Na^+ to some extent as a substitute for K^+, a known required cofactor for SAM-synthetases. The enzyme followed Michaelis–Menten kinetics (K_m = 1.82 mM, K_{cat} = 1.17 s^{-1}, V_{max} 243.9 µM. min^{-1}) and was not inhibited by spermidine, spermine or nicotianamine. Plant SAM-synthetases have not been characterized previously and the activity of the giant leucaena SAM-synthetase differed greatly from that of nonplant SAM-synthetases. Therefore, a second plant SAM-synthetase from *Acacia koa* was investigated. The activity of the *Acacia koa* SAM-synthetase resembles

that from the giant leucaena (K_m = 1.44 mM, K_{cat} = 1.29 s^{-1}, V_{max} 170 µM. min^{-1}) and exhibited similar alkali-thermophilic properties. Four single-point mutation variants of the *Acacia koa* SAM-synthetase were produced, each with varying degrees of reduced reaction rate, greater sensitivity to product inhibition and loss of thermophilic properties. Although an enhanced mutant was not produced, the addition of organic solvent was shown to have a beneficial effect on enzyme activity. Feedback inhibition was reduced in SAM-synthetase enzyme assays containing 25% acetonitrile, methanol or dimethylformamide and total SAM production improved by 30-65%.

Transcriptome sequence data and 5'-RLM-RACE methods identified the complete NA synthase coding sequence, which was cloned for heterologous expression and in vitro assays. Soluble expression was highly repressed, however heat-shocking and high-NaCl media improved recombinant enzyme production approximately 6-fold. Feedback inhibition by MTA is known to severely limit the in vitro activity of SAM dependent enzymes, however this work demonstrates comparable effects produced by substrate inhibition. Producing enantiomerically pure substrate in situ, using a recombinant SAM-synthetase, enabled 5-fold faster NA synthase activity (V_{max} = 1.25 µM. h^{-1}) and 2-fold net nicotianamine production than when commercially purified substrate, a racemate, is provided. Sequence and structural analyses suggest residues involved in azetidine ring formation, and other aspects of the mechanism are explored.

The complete coding sequence of a MTA nucleosidase was obtained from the giant leucaena transcriptome and cloned into *pet39b*, thereby expressing a fusion protein secreted into the *E. coli* periplasm. The crude periplasmic extract was tested for

MTA-nucleosidase activity and when combined with SAM-synthetase and NA-synthase, further improved the reaction rate 22-fold (V_{max} = 27.5 μM. h^{-1}) and net NA production 3-fold. In vitro NA production is optimal in solutions containing all three enzymes (SAM-synthetase, NA-synthase, and MTA-nucleosidase), however the reaction becomes fully inhibited upon producing 58.5 μM NA.

In addition to the in vitro characterization of recombinant enzymes, the *in plantae* transcription of NA synthase, SAM synthetase and 17 other genes was quantified in giant leucaena seedlings. In response to high-iron fertilization, real-time PCR performed on root and foliar tissue showed overall upregulation of most genes. Notable genes affected include glutathione synthase (20-fold increase in leaf), ferric chelate reductase (15-fold increase in root), mimosinase (20-fold increase in leaf) and nicotianamine synthase (30-fold increase in root). In response to iron fertilization, mimosine metabolism was shown to be increased by metal induced stress; that is oxidative stress and not iron itself. Furthermore, the gene expression profile of leaf tissue indicated that plants with high mimosinase activity were less affected by iron and experienced less oxidative stress. Therefore, mimosine metabolism may broadly affect iron-regulated processes and enable the hyperaccumulation of iron or other metals.

~~~~~~~~~~~~ INTRODUCTION ~~~~~~~~~~~~

The enzymes involved in nicotianamine biosynthesis are described in their sequential order; S-adenosylmethionine (SAM)-synthetase, nicotianamine (NA) synthase and 5'-methylthioadenosine (MTA) nucleosidase. Relevant/background information is provided for each step, as it pertains to the work in this dissertation.

S-adenosylmethionine (SAM) is a precursor for various transferase reactions in cells. For DNA or protein methylation, SAM is recognized as a primary source of methyl groups. Polyamines, notably spermine and spermidine, are important growth regulators and derived from aminopropyl groups of SAM. In addition to these essential processes, higher plant species require SAM for both primary and secondary metabolites. Nicotianamine is an essential metabolite in plants that chelates metallic ions (Carrillo and Borthakur, 2021); a single molecule of nicotianamine requires three molecules of SAM. Factors such as stress, flowering and fruit ripening can further increase SAM requirements to produce secondary metabolites and ethylene (Van de Poel et al., 2013; Roeder et al., 2009). While many separate pathways can be shown to involve SAM, in vivo studies often show that SAM production is increased in response to many abiotic stressors (Choi et al., 2022; Ding et al., 2015; Huang et al., 2021). N-methyltransferases transfer the methyl group of SAM to an accepting amine group, thus regulating gene expression and plant development. In plants specifically, histone lysine methylation is a strictly controlled process that determines the expression or suppression of various genes affecting shoot branching, seed development, and retrotransposon activity (Qin et al., 2010; Ebbs and Bender, 2006; Dong et al., 2008). Transcription factors and histone modification are dependent on the recognition of methylated CpG sites, the product of cytosine methylation by N-methyltransferases and SAM. A second class of methyltransferases, O-methyltransferases, are especially important in plants which produce methylated secondary metabolites.

Members of Fabaceae, such as *Leucaena* spp., are prolific producers of flavonoids and pterocarpans (Mottaghipisheh and Iriti, 2020). SAM is essential as a methyl donor to produce a diverse pool of flavonoids in plants. Pterocarpans are unique flavonoids produced by *Fabaceae* spp. and widely recognized as plant defense compounds; pterocarpan biosynthesis increases 2-4 fold in response to both abiotic stress and infection (Aisyah et al., 2013; Barz and Mackenbrock, 1994; Carlson and Dolphin, 1981). *Leucaena* spp. are producers of the unique secondary metabolite mimosine, a toxic nonprotein amino acid which is implicated in iron-uptake and stress tolerance (da Silva Rodrigues-Corrêa et al., 2019; Honda and Borthakur, 2020). While SAM is not directly required in mimosine biosynthesis, related pathways involved in methionine salvage may be affected. A key step in mimosine biosynthesis is performed by a cysteine synthase isozyme (Ikegami et al., 1990), suggesting competition between cysteine and mimosine production in Leucaena. Cysteine synthase kinetic studies have shown the enzyme favors cysteine over mimosine synthesis (Harun-Ur-Rashid et al.,2018), yet up to 10% (dry weight) mimosine has been measured in Leucaena shoot tips (Bageel et al., 2020). The carbon drain produced by mimosine synthesis may have downstream effects on cysteine/methionine availability, SAM-related pathways (Fig. 1) or on catalytic efficiency of SAM-dependent enzymes in Leucaena.

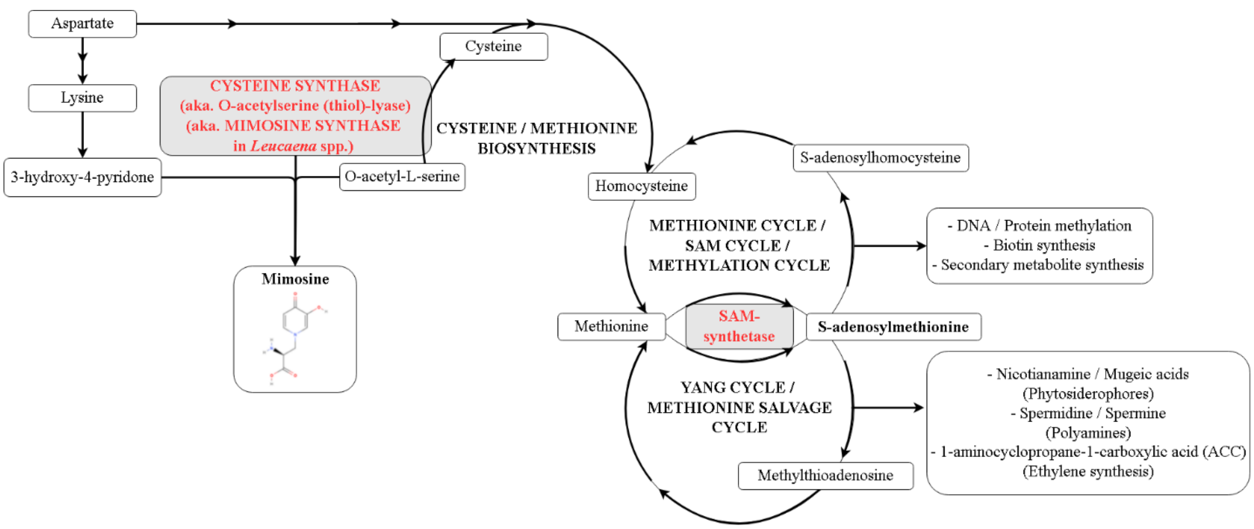

Figure 1: Methionine pathways in plants demonstrate the keystone role of S-adenosylmethionine for primary and secondary metabolism. Mimosine biosynthesis is included to illustrate potential competition between the essential amino acid methionine and non-protein amino acid mimosine. Intermediate compounds and most enzymes are omitted from the pathways shown for clarity.

Giant leucaena can tolerate high amounts of abiotic stress, nutrient poor alkaline soil and periodic drought more than common fodder crops. Many forms of abiotic stress have been shown to increase production of polyamines, ethylene, and S-adenosylmethionine (SAM) in plants. Huang et al. (2021) detected twice the spermine content in heat stressed lettuce varieties. In vivo plant studies often show increased salt tolerance and increased SAM production in response to stress (Li et al., 2013). Transgenic tobacco overexpressing *Suaeda salsa* SAM-synthetase exhibits healthier growth, high-salt tolerance and increased production of polyamines (Qi et al., 2010). In the cold-tolerant *Chorispora bungeana*, SAM-synthetase expression was strongly induced by low-temperature, ethylene, and NaCl (Ding et al., 2015).

Increasing the cellular pool of SAM is an efficient strategy to improve many genetically modified organisms. Yeast cells expressing a chimeric-plant enzyme accumulate 100-times greater cytosolic SAM (Chan and Appling, 2003). The same strain, further engineered to produce the plant metabolite nicotianamine, yields twice the amount compared to control yeast expression lines (Wada et al., 2006). Similarly, improved SAM production doubled the production of an antibiotic in *E. coli* (Wang et al., 2007b). Transgenic plant studies often correlate increased SAM production with increased stress tolerance (Heidari et al., 2020; Ma et al., 2017), thus increasing SAM may benefit expression systems limited by stress.

Few studies have characterized recombinant SAM-synthetases, fewer which focus on catalytic activity. Examples can be found from *Saccharomyces cerevisiae* SAM-synthetase expressed in *Pichia pastoris* (Zhou et al., 2008), *Bacillus subtilis* SAM-synthetase expressed in *E. coli* (Kamarthapu et al., 2008) and rat liver SAM-synthetase expressed in *E. coli* (Álvarez et al., 1994). The *Brassica rapa* SAM-synthetase was expressed in *E. coli*, however in vitro activity was not characterized (Kim et al., 2012). The optimal temperature of recombinant *Pichia ciferri* SAM-synthetase is 30^{o}C with activity greatly reduced at higher temperatures (Yoon et al., 2012). Native SAM-synthetase was purified and assayed from *Glycine max* ($K_{m\ ATP}$, 1.53 mM, $K_{m\ METHIONINE}$, 1.81 mM) (Kim et al., 1995) but plant SAM-synthetases from other plant species remain largely uncharacterized. In this work, the SAM-synthetase gene from giant leucaena

(*Leucaena leucocephala* subsp *glabrata*) and from the Hawaiian koa (*Acacia* koa) was cloned and heterologously expressed in *E. coli*.

The activity of the giant leucaena SAM-synthetase was unlike that of previous enzymes, those being from microbial species. The *A. koa* SAM-synthetase was cloned and used to confirm the activity of plant SAM-synthetases, as well as to test other techniques to overcome feedback inhibition. While very little is known regarding plant SAM-synthetases, the *E. coli* enzyme has been well characterized. Wang et al. (2019) identified four essential sites (**I303**, **I65**, **L186**, **N104**) in the *E. coli* SAM-synthetase (**EcMAT**) and produced mutants with enhanced activity. The corresponding sites were considered in this work with the aim of reducing feedback inhibition. Compared to nonplant SAM-synthetases, plant SAM-synthetases show less product inhibition and are more tolerant of extreme conditions. Two sites were selected to generate single point mutation variants of the *A. koa* SAM-synthetase: **Y65** and **I193**. Regarding the first site, **Y65**, the amino acid tyrosine is unique to eukaryote SAM-synthetases and highly conserved. Although this residue is not located near the active site, altering this site in **EcMAT** had a strong effect on enzyme Km and feedback inhibition. The second site, identified as **I193** in the *A. koa* enzyme, is also not directly implicated in catalysis but has a significant role in enzyme activity. In **EcMAT**, changes at this site had the greatest impact on enzyme activity; reduced K_m five-fold and improved SAM accumulation by 70%. These sites and other structural features of plant SAM-synthetases are illustrated and detailed in the result section. **EcMAT** has been studied extensively and continues to be a popular enzyme for mutagenesis (Gade et al., 2021; Kleiner et al., 2022; Cao et al., 2023). An enhanced variant of the *A. koa* SAM-synthetase was not produced in this study, however a close analysis reveals many distinctions between plant and nonplant SAM-synthetases.

Like mutagenesis, chemical additives can have pronounced effects on enzyme activity and inhibition. Organic solvents often have a denaturing effect on enzymes but their effect on other enzyme properties is less predictable. Polar solvents (e.g., dimethyl sulfoxide, acetonitrile, formamide), have improved enzyme activity or stability by orders of magnitude (Faulds et al., 2011; Shafiei et al., 2012; Wang et al., 2007a). Notable studies by Park et al. (1995, 1996) report zero product inhibition in **EcMAT** assays containing 2M urea, 20% acetonitrile, 8% β-mercaptoethanol or 400 mM p-toluenesulfonic acid. While interesting effects are observed in nonaqueous environments, there are few examples which consider SAM-synthetase specifically.

SAM metabolism fuels a unique and essential enzyme for plant metal homeostasis. The SAM-dependent enzyme nicotianamine (NA) synthase is highly expressed in plant root tissue and produces this essential phytosiderophore. Plants rely upon NA for the chelation of bivalent metallic ions, thereby maintaining their solubility, mobility and nonreactivity in plant tissues. As shown in this dissertation, successful in vitro activity of NA-synthase relies heavily upon two additional enzymes. They are SAM-synthetase, which was just described, and 5'-methylthioadenosine (MTA) nucleosidase, which will be addressed last.

The chelation of reactive metal species, especially iron, is critical to reduce their reactivity in cells and tissue. Small metabolites, such as proline or glutathione, have important roles in metal homeostasis but not specifically as metal chelators (Carrillo and Borthakur, 2021). The NA-iron chelate exhibits high stability and resistance to oxidation (von Wirén et al., 1999), thus iron is preserved effectively in a reduced state in vivo. With the exception of grass species, which produce variations of NA called mugineic acid compounds, NA is the primary phytosiderophore produced in higher plants. A few secondary metabolites in plants have been noted with metal chelating properties, however their role as phytosiderophore is not clear. Toxicity is often associated with metal-chelating secondary metabolites; examples include 8-hydroxyquinoline from *Centaurea diffusa* (Tharayil et al., 2009), juglone from the walnut tree (Chobot and Hadacek, 2009) and mimosine (Gilbert et al., 1995). Other interesting effects in plants have been reported as well, such as improved nutrient acquisition, stress tolerance or overall growth (Santos et al. 2016). Therefore, metal homeostasis is an interesting process in plants which produce such potent metal chelators. This study attempts to show relationships between iron translocation, iron induced stress and mimosine metabolism in giant leucaena (*Leucaena leucocephala* subsp *glabrata*).

NA biosynthesis is not well understood, specifically the activity of the enzyme NA-synthase (EC 2.5.1.43). In total, three aminopropyl moieties from S-adenosylmethionine (SAM) are polymerized to form one molecule of NA and three molecules of MTA (Fig. 2). NA-synthases are mostly absent outside of higher plants, except for the bryophyte *Physcomitrella patens* (Trampczynska et al., 2006), fungi *Neurospora crassa* (Rensing et al., 2008), and *Streptomyces* SANK 62595 (Suzuki et al., 1996). A variety of bacterial siderophores have been characterized which are referred to as NA-like (Laffont and Arnoux, 2020), however their biosynthesis is distinctly different. Compared to known aminopropyl-transferases, the reaction performed by NA-synthase is unique for three reasons:

1) *Only* SAM serves as a substrate. (3 eq. SAM ☐ 1 eq. NA).

2) Four *distinct* reactions are performed by NA-synthase. 1) Cleaving the initial aminopropyl group from SAM, 2) condensation reaction using second molecule of SAM, 3) second condensation reaction using third molecule of SAM and 4) azetidine ring synthesis.

3) Compounds containing azetidine rings are extremely rare in nature, observed only in two plant metabolites, NA and azetidine-2-carboxylic acid.

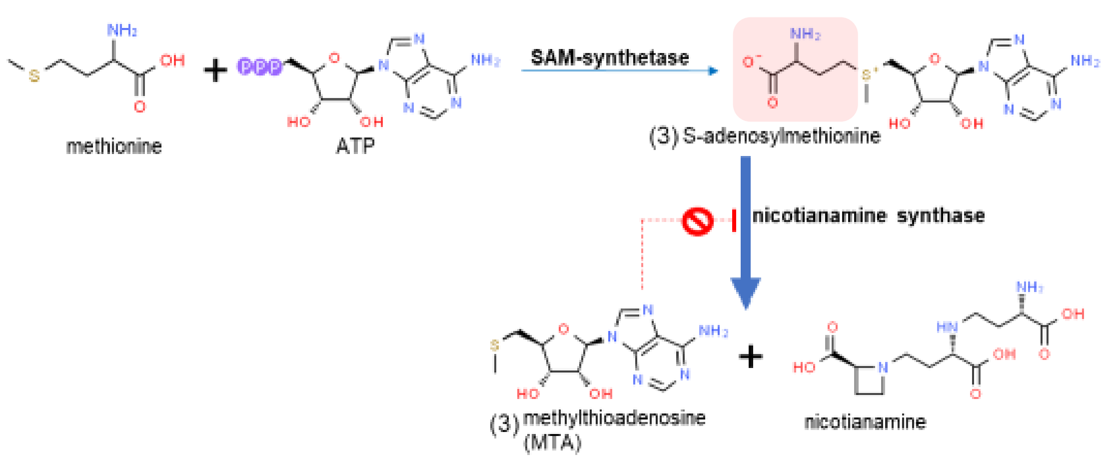

Figure 2: Biosynthetic pathway for nicotianamine. The portion of SAM which is used in NA synthesis is highlighted with a red box. The byproduct S-methyl-5'-thioadenosine (MTA) has a strong inhibitory effect on NA synthase activity.

NA studies are ultimately limited by the availability of purified compound, which is scarce and expensive. Despite being produced by all plant species, its purification from plant material is difficult and labor intensive (Asai et al., 2005). Although NA production has been achieved using engineered yeast (Wada et al., 2006), purification remains a challenging step which may be overcome using cell-free methods. In vitro studies have indicated other limitations, namely the poor expression of recombinant NA-synthase and strong feedback inhibition by 5'-methylthioadenosine (MTA) (Schmiedeberg et al., 2003; Herbik et al., 2009). Poor expression and insoluble expression of recombinant enzymes are common issues in bacteria. Methods such as heat-shocking *E. coli* cultures (Oganesyan et al., 2007) were highly effective in improving NA-synthase activity, yet renaturation of the recombinant NA-synthase was ultimately required. Only recently was the activity of an NA-synthase described, albeit not completely (Seebach et al., 2023). In that study, the paralyzing effects of MTA were properly addressed yet NA-synthase activity is repressed by substrate inhibition as well. Shown in this dissertation is the essential nature of enzymatically fresh substrate, catalyzed by SAM-synthetase. Substrate inhibition is not often considered among SAM-dependent enzymes, though it has been demonstrated among methltransferases (Borchardt and Wu, 1976). When enzymatically produced from SAM-synthetase (L-methionine + ATP → SAM) only the (S, S) enantiomer is formed, which inevitably forms a (R, S) / (S, S) racemic mixture. Commercially available purified SAM contains 20 to 40% of the inactive (R, S)-SAM diastereomer (Desderio, 2005; Zhang and Klinman, 2015). Our lab has previously assayed recombinant plant SAM-synthetases (Carrillo and

Borthakur, 2022, 2023) and present a significant benefit to producing (S, S)-SAM in situ for NA-synthase.

When performed in plantae, NA biosynthesis may be considered complete. However, proper NA-synthase activity in vitro requires the byproduct to be further degraded. Therefore, the third and final enzyme characterized in this work is the giant leucaena MTA-nucleosidase. A few other plant MTA-nucleosidases have been previously characterized; *Oryza sativa* L. (Rzewuski et al., 2007), *Arabidopsis thaliana* (Park et al., 2009; Siu et al., 2008) and *Lupinus luteus* (Guranowski et al., 1983). This work describes the successful periplasmic expression of a fusion MTA-nucleosidase from giant leucaena. Due to issues in purifying the fusion protein, the crude periplasmic extract was not characterized in detail. Regardless, the crude periplasmic extract was effective for use with NA-synthase. Compared to when NA-synthase is assayed alone, when all three enzymes are present (SAM-synthetase, NA-synthase and MTA-nucleosidase) NA production is roughly 100-fold higher. Despite this vast improvement, overall productivity in vitro is very low and not practical on an industrial scale.

~~~~~~~~ RESEARCH OBJECTIVES ~~~~~~~~

To characterize the in vitro activity of three essential genes in nicotianamine biosynthesis; SAM-synthetase, nicotianamine synthase and 5'-methylthioadenosine nucleosidase

To determine if in vitro synthesis is a viable method for commercial nicotianamine production

To measure the change in giant leucaena gene expression in response to iron fertilization, specifically to show differences…

1) *… between leaf and root tissue*
2) *… between foliar and soil fertilization methods*
3) *… which can be attributed to mimosine catabolism*

~~~~~~~~~~~ METHODOLOGY ~~~~~~~~~~~

Divided into six parts, beginning with the individual characterization of each enzyme involved in nicotianamine biosynthesis.

***Part I:* SAM-synthetase from giant leucaena**

***Part II:* SAM-synthetase from Acacia koa and mutagenesis experiments**

***Part III:* 5'-methylthioadenosine nucleosidase from giant leucaena**

***Part IV:* nicotianamine synthase from giant leucaena**

***Part V:* Gene expression analysis following iron fertilization of giant leucaena seedlings**

Part I: SAM-synthetase from giant leucaena

1.1. 5'-RLM-RACE to obtain full-length SAM-synthetase transcript sequence

Giant leucaena (*Leucaena leucocephala* subsp *glabrata*, cultivar K636) seeds were harvested from the University of Hawaii Waimanalo Research Station (Oahu, Hawaii). Seeds were scarified using concentrated sulfuric acid, rinsed and planted directly into 4" pots containing generic potting soil. Plants were maintained indoors under fluorescent lighting and successful germination was observed between 1-2 weeks. Giant leucaena root tissue from three-week old seedlings were snap frozen and finely ground for total RNA extraction using RNeasy Plant Mini Kit (Qiagen). Full-length mRNA transcripts were selected for 5'-RLM-RACE and cDNA synthesis using the FirstChoice RLM-RACE Kit (Thermo Fischer).

PCR primers were designed from a partial coding sequence for SAM-synthetase obtained from giant leucaena K636 transcriptome data (Ishihara et al., 2016). Conventional PCR methods were used to amplify the adapter ligated cDNA and identify the complete transcript. Additional PCR primers were then designed (Table 1) to obtain the complete SAM-synthetase coding sequence, designated hereafter as *sams*.

Table 1: List of primers using for amplification of the giant leucaena SAM-synthetase coding sequence. The start codon is indicated with red and restriction enzyme sites used for cloning are indicated in bold italics.

Primer Description	Primer Sequence
Forward primer	**ATG** GAG ACC TTT TTG TTC ACT TCT GAA TCT GTC AAC GAG GGT C
Reverse primer	TTA AGC TTG AGG CTT CTC CCA CTT GAG TGG CTT C
Xho 1 site insertion (Forward primer)	TTA GCA ***CTC GAG*** **ATG** GAG ACC TTT TTG TTC ACT TCT GAA TCT GTC
Bam H1 site insertion (Reverse primer)	TTA GCA ***GGA TCC*** TTA AGC TTG AGG CTT CTC CCA C

1.2. Bioinformatics and sequence analysis of giant leucaena SAM-synthetase

Recently the first crystal structure of plant SAM-synthetases was determined from *Arabidopsis thaliana* (Sekula et al., 2020). Using the Arabidopsis model as a template, SWISS-MODEL (Waterhouse et al., 2008) was used to generate a 3d-model of the giant leucaena SAM-synthetase. The web application POLYVIEW-3D (Porollo and Meller, 2007) was used to color and highlight select residues.

The giant leucaena SAM-synthetase sequence was used to collect similar sequences using the NCBI BLAST program. Results were selected for use in multiple sequence alignment by CLUSTAL-OMEGA (Sievers et al., 2011) and to construct a simple phylogenetic tree using Phylogeny.fr (Dereeper et al., 2008).

1.3. Construction of pET14b-sams and heterologous expression

Q5 High-Fidelity Polymerase (New England Biolabs) was used to amplify *sams* from cDNA and the identity of the gel-purified amplicon was confirmed by Sanger sequencing (Advanced Studies in Genomics, Proteomics and Bioinformatics (ASGPB), University of Hawaii at Manoa). The Codon Optimization Tool (Integrated DNA Technologies) was used to check for codon biases in *sams* and none were detected. Primers were designed which include *Xho*1 and *Bam*H1 restriction sites and conventional PCR was used to generate a *sams* amplicon suitable for cloning. The subsequent PCR product was gel-purified, digested for 4 h at 37^{o}C using FastDigest *Bam*HI and FastDigest *Xho*1 restriction enzymes (Thermo Scientific), and gel purified to remove enzyme, salt, and oligonucleotide fragments. The T_7-expression vector *pet14b* (Novagen) was digested and dephosphorylated in a three-enzyme reaction using FastDigest *Bam*HI, FastDigest *Xho*1 (Thermo Scientific) and Shrimp Alkaline Phosphatase (New England Biolabs) in 1X CutSmart Buffer (New England Biolabs) prior to gel-purification. *pET14b-sams* was produced by a standard ligation reaction using T4 DNA Ligase (New England Biolabs) and transformed into *E. coli* DH5-α. Purified *pET14b-sams* was sequence verified and used to transform *E. coli* BL21(DE3) cells for protein expression.

Overnight cultures of the transformed BL21(DE3) line were prepared by inoculating Luria-Bertani (LB) media containing ampicillin and chloramphenicol. Fresh LB (no antibiotics) media was inoculated using 1/1000th vol. overnight culture and grown at 37 ^{o}C until O.D.$_{600}$(0.7). Protein expression was induced with the addition of 0.2 mM IPTG for 12 h at 25 ^{o}C with gentle mixing. Cells were harvested by pelleting cultures and lysed by sonication in 1/10th vol. of HisLink Binding/Washing Buffer. Methods and materials outlined in the HisLink Protein Purification System (Promega) were followed for the purification of the recombinant Leucaena SAM-synthetase enzyme, designated hereafter as **LSAMS**.

Purified **LSAMS** was subject to buffer exchange using Amicon Ultra-15 Centrifugal Filters to a protein storage solution (100 mM TRIS-HCl (pH 8.5), 50 mM NaCl, 5 mM dithiothreitol (DTT), 1 mM EDTA, 50% glycerol) and concentrated to 5 mg. mL^{-1}. Small aliquots were prepared, snap frozen and stored at -80 ^{o}C.

1.4. Determining optimal assays conditions and RP-HPLC analysis of activity

Optimal conditions were determined for pH, temperature and ionic strength of the enzyme assay solution prior to investigating kinetic constants of **LSAMS**. Unless otherwise stated, assay composition and conditions are as follows: 100 mM Tris-HCl, 200 mM KCl, 10 mM $MgCl_2$, 5 mM DTT, 1 mM ATP, and 1 mM L-methionine. The pH of assay solutions was carefully adjusted at the designated temperature prior to the addition of substrate, DTT or enzyme. Necessary considerations were made to ensure accurate pH of heated assay solutions. The relative volume of solution and type of pH probe must be considered as a large glass pH probe must reach a temperature equilibrium with the solution, taking up to 10 min.

Discontinuous assays were performed under a range of conditions to determine optimal pH, ionic strength, and temperature. Assays (2 mL volume) were performed in 15 mL Falcon centrifuge tubes with the use of a heated water bath. Assays were started by addition of enzyme (final concentration of **LSAMS**: 0.1 mg. mL^{-1}), gently mixed by hand and allowed to proceed for 20 min. Assays were terminated by the addition of an equal volume of ice cold 0.2 M o-phosphoric acid (OPA) and kept on ice until analysis by HPLC. Reversed-phase HPLC was performed using a C18 column (Phenomenex C18; 5 µm; 4.6 × 250 mm) and mobile phase of 0.02 M OPA (isocratic elution, 1 mL/min). Formation of S-adenosylmethionine was measured at λ = 260 nm, retention time of 2.4 min. A standard curve was constructed using pure SAM (New England Biosciences) and used for determining kinetic values. The decomposition of SAM, determined largely by heat and alkalinity, was measured by the production of adenine (retention time, 4.0 min).

1.5. Kinetic analyses of recombinant LSAMS

Discontinuous time course assays (400 µL) were performed in a dry bath (50 ^{o}C) using the determined optimal assay conditions (100mM Tris-HCl pH 8.5, 50 ^{o}C, 200 mM KCl, 10 mM $MgCl_2$ and 5 mM DTT). The assay solution master mix was adjusted to pH 8.5 at the optimal temperature of 50 ^{o}C prior to the addition of any substrate, DTT, or enzyme. ATP and L-methionine were supplied in equal concentrations and varied equally, thus **LSAMS** was treated as a single substrate enzyme. Substrate concentrations of 0.8, 1.6, 2.4, 4.0, 4.8 and 5.6 mM were tested. Upon reaching temperature, assays were started by the addition of **LSAMS** (final concentration 0.16 mg. m/L^{-1} enzyme). Aliquots were transferred from the assay at 2, 4, 8, 15, 60, and 120 min to chilled tubes prior to complete termination by 2 vol. of 0.16 M o-phosphoric acid, velocity values were calculated using the 4 min measurements. Intermediate quenching on ice prior to complete termination of assay was required to minimize pipette error in transferring the heated solution.

A maximum concentration of 15 mM ATP and L-methionine was evaluated for potential substrate inhibition on **LSAMS**. Inhibitory properties of spermidine (1 mM), spermine (1 mM) and nicotianamine (0.2 mM) were investigated.

Part II: SAM-synthetase from Acacia koa and mutagenesis experiments

2.1. Isolating the complete coding sequence of SAM-synthetase and construction of the expression vector pET14b-ksams

Total RNA extraction (RNeasy Plant Mini Kit, Qiagen) was performed from seedling root tissue. Seeds were obtained from the Hawaii Agriculture Research Center (Kailua, HI) and seedlings cultivated indoors in ordinary potting soil. After 12-weeks, seedlings reached approximately 4” in height and had developed root tissue suitable for RNA extraction. Partial sequences (GENBANK ACCESSION No. GBYE01000801, GBYE01002034) and one complete transcript (GBYE01000159) were identified from the *A. koa* transcriptome sequence archive (Ishihara et al., 2015). Untranslated regions were identified from the complete transcript sequence (GBYE01000159), which includes a 5'-untranslated region of 251 bp and a 3'-untranslated region of 394 bp. The partial transcript GBYE01002034 likely encodes a homologue of the SAM-synthetase in this study. Based on the translated sequence, GBYE01002034 encodes a SAM-synthetase sharing 92% similarity to the other two transcripts. Therefore, cloning efforts were solely focused on the coding sequence of the complete transcript. Sanger sequencing (Advanced Studies in Genomics, Proteomics and Bioinformatics (ASGPB)) confirmed the full coding sequence (>99% identical to transcriptome sequence data) of SAM-synthetase from *A. koa* cDNA, referred to hereafter as *ksams*.

Primers containing *BamH*1 restriction sites were designed to produce a suitable gene insert for cloning. The T_7-expression vector *pet14b* (Novagen) was digested, dephosphorylated and purified. *pET14b-ksams* was produced by a standard ligation reaction and used to transform *Escherichia coli* DH5-α competent cells. Colonies were selected on Luria-Bertani (LB)-ampicillin plates, subcultured for plasmid purification and reconfirmed by sequence analysis.

2.2. Production of mutant constructs

Two sites were selected for site-directed mutagenesis and a total of four mutants were produced. The original construct and mutant variants were analyzed for codon biases in *E. coli* (IDT-DNA Codon Optimization Tool), which were not detected.

The mutations are Y65A, Y65V, I193V and I193A. Using a high-fidelity DNA polymerase and *pET14b-ksams* plasmid template, conventional PCR produced linear blunt-ended vectors with the intended mutation. The PCR product was purified, circularized and used to transform *E. coli* DH5-α competent cells. Transformants were subcultured and sequenced to confirm the intended mutation. A list of primers and their sequence is available to view in Table 2.

Table 2: List of primers used for amplification of the *A. koa* SAM-synthetase coding sequence. Primers used in cloning and mutagenesis are included with relevant sites indicated in bold text.

Primer Description	Primer Sequence
Forward Primer	ATG GAG ACT TTT CTA TAC ACC TCC GAA TCA GTG AAC G
Reverse Primer	TTA AGC TTG AGG TTT TTC CCA CTT AAG TGG CTT CAC
***Bam*H1** Restriction site insertion (Forward primer)	TTA GCA **GGA TCC** ATG GAG ACT TTT CTA TAC ACC TCC GAA TCA GTG
***Bam*H1** Restriction site insertion (Reverse primer)	GAC TAT **GGA TCC** TTA AGC TTG AGG TTT TTC CCA CTT AAG TGG C
I193_REV	GAG CAC GGT GTG GAC CCG AAT GG
I193**A**_FWD	**GCC** TCC ACC CAG CAC GAC GAG
I193**V**_FWD	**GTC** TCC ACC CAG CAC GAC GAG ACT G
Y65_REV	GTC TAC GTT GGC CTT GGT GGT GAT CTC TCC
Y65**A**_FWD	**GCC** GAG AAG ATC GTC CGT AAC ACT TGC AGG
Y65**V**_FWD	**GTC** GAG AAG ATC GTC CGT AAC ACT TGC AGG AAC

2.3. Expression conditions and protein purification

E. coli BL21(DE3) competent cells were transformed using purified *pET14b-ksams*, similarly cell lines were created for each of the mutant constructs. Overnight cultures were prepared by subculturing single colonies in LB media containing ampicillin and chloramphenicol. Fresh LB (no antibiotics) media was inoculated using 1/1000th vol. overnight culture and grown at 37 ^{o}C until O.D.$_{600}$(0.7). Protein expression was induced with the addition of 0.2 mM IPTG for 12 h at 25 ^{o}C with gentle mixing. Cell lysis was achieved by subjecting pelleted cell cultures to freeze-thaw cycles and ultrasonic probe sonication. Lysate was clarified by high-speed centrifugation (5,000 x g for 30 min) prior to the addition of Ni-NTA affinity resin. Purification of the recombinant *A. koa* SAM-synthetase enzyme, designated hereafter as **KSAMS**, was achieved by methods and materials outlined in the HisLink Protein Purification System (Promega). Special considerations or customization of solutions were not deemed necessary.

Purified **KSAMS** was subject to buffer exchange using Amicon Ultra-15 Centrifugal Filters to a protein storage solution (100 mM Tris-HCl (pH 8.5), 50 mM KCl, 5 mM dithiothreitol (DTT), 1 mM EDTA, 50% glycerol) and concentrated to 5 mg/mL. Quantification of purified protein was achieved using the Nanodrop ND-1000 spectrophotometer (Thermo Scientific) and qualitative assessment of purity by SDS-PAGE. Small aliquots were prepared, snap frozen and stored at -80 ^{o}C.

Every mutant variant was expressed and purified using the described methods, designated as **KSAMS(Y65V)**, **KSAMS(Y65A)**, etc., no differences in expression levels or solubility were observed.

2.4. Enzyme assays and RP-HPLC methods

Optimal conditions (pH, KCl concentration, and temperature) were investigated for **KSAMS**. Unless otherwise stated assay composition and conditions are as follows: 100 mM Tris-HCl (pH 8.5 at 35 °C), 20 mM KCl, 10 mM $MgCl_2$, 5 mM DTT, 4 mM ATP, 4 mM L-methionine and performed in triplicate. Prior to the addition of substrate, DTT or enzyme, the pH of 2x conc. assay solutions was carefully adjusted with respect to the intended temperature. Necessary considerations were made to ensure accurate pH of heated assay solutions. The relative volume of solution and type of pH probe must be considered as a large glass pH probe must reach a temperature equilibrium with the solution, taking up to 10 min.

Discontinuous assays (100 µL) in a dry bath were started by the addition of 20 µL enzyme solution (final concentration: 0.1 mg. mL^{-1} enzyme). Assays were terminated at 5 min by the addition of an equal volume of ice cold 0.4 M o-phosphoric acid (OPA). Temperature (25, 35, 40, 45, 50, 55, 60 °C), pH (5.5, 6, 7, 8, 8.5, 9, 10.5, 11.5) and KCl concentration (0.02, 0.2, 0.5, 1, 1.5, 2, 3 M). Reversed-phase HPLC analysis was achieved using a C18 column (Phenomenex C18; 5 µm; 4.6 × 250 mm) and a completely aqueous mobile phase of 0.04 M OPA (isocratic elution, 1 mL. min^{-1}). SAM was measured at λ = 256 nm, retention time of 2.75 min (Fig. 3) A standard curve was constructed using pure SAM (New England Biosciences) and used for determining kinetic values.

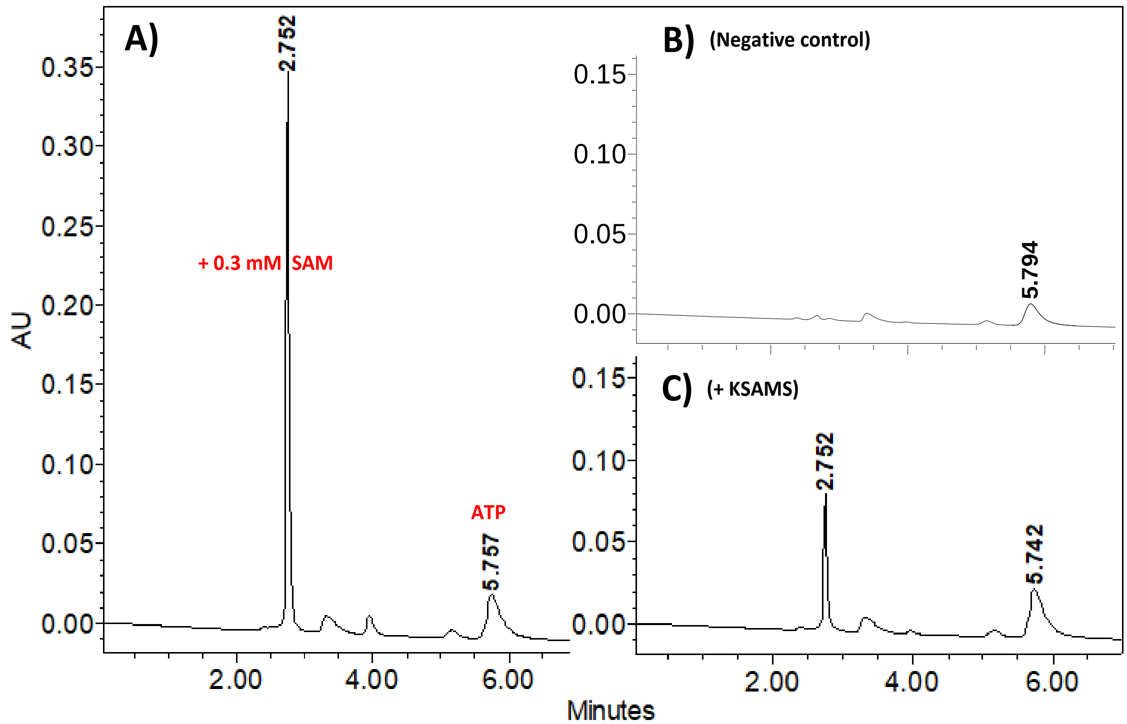

Figure 3: HPLC chromatograms depicting the retention times of analytes measured at 256 nm. Enzyme assay solutions, described and terminated as described in "**MATERIALS AND METHODS, 2.4**", were spiked with 0.3 mM purified SAM **(A)**, started with heat-inactivated **KSAMS (B)** or started with active **KSAMS (C)**. Substrate concentration: 4 mM ATP, 4 mM L-methionine, final concentration enzyme: 0.05 mg. mL^{-1} **KSAMS**, conditions: 35 °C for 60 min.

2.5. Enzyme kinetics and total SAM production: KSAMS, mutants and organic solvent assays

Continuous time course assays (100 µL) were performed under optimal assay conditions (100mM Tris-HCl pH 8.5, 50 °C, 20 mM KCl, 10 mM $MgCl_2$ and 5 mM DTT). Highly alkaline solutions and heat rapidly degrades the product SAM, so optimal conditions are defined as previously determined by Carrillo and Borthakur (2022). The combined effect of temperature and pH on SAM degradation suggests pH 8.5 / 50 °C as optimal. The assay solution master mix was adjusted to pH 8.5 at the optimal temperature of 50 °C prior to the addition of any substrate, DTT, or enzyme. Assays containing both ATP and L-methionine in equal concentrations of 0.4, 0.8, 2.4, 4.0, and 10 mM were used to determine kinetic constants for **KSAMS**. Upon reaching temperature, assays were started by the addition of 20 μL enzyme solution (final concentration 0.1 mg. mL^{-1} enzyme). Aliquots were transferred to ice-chilled tubes at 5 and 60 min, followed by complete termination by the addition of an equal volume of 0.4 M o-phosphoric acid. Intermediate quenching on ice was necessary to minimize error when pipetting hot solutions. Velocity and K_{cat} were calculated from 5 min measurements and total SAM production from 60 min measurements. Mutants were investigated using similar methods.

The addition of six organic solvents (ß-mercaptoethanol, methanol, acetonitrile, formamide, dimethylformamide, dimethylsulfoxide) were investigated at 5%, 10%, 25% and 40%. Supplementing assays with low concentration urea (500 mM) was investigated as well. Continuous time course assays (100 μL) were conducted as previously described; 4 mM ATP/L-met, measured at 5 min and 60 min. Assays were performed at 35 °C and were prepared using a 4x conc. assay solution to accommodate for 40% organic solvent volume. Higher concentrations of acetonitrile were omitted due to phase separation.

2.6. Modeling and sequence analysis

The crystal structure of an Arabidopsis SAM-synthetase (PDB ID:6VCX, Sekula et al., 2020) provided a template for modeling the *A. koa* SAM-synthetase in SWISS-

MODEL (Waterhouse et al., 2008). The web application POLYVIEW-3D (Porollo and Meller, 2007) was used to color and highlight select residues.

A sequence alignment for performed using CLUSTAL-OMEGA (Sievers et al., 2011) for SAM-synthetases from *E. coli,* giant leucaena and *A. koa*. Conserved regions, as indicated by Sekula et al. (2020), are colored similarly in the 3d model and sequence alignment (gate-loop region in blue, ATP binding site in yellow, a proposed regulatory site in green, strict conservation of active site and interior residues in red).

Additional models were made using UCSF ChimeraX (Pettersen et al., 2021) to illustrate structural changes due to mutagenesis and to compare plant and nonplant SAM-synthetases. Species name and PDB numbers of the structures used are: (from bacteria: *E. coli* (1XRA), *Burkholderia pseudomallei* (3IML), *Neisseria gonorrhoeae* (5T8T), *Lactiplantibacillus plantarum* (7R3B). From eukarya: *Entamoeba histolytica* (3SO4), *Cryptosporidium parvum* (6C07), *Medicago truncatula* (6VCW), *Arabidopsis thaliana* (6VD2), *Homo sapiens* (2P02), *Rattus norvegicus* (1O90)).

Part III: 5'-methylthioadenosine nucleosidase from giant leucaena

3.1. Cloning and expression of an MTA-nucleosidase from giant leucaena

The giant leucaena transcriptome (Ishihara et al., 2016) was screened for sequences matching the *Prosopis alba* MTA-nucleosidase (ACCESSION: XM_028909832), yielding 16 hits. The 5' and 3' ends of the coding sequence were identified by transcriptome reads: GDSA01070893, GDRZ01021632, GDSA01081242, GDRZ01245256, GDSA01177384, and GDSA01172186. Primers were designed and used to amplify the full coding sequence from root cDNA with Q5 High-Fidelity DNA Polymerase. Sanger sequencing (Advanced Studies in Genomics, Proteomics and Bioinformatics) confirmed an MTA-nucleosidase, referred to hereafter as *mtan* (GENBANK#: OR995291). The addition of restriction digest sites produced the insert (*NcoI)-mtan-(XhoI)* and was cloned into the expression vector *pet39b* in frame following a DsbA secretion tag. Thus, the recombinant giant leucaena MTA-nucleosidase, hereafter referred to as **LMTAN**, was secreted into the cell periplasm as the fusion protein DsbA-**LMTAN**. Following *Escherichia coli* DH5-alpha transformation and sequence reverification of clones, the purified plasmid was used to transform the *E. coli* expression line Origami B(DE3). Transformed colonies were selected for expression testing, subcultured and saved as glycerol stocks to be stored at -80 C°.

5 mL of LB (35 µg. μL^{-1} kanamycin) was inoculated from glycerol cell stocks and grown overnight in a 37 C° shaker (200 rpm). The overnight culture (5 mL) was added to 1 L of sterile LB (no antibiotics) and grown in a 37 C° shaker (200 rpm). Upon reaching OD_{600} 0.5, expression was induced using 0.8 mM IPTG and proceeded in a 37 C° shaker (200 rpm) for 5 hours. Preliminary testing suggested improved expression of DsbA-**LMTAN** when induced at early log-phase and at 37 C°.

Cells were pelleted by centrifugation (5,000 x g, 20 min) and maintained at 4 C°. Various protocols for osmotic shock and purification of periplasmic proteins emphasize keeping equipment, solutions and cells at 4 C° (Neu and Heppel, 1965). Therefore, all steps, centrifugation and resuspension, were performed on ice or below 10 C°. A sucrose solution of 500 mM was used to resuspend the cell pellet in 1/10th the original culture volume. The resuspension was agitated on ice for 90 min. It is worthy to note that pipetting, even gently pipetting, can result in cell lysis at this stage and should be avoided entirely. Cells were pelleted (5,000 x g, 30 min) and the supernatant discarded. The cell pellet was respun briefly (5,000 x g, 2 min) to remove any remaining sucrose liquid by micropipette. MilliQ water, equal to 1/10th the original culture volume, was used to resuspend the cell pellet and gently agitated on ice for 30 min. The periplasmic extract was separated by centrifugation (5,000 x g, 30 min) and the supernatant retained. The periplasmic extract containing recombinant DsbA-**LMTAN** was concentrated to 10 mg. ml^{-1} protein, buffered/stored in 50 mM sodium phosphate (pH 8.0, 5 mM DTT, 20% glycerol) and stored at -80 C°.

Initial testing of the periplasmic extract indicated strong MTA-nucleosidase activity; however further purification was not possible. The recombinant protein DsbA-**LMTAN** features an internal/hidden histidine-tag and removal of the DsbA-tag by thrombin digestion was unsuccessful. Regardless, the optimal pH and temperature for MTA-nucleosidase activity was determined and the periplasmic extract used to enhance LNAS activity.

3.2. Discontinuous assays and optimal conditions for DsbA-LMTAN

Discontinuous DsbA-**LMTAN** assays were performed in 100 mM sodium phosphate (pH 4.0 - 8.5), CHES (pH 8.5 – 9.5) and Tris (pH 8.5) buffers. Activity in phosphate buffer (pH 7.0) was evaluated across a range of temperatures (25 - 70°C).

Assays were performed in triplicate as follows: total volume 50 µL (50 µg. mL^{-1} periplasmic extract), 100 µM MTA, 15 min duration. Assays were started by the gentle pipetting of substrate and diluted enzyme; termination of assays was achieved by the addition of eq. vol. (50 µL) of ice cold 0.4 M OPA. The hydrolysis of MTA was measured by reversed-phase HPLC (5 µL injection volume), using a C-18 column (Phenomenex Synergi 4 µm Hydro-RP 80 Å, 150 x 2 mm) and by a mobile phase of 0.04 M OPA (7% acetonitrile, isocratic elution, 0.25 mL. min^{-1}). MTA was measured at λ = 256 nm, retention time of 5.9 min.

Part IV: nicotianamine synthase from giant leucaena

4.1. 5'-RLM-RACE to obtain full-length NA-synthase mRNA

Incomplete RNA sequences (GENBANK ACCESSION No. GDRZ01213130, GDRZ01213129) for a NA-synthase were identified in the giant leucaena K636 transcriptome data (Ishihara et al., 2016b). Both RNA sequences encoded for an identical NA-synthase and highly similar ~250 bp 3'-untranslated region. The FirstChoice RLM-RACE Kit (Thermo Fisher) was used to obtain the 5'-untranslated region of a NA-synthase. A standard RNA ligation reaction (10 µg total RNA), cDNA synthesis reagents and conventional PCR methods were used to amplify the complete NA-synthase transcript. Sanger sequencing services (Advanced Studies in Genomics, Proteomics and Bioinformatics (ASGPB), University of Hawaiʻi at Manoa) of the PCR product confirmed the identity of a NA-synthase transcript and new primers were designed to isolate the complete NA-synthase coding sequence, designated hereafter as *nas,* for cloning.

4.2. Construction of expression vector pET14b(nas)

Q5 High-Fidelity Polymerase (New England Biolabs) was used to amplify *nas* from cDNA and the identity of the gel-purified amplicon was confirmed by sequencing services. The IDT-DNA Codon Optimization Tool detected no codon bias for the expression of protein by *E. coli*. Primers were designed with flanking *Nde*1 and *Bam*H1 restriction sites and conventional PCR was used to generate a *nas* amplicon suitable for cloning. Purified PCR product and the T_7-expression vector *pet14b* (Novagen) were digested and combined to construct *pET14b-nas* by overnight ligation. The ligation reaction was used directly to transform *E. coli* DH5-α competent cells and clones were selected from ampicillin plates for plasmid purification and sequencing. Sequence verified *pET14b-nas* was subsequently used to transform *E. coli* BL21(DE3) cells for protein expression.

4.3. Production and purification of soluble recombinant enzyme

Initial testing of recombinant giant leucaena NA-synthase, designated hereafter as **LNAS**, resulted in suppressed expression levels and inclusion body formation. Almost no soluble recombinant enzyme could be recovered using standard expression conditions or common solutions to insoluble protein production (e.g. reducing expression temperature, reducing IPTG concentration, synthetic minimal media).

Instead, modified expression media and heat-shocking *E. coli* cultures were investigated for their effect on improving soluble protein expression. Three types of LB expression media were used: Standard LB broth ("*low-salt*"), LB broth "*med-salt*" (+250 mM NaCl, +250 mM sorbitol) and LB broth "*high-salt*" (+500 mM NaCl, +500 mM sorbitol).

Overnight cultures of *E. coli* BL21(DE3) *pet14b-nas* were grown from glycerol stocks and 5 mL was used to inoculate 1 L of expression media. Flasks were agitated at 37 ˚C until reaching O.D.$_{600}$ (0.7). Cultures were subjected to heat shock at this time (20 min in 48˚C water bath) and placed briefly on ice to reach room temperature. Protein expression was induced by 0.2 mM IPTG and allowed to proceed at 25 ˚C for 12 hours with vigorous shaking (240 rpm). Cells were pelleted by centrifugation and stored at -80 ˚C.

Purification was achieved by methods and materials outlined in the HisLink Protein Purification System (Promega). Cell lysis was achieved by resuspending pellets in 50 mL binding buffer, sonication on ice and clarification by high-speed centrifugation. 100 µL of resin was used per purification, incubated for 30 min and collected by gravity flow column. The total amount of purified LNAS from each liter of culture (*low-, med- and high-salt*) was eluted using 500 mM imidazole and concentrated to 200 µL using Amicon Ultra-0.5 Centrifugal Filters prior to analysis by SDS-PAGE. The relative purity and quantity of **LNAS** was observed by SDS-PAGE to observe effects on soluble expression.

4.4. Purification of denatured enzyme and optimization of refolding procedures

The amount of soluble **LNAS** recovered was not sufficient for activity studies, thus denaturing conditions and subsequent renaturation procedures were developed. The addition of 8 M urea to buffers and purification of **LNAS** was performed according to procedures outlined in the HisLink Protein Purification System (Promega). Elution from the resin was achieved using 400 mM imidazole and fractions containing **LNAS** were concentrated using Amicon Ultra-15 Centrifugal Filters to 1 mg. mL^{-1}.

Optimal refolding conditions were determined by small-scale rapid dilution of purified denatured **LNAS**, fifteen different refolding solutions were tested. Detailed procedure for screening can be found in the QuickFold™ Protein Refolding Kit manual (Athena Enzyme Systems); the composition of refolding solutions #1-15 are included for reference (Fig. 4). To evaluate the effect that substrate binding has on refolding efficiency, refolding solutions #1-15 were supplemented with either 20 μM SAM. Pure denatured **LNAS** was diluted with 8 M urea H_2O to a protein concentration of 0.2 mg. mL^{-1} prior to refolding procedures. Each dilution consisted of the slow-dropwise addition of 35 μL **LNAS** (25 °C) to 465 μL of selected refolding solution (<10 °C while gently vortexed). The resulting solution was kept on ice for 1 h, clarified by high-speed centrifugation and the soluble fraction analyzed by reversed-phase HPLC (Phenomenex C18; 5 μm; 4.6 × 250 mm, isocratic elution, 0.8 mL. min^{-1}, 50 mM ammonium acetate, pH 8.5). Detection of soluble **LNAS** (280 nm) was used to determine relative efficiency of enzyme renaturation.

QuickFold™ Protein Refolding Buffer Formulation			
Component	**Formulation after Preparation (Addition of DTT, GSH, and GSSH)**	**DTT**	**GSH/GSSH**
Buffer 1	50 mM MES pH 6.0, 9.6 mM NaCl, 0.4 mM KCl, 2 mM $MgCl_2$, 2 mM $CaCl_2$, 0.75 M Guanidine HCl, 0.5% Triton X-100, 0.1 mM DTT	●	
Buffer 2	50 mM MES pH 6.0, 9.6 mM NaCl, 0.4 mM KCl, 2 mM $MgCl_2$, 2 mM $CaCl_2$, 0.5 M arginine, 0.05% polyethylene glycol 3,550, 0.1 mM GSH, 0.01 mM GSSH		●
Buffer 3	50 mM MES pH 6.0, 9.6 mM NaCl, 0.4 mM KCl, 1 mM EDTA, 0.4 M sucrose, 0.75 M Guanidine HCl, 0.5% Triton X-100, 0.05% polyethylene glycol 3,550, 0.1 mM DTT	●	
Buffer 4	50 mM MES pH 6.0, 240 mM NaCl, 10 mM KCl, 2 mM $MgCl_2$, 2 mM $CaCl_2$, 0.5 M arginine, 0.5% Triton X-100, 0.1 mM GSH, 0.01 mM GSSH		●
Buffer 5	50 mM MES pH 6.0, 240 mM NaCl, 10 mM KCl, 1 mM EDTA, 0.4 M sucrose, 0.75 M Guanidine HCl, 0.1 mM DTT	●	
Buffer 6	50 mM MES pH 6.0, 240 mM NaCl, 10 mM KCl, 1 mM EDTA, 0.5 M arginine, 0.4 M sucrose, 0.5% Triton X-100, 0.05% polyethylene glycol 3,550, 0.1 mM GSH, 0.01 mM GSSH		●
Buffer 7	50 mM MES pH 6.0, 240 mM NaCl, 10 mM KCl, 2 mM $MgCl_2$, 2 mM $CaCl_2$, 0.75 M Guanidine HCl, 0.05% polyethylene glycol 3,550, 0.1 mM DTT	●	
Buffer 8	50 mM Tris-Cl pH 8.5, 9.6 mM NaCl, 0.4 mM KCl, 2 mM $MgCl_2$, 2 mM $CaCl_2$, 0.4 M sucrose, 0.5% Triton X-100, 0.05% polyethylene glycol 3,550, 0.1 mM GSH, 0.01 mM GSSH		●
Buffer 9	50 mM Tris-Cl pH 8.5, 9.6 mM NaCl, 0.4 mM KCl, 1 mM EDTA, 0.5 M arginine, 0.75 M Guanidine HCl, 0.05% polyethylene glycol 3,550, 0.1 mM DTT	●	
Buffer 10	50 mM Tris-Cl pH 8.5, 9.6 mM NaCl, 0.4 mM KCl, 2 mM $MgCl_2$, 2 mM $CaCl_2$, 0.5 M arginine, 0.4 M sucrose, 0.75 M Guanidine HCl, 0.1 mM GSH, 0.01 mM GSSH		●
Buffer 11	50 mM Tris-Cl pH 8.5, 9.6 mM NaCl, 0.4 mM KCl, 1 mM EDTA, 0.5% Triton X-100, 0.1 mM DTT	●	
Buffer 12	50 mM Tris-Cl pH 8.5, 240 mM NaCl, 10 mM KCl, 1 mM EDTA, 0.05% polyethylene glycol 3,550, 0.1 mM GSH, 0.01 mM GSSH		●
Buffer 13	50 mM Tris-Cl pH 8.5, 240 mM NaCl, 10 mM KCl, 1 mM EDTA, 0.5 M arginine, 0.75 M Guanidine HCl, 0.5% Triton X-100, 0.1 mM DTT	●	
Buffer 14	50 mM Tris-Cl pH 8.5, 240 mM NaCl, 10 mM KCl, 2 mM $MgCl_2$, 2 mM $CaCl_2$, 0.5 M arginine, 0.4 M sucrose, 0.75 M Guanidine HCl, 0.5% Triton X-100, 0.05% polyethylene glycol 3,550, 0.1 mM GSH, 0.01 mM GSSH		●
Buffer 15	50 mM Tris-Cl pH 8.5, 240 mM NaCl, 10 mM KCl, 2 mM $MgCl_2$, 2 mM $CaCl_2$, 0.4 M sucrose, 0.1 mM DTT	●	

Figure 4: Composition of fifteen refolding buffers from the QuickFold™ Protein Refolding Kit manual from Athena Enzyme Systems. The refolding procedure was not followed in this manual, please see 2.4. Optimization of refolding procedures for details.

Optimal refolding conditions were selected and scaled up to produce similar yields of refolded **LNAS** (50 mL refolding solution #15 + 4 mL 0.2 mg. mL^{-1} denatured **LNAS**). The post-dilution solution was clarified by high-speed centrifugation, dialyzed against (50 mM Tris-Cl pH 9.0, 50 mM KCl ,10 mM dithiothreitol, 10% glycerol), and concentrated to 0.8 mg. mL^{-1} using Amicon Ultra-15 Centrifugal Filters. The filtrate was saved from protein concentration for enzyme assay negative control experiments. Aliquots of 50 µL were prepared, snap frozen and stored at -80 °C. Each 50 µL aliquot (0.8 mg. mL^{-1} **LNAS**) was required for a single assay.

4.5. Two-enzyme continuous assays and HPLC method

High-pressure liquid chromatography (HPLC) was performed using a Waters Alliance 2696 and 996 PDA detector. **LNAS** assays were designed to satisfy two essential requirements, 1) a high concentration of **LNAS** is required for measurable activity and 2) buffer composition and conditions must also permit the activity of recombinant SAM-synthetase (Carrillo and Borthakur, 2022). 50 µL aliquots of refolded **LNAS** and 50 µL of an "activating" solution were mixed to start enzyme assays. Negative controls were prepared using the **LNAS**-free filtrate (saved from concentrating the dialysate). The "activating" solution (100mM Tris-HCl, pH 9.0, 200 mM KCl, 10 mM $MgCl_2$ and 10 mM DTT) was supplemented with 25 µM commercial SAM (New England Biolabs) or components for enzymatic synthesis of SAM (25 µM L-methionine, 25 µM ATP, 50 ng recombinant SAM-synthetase). Additional supplementation of two-enzyme assays (recombinant SAM-synthetase + **LNAS**) were performed containing either alternative substrates (40 uM homoserine or azetidine-2-carboxylic acid) or organic solvents (5% acetonitrile, 5% methanol) to evaluate the effect on **LNAS** activity.

The rationale for these experimental substrates/additives is explained in the discussion section.

Continuous-enzyme assays (200 µL, 25 °C), performed in triplicate, were analyzed by reversed-phase HPLC (Phenomenex C18; 5 µm; 4.6 × 250 mm, isocratic elution, 1 mL. min^{-1}, 0.02 M o-phosphoric acid) by repeated injections (10 µL every 2 h) over the course of 18 h. A standard curve was constructed using commercial SAM (λ = 260 nm, retention time of 2.4 min) and substrate depletion was used to quantify **LNAS** activity.

4.6. MTA degradation on LNAS activity and three-enzyme continuous assays

Two sets of **LNAS** assays were designed to distinguish the effects that DsbA-**LMTAN** and/or **LSAMS** has on **LNAS** activity. Freshly purified **LSAMS** and **LNAS** were required to exclude the presence of Tris in all solutions, which strongly inhibits the activity of DsbA-**LMTAN**.

To provide a precise starting amount of enzymatically produced SAM, the multi-enzyme assays were broken up into two stages.

1) **Enzymatic production of SAM**: The "activating" solution (100mM CHES (pH 9.0) 5 mM $MgCl_2$, 40 mM KCl, 5 mM DTT) was supplemented with components for enzymatic synthesis of SAM (200 µg. mL^{-1} **LSAMS**, 500 µM L-methionine, 500 µM ATP) and allowed to proceed to near completion. **LSAMS** activity and

future SAM production was prevented by adjusting the “activating” solution to 10 mM EDTA. This source of enzymatically produced SAM was analyzed by HPLC and diluted to produce a solution of 400 μM SAM.

2) **NA synthase activation:** An enzyme solution containing 0.30 mg. mL^{-1} refolded **LNAS** and 200 μg. mL^{-1} DsbA-**LMTAN** periplasmic extract was prepared in 100mM CHES (pH 9.0).

When commercial SAM substrate was to be used instead, **LSAMS**, ATP and L-methionine were omitted from the “activating” solution and instead adjusted to contain 200 μM commercial SAM (New England Biolabs). 50 μL from either source, containing the substrate or (**LNAS** + DsbA-**MTAN**) were mixed buy gentle pipetting to start the assay. Negative controls were prepared using the **LNAS**-free filtrate (saved from centrifugal filter devices). Preliminary testing indicated that assays containing commercial SAM were not highly active, especially compared to three-enzyme assays (**LSAMS** + **LNAS** + DsbA-**LMTAN**). Therefore, assays using commercial SAM consisted of a final concentration of 100 μM SAM and assays containing enzymatic SAM received 200 μM.

Continuous-enzyme assays (100 μL, 25 °C), performed in triplicate, were analyzed by reversed-phase HPLC (Phenomenex C18; 5 μm; 4.6 × 250 mm, isocratic elution, 1 mL. min^{-1}, 0.04 M o-phosphoric acid) by repeated injections (5 μL every 60 min) over the course of 6 h. A standard curve was constructed using commercial SAM (λ = 256 nm, retention time of 2.4 min) and substrate depletion was used to quantify **LNAS** activity.

4.7. Structural and sequence analysis of LNAS and other NA-synthases

The giant leucaena NA-synthase amino acid sequence was used to collect related sequences using the NCBI BLAST program. Multiple sequence alignment of NA-synthases (4 sequences from plant, 3 from fungi, 1 from bacteria) and NA-synthase-like enzymes (MtNAS from *Methanothermobacter thermautotrophicus*) and CntL (from *Staphylococcus aureus, Psuedomonas aeruginosa* and *Yersinia pestis)* was constructed using CLUSTAL-OMEGA (Sievers et al., 2011).

Structural studies and X-ray crystallography of thermo-NA-synthase (MtNAS) (Dreyfus et al., 2009, 2011) served as a template structure to model the giant leucaena NA-synthase. The crystal structure of NA-synthases, from plant or otherwise, has yet to be determined. SWISS-MODEL (Waterhouse et al., 2008) was used for modelling and the web application POLYVIEW-3D (Porollo and Meller, 2007) was used to color and highlight select residues.

Part V: Gene expression analysis following iron fertilization of giant leucaena seedlings

5.1. Plant growth conditions and iron fertilization methods

Giant leucaena (*Leucaena leucocephala* subsp *glabrata*, cultivar K636) seeds were obtained from a fully grown tree at the University of Hawai‘i Waimanalo Research Station (O‘ahu, Hawai‘i). Seeds were scarified for 1 min using concentrated sulfuric acid, rinsed and planted into 4” pots containing well-draining potting soil (50% perlite : 50% Miracle-Gro potting mix). Indoor growth conditions are as follows: 25 °C, 16/8 light cycle, fluorescent lighting (Four 40W 5000K bulbs). When plants reached 4” in height, approximately 2 months, they were organized into experimental groups and subjected to iron treatments. Aside from slow-release fertilizer (N-P-K : 21-7-14) supplied in Miracle-Gro potting mix, no other fertilizers were used. The four treatment groups (three biological replicates per group) are as follows:

Group #1: Negative control

Group #2: Foliar spray only

Group #3: Soil application only

Group #4: Both spray and soil application

Preliminary tests were performed to determine the highest concentration of iron which may be used to treat giant leucaena plants. Solutions containing 10 mM Fe-DTPA (+0.05% Triton X-100 surfactant) produced visible toxic effects and leaf necrosis after 2 days. Therefore, a solution of 5 mM Fe-DTPA (+0.05% Triton X-100 surfactant) was prepared and 100 mL applied to soil and/or sprayed thoroughly on and under leaves. The concentration of Triton x-100, 0.05%, was the lowest concentration which was observed to break surface tension and allow the foliar spray to effectively stick to leaves. Paper towels were used to block soil for plants in Group #2. Plants which do not receive iron were treated identically by foliar spray or soil application using water containing 0.05% Triton X-100. Treatment commenced at the end of the 16-hour light cycle and plants were harvested in the middle of the proceeding light cycle; the total exposure time of 16-hours (8-hours dark period and 8-hours of light period). The root mass was gently removed from pot, cleaned of soil and briefly dried. The plant was cut into three sections and immediately submerged in a mortar filled with liquid nitrogen. The base of the stem, approximately 1 cm above the uppermost root development, was discarded. Root tissue and aerial tissue were separately ground into a fine powder and stored at -80 °C.

5.2. cDNA synthesis and real-time PCR

Total RNA extraction was performed using the Qiagen RNeasy Plant Mini kit, using the provided “RLC” lysis buffer for root tissue. Identical procedures were performed for leaf tissue, except a non-kit lysis reagent was used. Macerated leucaena leaf tissue produced a highly viscous lysate and RNA yield was poor using Qiagen kit reagents. Fruit-Mate (Takara Biosciences), recommended for woody plant species (Ishihara et al., 2016a), improved RNA yield when used in place of kit lysis reagents. Rapid freeze-thaw cycles (3 times), between liquid nitrogen (2 min) and 80 °C water bath (5 min) was effective at lysing leaf tissue. DNAse treatment and RNA clean-up, as outlined in the Qiagen RNeasy Handbook, were performed prior to final quantification by Nanodrop ND-1000 spectrophotometer. Complementary DNA was synthesized using the SensiFAST cDNA synthesis kit, heat-terminated and diluted with low-EDTA Tris-buffer (10 mM Tris-HCl (pH 8.0) + 0.1 mM EDTA) to stock solutions of 15 ng. µL-1 cDNA. Purified cDNA/RNA stocks were stored at -80 °C.

The giant leucaena transcriptome archive (Ishihara et al., 2016b) was screened for genes associated with metal transport, SAM-related pathways and stress related genes. Primers were designed to amplify 100-120bp of the coding sequence 3'-terminus for each target gene. PCR specificity was confirmed by agarose gel electrophoresis and melting curve analysis. Nineteen target genes were successfully amplified and selected for real-time PCR analysis.

All reactions were performed using the StepOne Real-time PCR system (Applied Biosystems) SensiFAST SYBR Hi-ROX mix. Reaction details, PCR conditions and target genes details (accession numbers, primer sequence, etc.) are provided below (Table 3, 4). Recommended conditions by SensiFAST and a final concentration of 3 ng. μL-1 cDNA (10 μL reaction) produced a desirable range of Ct-values ≤ 30. Relative gene expression changes between untreated (Group #1) and iron-induced treatments were normalized using elongation factor-1α (ef1α) as an internal reference gene. Multiple reference genes for giant leucaena were previously investigated by Honda and Borthakur (2020) and ef1α produced consistent Ct-values for all groups in this study. Relative quantification of transcripts (the 2−ΔΔCt method) and data analysis methods were performed as described by Livak and Schmittgen (2001). Technical replicates (n=3) were averaged, per biological replicate, thus variance in gene expression change (Fig. 30) depicts the standard deviation between biological replicates.

Table 3: Complete details for the nineteen genes evaluated by real-time PCR.

GENE	FORWARD PRIMER	REVERSE PRIMER	ACCESSION
methionine synthase	AGC TTG ATA TTG ATG TCC TTG TAC ATG GGG	ATC CAT AAG ATT GCA CCC ACC CAT TAA CG	GDRZ01176135
SAM-synthetase	GAG GGG TGG CCA TAG G	TTA AGC TTG AGG CTT CTC CCA CTT GAG T	GDRZ01071457
nicotianamine synthase	CAT TCT TGT ACC CTA TTG TGG AGG	CTA AGC CAT AGG CTT GCG AAG AAG AAG AA	GDRZ01190472
MTA-nucleosidase	CAG AAG AAT TCC TTC AGA ATT TGG C	TCA AAG TTC AGA TAG GCA CTG TC	GDRZ01230955
SAM-decarboxylase	GAC TCT GTT TAC ACC CTC GAG ATG TGC	CTT TCG GAT TCC AGA TTT CGA GGT CAT GT	GDRZ01219250
spermidine synthase	CGG CAT TCT TCT GTC GAG AAG ATA GAC ATT TG	TGT CAC ACG TGG ATC ATC AAA CCC TAC	GDRZ01216731
spermine synthase	TGA ATG TGC TTA CCA GGA GAT GAT AGC TCA	ACG GGA TAC TTC CCT CAG AAC CC	GDRZ01136447
ACC-synthase	AGT TCC TGG GTT TAG AGT TGG AAT CAT CTA CTC	CGC AAG AAG ATT CTG GGT TTG TGT CG	GDRZ01241016
ACC-oxidase	ATG GAG AAG GTG AAG CAT CTG GTA AAT ACA TAC TTC	CGT GTC AGA GAT GGA GAC AGA CTT GTT C	GDRZ01231262
catalase	ATG GAT CCC TAC AAG CAT CGA CCA TC	GGA CCT CTA GAT CCA AGC GTC AGA G	GDRZ01203232
γ-glutamylcysteine synthetase	TGG TTT CCA GCC AAA GTG GGG	GTT CTG AAC ATC ATG TTA AGT CCA AGG GAA CC	GDRZ01216397
glutathione synthase	GAG ATC AGG AAG CGT TCC TGG C	TTC ATT GAA TAT TGG GGC TAA CTC ACA CGC	GDRZ01125524
glutathione reductase	ACG GCA GAA AAA AGT TTT ACG GGG ATT TG	TTG GGG AGA TTC CTC GAC ATG AAA CTC	GDRZ01146332
homophytochelatin synthase	AGT TGA AGC CTT TCG TGC AAA TCA AAG C	TTG TTT GAG AGC AGC TCT GTG GTA TGA AG	GDRZ01150333
FRO2	TCA TTA CCC TCC TCG TTT GGT CTC TTT CT	TGC CAC ACT TTC TCG CCG GAT T	GDRZ01178233
IRT2	TCG CCG CTT TGG CAT TTC ATC A	AAG CAC ATA TAA GCC GTG GTT CCA A	GDSA01150373
YSL6	CAC CTG ATG GTC CCT ATA AAG TAC CCT	GCA ATG CTT TGG AAG CCC AGA GA	GDRZ01179279
YSL8	TAC CAA AGA ACT GCC TCC TGC TGT G	CAC CCT CTT TCA CCC ATC AGG TCT TT	GDSA01147456
mimosinase	TTC TCA ACC CTC TCG TTT CTT C	CAT GGG CTA TCC TGG CTA TTT	GDSA01216745
ef1α	AAG CTG ACT GTG CTGTCC TCA TCA	GCT TCA CAC CAA GGG TGA AAG CAA	GDSA01219315

Table 4: Real-time PCR conditions and reaction details. The recommended reaction conditions by SensiFAST SYBR Hi-ROX mix were used.

Final concentration				
Forward primer	250 nM			
Reverse primer	250 nM			
SensiFAST SYBR Hi-ROX mix	1x			
cDNA	3 ng. µL-1			
Final Reaction volume	10 µL			
Run conditions for 2-step cycling				
Cycles	**Temp. (°C)**		**Time**	
1	95		2 min	
40	95		5 sec	
	55		20 sec	
1 (Melt curve analysis)	55 + 0.3 min^{-1}		---	

~~~~~~~~~~~~~~ RESULTS ~~~~~~~~~~~~~~

Divided into six parts, as in methodology.

***Part I:** SAM-synthetase from giant leucaena*

***Part II:** SAM-synthetase from Acacia koa and mutagenesis experiments*

***Part III:** 5'-methylthioadenosine nucleosidase from giant leucaena*

***Part IV:** nicotianamine synthase from giant leucaena*

***Part V:** Gene expression analysis following iron fertilization of giant leucaena seedlings*

Part I: SAM-synthetase from giant leucaena

1.1. Characterization of giant leucaena SAM-synthetase

The identified giant leucaena SAM-synthetase transcript consists of a 5'-untranslated region of 133 nucleotides and a 3'-untranslated region of 121 bp. The full mRNA transcript of giant leucaena SAM-synthetase (GENBANK ACCESSION No. MZ419855) contains a 1179 bp coding sequence for a 43.2 kDa protein. Purified recombinant enzyme (**LSAMS**) was observed by NATIVE-PAGE analysis to form a homodimer under reducing and nonreducing conditions (results not shown). Strong hydrophobic forces in homodimer formation were previously demonstrated using a recombinant bacterial SAM-synthetase (Kamarthapu et al., 2008). Plant SAM-synthetases have not been characterized to the extent of bacterial variants however physical and structural properties, such as size and dimerization, agrees with previous reports (Li et al., 2013; Mathur et al., 1993).

1.2. Sequence and structure-based analysis

The location and function of these enzyme sites were inferred from the Arabidopsis model (92% similarity) and structural analysis by Sekula et al., 2020, though all residues described and illustrated in this section are based on the giant leucaena SAM-synthetase sequence. Two active sites are formed upon assembly of the native homodimeric enzyme, however conserved regions are best visualized by the monomer model (Fig. 5). Twelve notable residues (Fig 5.A and inserted table) were identified in the giant leucaena sequence which otherwise appear as conserved in most plant SAM-synthetases. These residues may have significance in effecting thermoalkaliphilic properties of SAM-synthetases, though until other plant variants are assayed this is pure speculation. Conserved regions and residues may be viewed in greater detail within the multienzyme sequence alignment (Fig. 6). The highly conserved "gate-loop" motif (region **Q98-Q123**) stabilizes L-methionine, encloses the active site and produces a positively charged region exterior to the active site. The **K227-Y284** region appears as strictly conserved in all plant SAM-synthetases and includes five amino acids (**G236-I240**) which are directly involved in binding the adenosine moiety of ATP. The suspected regulatory site (formed by residues **F4, F6, F127, N178, G261, W262, G263, A264, R301, L303, F319, D321, Y323, G324, E330,**), is highly conserved and is accessible as a small pocket near the polypeptide termini. Sekula et al. (2020) observed a molecule of polyethylene glycol (PEG-8) bound to this site and proposed regulation by spermidine (K_d = 654 nM ± 256 nM). However, this dissertation suggests that spermidine, spermine or nicotianamine have no apparent regulatory effect in vitro.

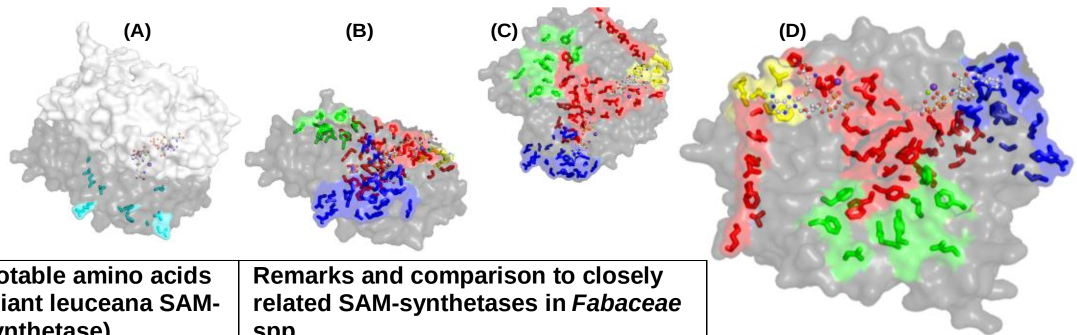

Notable amino acids (giant leuceana SAM-synthetase)	Remarks and comparison to closely related SAM-synthetases in *Fabaceae* spp.
H359	Not observed in plant or *Fabaceae* spp. Unique to **LSAMS** and few closely related legume species.
A162	
I348	Methionine conserved in other *Fabaceae* spp.
F111→L	Gate-loop region (Q98→Q123), the entrance to active site. Conserved residues observed in Fabaceae spp. are indicated by arrow.
R114→P, N, Q, L, K	
V118→I	
V23	Isoleucine conserved in other *Fabaceae* spp.
V285 & A286	Isoleucine and valine conserved in other *Fabaceae* spp.
A61, N62, V63	High variability in these three amino acids among plant SAM-synthetases.

Figure 5: (A) Homodimeric assembly shown with cyan-colored residues to highlight notable sites in giant leucaena SAM-synthetase. Details for these twelve notable residues are compiled in the above table. Multiple views of the monomeric giant leucaena SAM-synthase **(B)** monomer, **(C)** monomer (top view), **(D)** monomer (enlarged top view of regulatory site). The enzyme active site and conserved residues are clearly seen in the monomeric form; (gate-loop region in blue, ATP binding site in yellow, regulatory site in green, strict conservation of active site and interior residues in red).

```
                     cov    pid   1 [         .         .    *    .         .         :         .  ***    .         .  80
1 Giant_leucaena 100.0% 100.0%    --METFLFTSESVNEGHPDKLCDQVSDAVLDACLEQDPDSKVACETCTKTNMVMVFGEITTKANVDYEKIVRDTCRNIGF
2 Soy            100.0%  95.2%    MAQETFLFTSESVNEGHPDKLCDQISDAVLDACLEQDPDSKVACETCTKTNMVMVFGEITTKANVDYEKIVRDTCREIGF
3 Alfalfa         99.5%  92.3%    --METFLFTSESVNEGHPDKLCDQISDAVLDACLEQDVDSKVACETCTKTNMVMVFGEITTKAKVDYEKIVRDTCRKIGF
4 Arabidopsis    100.0%  92.1%    --METFLFTSESVNEGHPDKLCDQISDAVLDACLEQDPDSKVACETCTKTNMVMVFGEITTKATVDYEKIVRDTCRAIGF
5 Corn            99.5%  89.8%    MAAESFLFTSESVNEGHPDKLCDQVSDAVLDACLAQDPDSKVACETCTKTNMVMVFGEITTKASVDYEKIVRDTCREIGF
6 E. coli         96.9%  54.5%    --MAKHLFTSESVSEGHPDKIADQISDAVLDAILEQDPKARVACETYVKTGMVLVGGEITTSAWVDIEEITRNTVREIGY

                     cov    pid  81         .         1         .  *  *   *     .         .         :         . 160
1 Giant_leucaena 100.0% 100.0%    VSDDVGLDADKCKVLVNIEQQSPDIAQGVHGHFTKRPEEVGAGDQGHMFGYATDETPEYMPLSHVLATKLGARLTEVRKN
2 Soy            100.0%  95.2%    ISDDVGLDADKCKVLVNIEQQSPDIAQGVHGHFTKRPEEVGAGDQGHMFGYATDETPEYMPLSHVLATKLGARLTEVRKN
3 Alfalfa         99.5%  92.3%    VSDDVGLDADNCKVLVNIEQQSPDIAQGVHGHLTKRPEEIGAGDQGHMFGYATDETPELMPLSHVLATKLGARLTEVRKN
4 Arabidopsis    100.0%  92.1%    VSDDVGLDADKCKVLVNIEQQSPDIAQGVHGHFTKCPEEIGAGDQGHMFGYATDETPELMPLSHVLATKLGARLTEVRKN
5 Corn            99.5%  89.8%    TSDDVGLDADRCKVLVNIEQQSPDIAQGVHGHFTKRPEEIGAGDQGHMFGYATDETPELMPLSHVLATKLGARLTEVRKD
6 E. coli         96.9%  54.5%    VHSDMGFDANSCAVLSAIGKQSPDINQGVDR---ADPLEQGAGDQGLMFGYATNETDVLMPAPITYAHRLVQRQAEVRKN

                     cov    pid 161  *      .         .         .         2         .         .         .         . 240
1 Giant_leucaena 100.0% 100.0%    GTCAWLRPDGKTQVTVEYYNDNGAMVPVRVHTVLISTQHDETVNNEQIAADLKEHVIKPVIPEKYLDDKTIFHLNPSGRF
2 Soy            100.0%  95.2%    GTCAWLRPDGKTQVTVEYYNDNGAMVPVRVHTVLISTQHDETVSNDQIAADLKEHVIKPVIPEKYLDEKTIFHLNPSGRF
3 Alfalfa         99.5%  92.3%    GTCPWLRPDGKTQVTVEYYNDNGAMVPVRVHTVLISTQHDETVTNDEIAADLKEHVIKPVIPEKYLDSKTIFHLNPSGRF
4 Arabidopsis    100.0%  92.1%    GTCAWLRPDGKTQVTVEYYNDKGAMVPIRVHTVLISTQHDETVTNDEIARDLKEHVIKPVIPEKYLDEKTIFHLNPSGRF
5 Corn            99.5%  89.8%    GTCAWLRPDGKTQVTVEYVNEGGAMVPVRVHTVLISTQHDETVTNDEIAADLKEHVIKPVIPERYLDEKTIFHLNPSGRF
6 E. coli         96.9%  54.5%    GTLPWLRPDAKSQVTFQYDDGK--I--VGIDAVVLSTQHSEEIDQKSLQEAVMEEIIKPILPAEWLTSATKFFINPTGRF

                     cov    pid 241         :         .         .         .  **     .    3         .         . 320
1 Giant_leucaena 100.0% 100.0%    VIGGPHGDAGLTGRKIIIDTYGGWGAHGGGAFSGKDPTKVDRSGAYVARQAAKSVVANGLARRCLVQVSYAIGVPEPLSV
2 Soy            100.0%  95.2%    VIGGPHGDAGLTGRKIIIDTYGGWGAHGGGAFSGKDPTKVDRSGAYIVRQAAKSVVANGLARRCIVQVSYAIGVPEPLSV
3 Alfalfa         99.5%  92.3%    VIGGPHGDAGLTGRKIIIDTYGGWGAHGGGAFSGKDPTKVDRSGAYIVRQAAKSIVASGLARRCIVQVSYAIGVPEPLSV
4 Arabidopsis    100.0%  92.1%    VIGGPHGDAGLTGRKIIIDTYGGWGAHGGGAFSGKDPTKVDRSGAYIVRQAAKSVVANGMARRALVQVSYAIGVPEPLSV
5 Corn            99.5%  89.8%    VIGGPHGDAGLTGRKIIIDTYGGWGAHGGGAFSGKDPTKVDRSGAYVARQAAKSIVASGLARRCLVQVSYAIGVPEPLSV
6 E. coli         96.9%  54.5%    VIGGPMGDCGLTGRKIIVDTYGGMARHGGGAFSGKDPSKVDRSAAYAARYVAKNIVAAGLADRCEIQVSYAIGVAEPTSI

                     cov    pid 321         .         .         *         .*        .         .         .      ] 398
1 Giant_leucaena 100.0% 100.0%    FIDTYGTGKIPEREILQLVKDNFDFRPGMITINLDLKRGGH-RFLKTAAYGHFGREDPDFTWEVVKPLKWEKPQA---
2 Soy            100.0%  95.2%    FVDTYGTGKIPDKEILQIVKENFDFRPGMITINLDLKRGGH-RFLKTAAYGHFGRDDPDFTWEVVKPLKSEKPQA---
3 Alfalfa         99.5%  92.3%    FVDTYGTGKIPDKEILNIVKQNFDFRPGMISINLDLLRGGNGRFLKTAAYGHFGREDADFTWEVVKPLKWEKA-----
4 Arabidopsis    100.0%  92.1%    FVDTYETGLIPDKEILKIVKESFDFRPGMMTINLDLKRGGNGRFLKTAAYGHFGRDDPDFTWEVVKPLKWDKPQA---
5 Corn            99.5%  89.8%    FVDSYGTGTIPDKEILKIVKENFDFRPGMVTINLDLKKGGN-RFIKTAAYGHFGRDDADFTWEVVKPLKKASA-----
6 E. coli         96.9%  54.5%    MVETFGTEKVPSEQLTLLVREFFDLRPYGLIQILDLLH---PIYKETAAYGHFGREH--FPWEKTDKAQLLREAAGLK
```

Figure 6: Multienzyme sequence alignment of select plant SAM-synthetases and one from the bacteria *E. coli*. Conserved regions are shown by colored text, consistent with the colors used in 3d models from Fig. 5 (gate-loop region in blue, ATP binding site in yellow, regulatory site in green, active site and interior residues in red). Notable amino acids in the giant leucaena SAM-synthetase sequence (from the table in Fig. 5) are indicated by a cyan-asterisk and black background.

The phylogenetic tree shows five bacterial SAM-synthetases with surprising similarity to plant variants (Fig. 7). SAM-synthetases from higher plants exhibit a high degree of conservation (< 89% similarity) and typically share 60-70% similarity to bacterial SAM-synthetases. Two bacterial variants with approximately 90% similarity to giant leucaena SAM-synthetase are worth noting as they have been recently discovered from extremophilic species. Psychrotrophic *Paenibacillus* sp. isolated from the Western Himalayas (Dhar et al., 2015) and *Nitriliruptor alkaliphilus* isolated from alkali lakes in

Siberia (Sorokin et al., 2009) share higher sequence identity to plant SAM-synthetases than do members of cryptogamae (non-flowering, non-seed bearing plants).

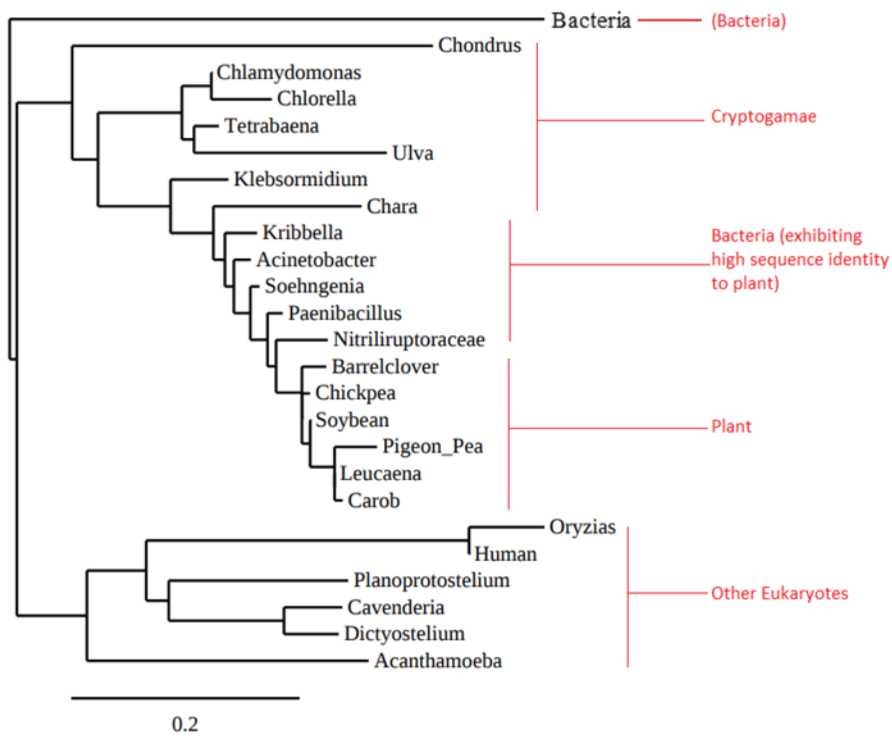

Figure 7: Phylogenetic tree based on protein sequences of SAM-synthetase. Select examples with high similarity to *Leucaena* are shown from various taxonomical groups. Most bacterial sequences group together, within the branch labelled "Bacteria", however few exceptions from extremophilic species exhibit high sequence identity to higher plants. The scale bar corresponds to a 0.2 change per amino acid.

1.3. Expression and purification of recombinant LSAMS

His$_6$-tagged **LSAMS** was expressed in high amounts by *E. coli*, as a soluble protein and eluted from Ni-resin using 500 mM imidazole (Fig. 8). High quality purified **LSAMS** was accomplished by extensive washing of the enzyme bound resin with buffers containing 50 mM and 100 mM imidazole. His$_6$-tag removal by thrombin had no effect on enzyme activity.

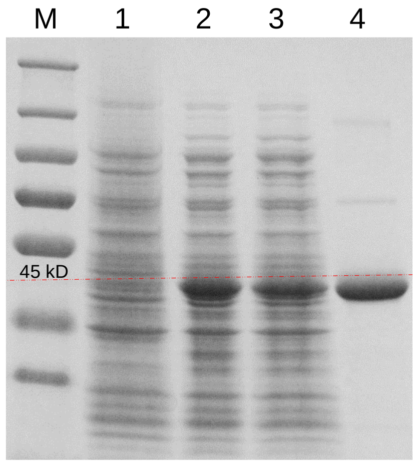

Figure 8: SDS-PAGE analysis of recombinant giant leucaena SAM-synthetase (**LSAMS**) expression by *E. coli* BL21(DE3). Cells were pelleted and lysed in 1/10th the original culture volume prior to loading (5 µL sample per well 12%-NOVEX precast gels by Thermo Fisher Scientific). Purified SAM-synthetase was quantified by nanodrop prior to loading. Lane M: BIO-RAD Precision Plus Protein Standard, Lane 1: Uninduced Lysate, Lane 2: Induced Lysate, Lane 3: Induced Soluble fraction, Lane 4: Purified **LSAMS** (0.5 ug).

1.4. Enzymatic properties of recombinant LSAMS

Production of S-adenosylmethionine was measured by RP-HPLC and presented in terms of relative activity (Fig. 9). Both Mg^{2+} and K^+ are required cofactors for SAM-synthetase enzymes, however Na^+ is shown here to restore activity approximately 20% of that when K^+ is present (Fig. 9.A). Tolerance to high salinity was observed as shown by **LSAMS** activity at 4 M KCl, the maximum solubility of KCl at room temperature. The product, SAM, is degraded by high temperature and by alkalinity however enzyme activity was shown to be highest in these conditions. In assays buffered with 100mM Tris-HCl pH 8.0, enzyme activity was highest at 55 °C (Fig. 9.B). In assays conducted at room temperature (25 °C), enzyme activity was highest at pH 10.0 (Fig. 9.C). Since the combined effects of alkaline pH and high temperature rapidly degraded the substrate SAM, additional tests were performed which considered both pH, temperature and the degradation product adenine. SAM-synthetase activity was shown to be highest in Tris-HCl buffered solution pH 8.5 at temperature of 50 °C with slight degradation of SAM (Fig. 10). Therefore, these conditions were deemed as optimal and used to further characterize the kinetic properties of **LSAMS**.

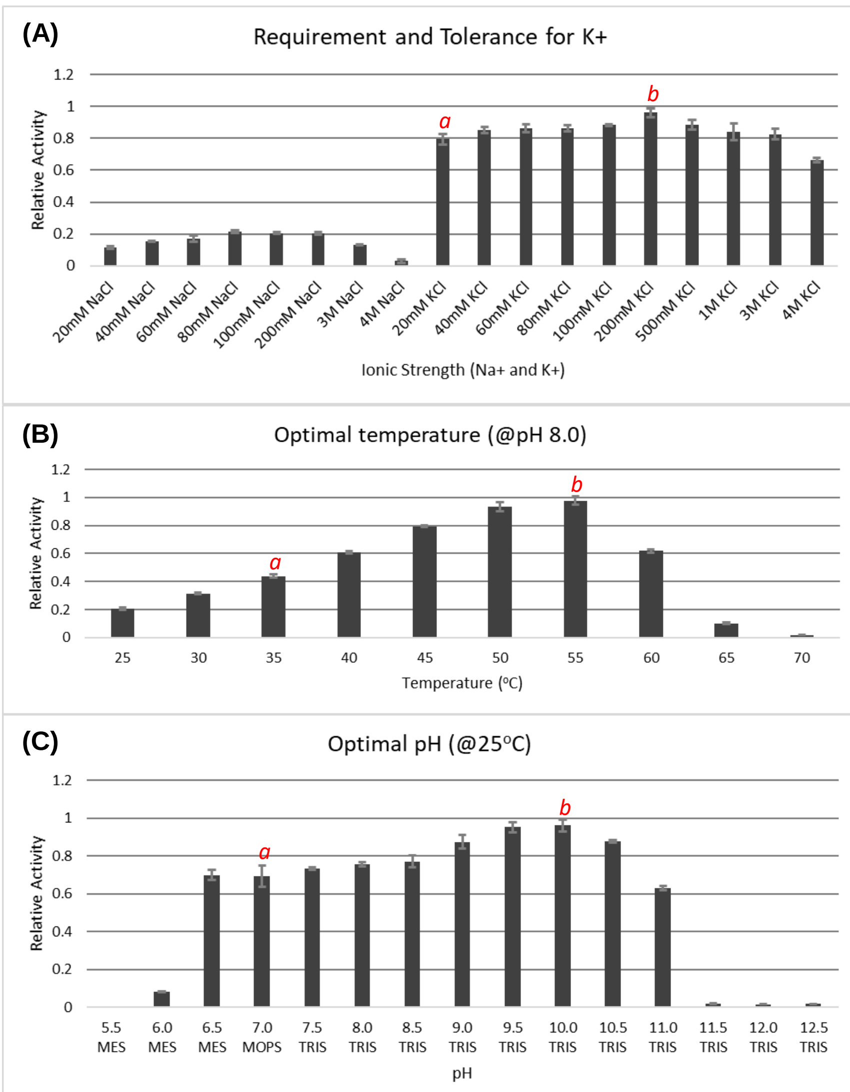

Figure 9: (A) LSAMS activity at different concentrations of NaCl and KCl (n=3), **(B) LSAMS** activity at different temperatures (n=4) **(C) LSAMS** activity at different pH values (n=4). Compared to activity in minimal KCl solutions, 35 ˚C or at neutral pH, **LSAMS** activity is significantly higher ($p < 0.05$).

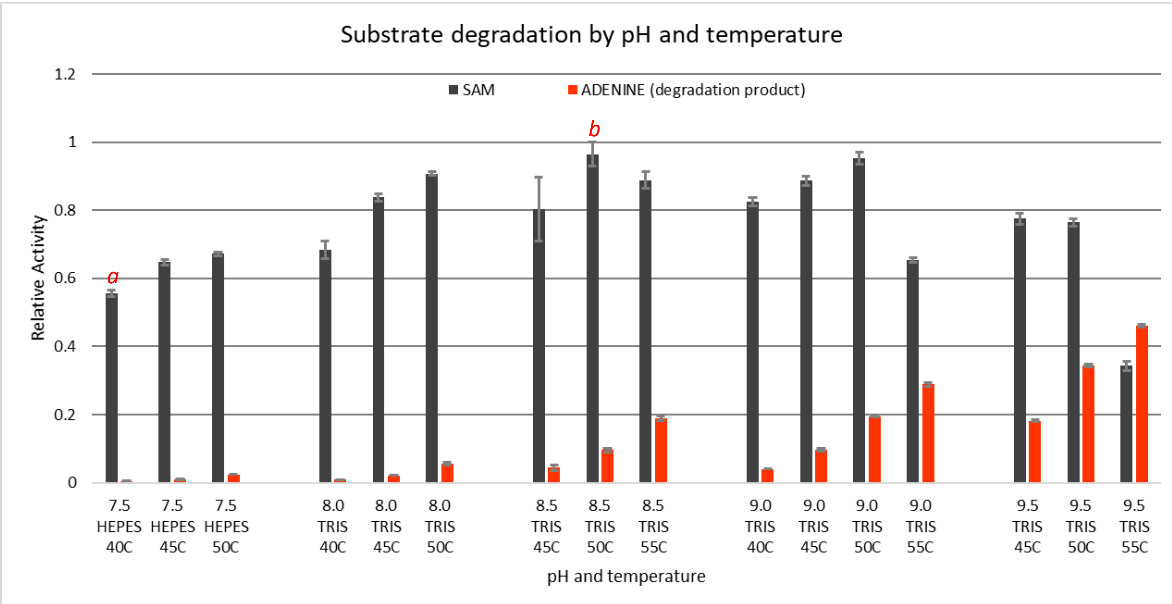

Figure 10: The effect of temperature and pH on SAM degradation in **LSAMS** assays, (n=3). Compared to activity in milder conditions (pH 7.5, 40 ˚C), **LSAMS** activity is increased significantly ($p < 0.05$).

1.5. Kinetic analyses of recombinant LSAMS

Kinetic values for **LSAMS** were determined from the Lineweaver-Burke plot (Fig. 11). Required calculations (K_m = 1.82 mM, K_{cat} = 1.17 s^{-1}, V_{max} 243.9 µM. min^{-1}) were based on the molecular weight of **LSAMS** (45.9 kDa w/tag) and that [E_{TOTAL}] = [**LSAMS**]. High concentration of substrate (>10 mM) did not affect enzyme activity however complete inhibition was observed upon accumulation of 2.5 mM of product.

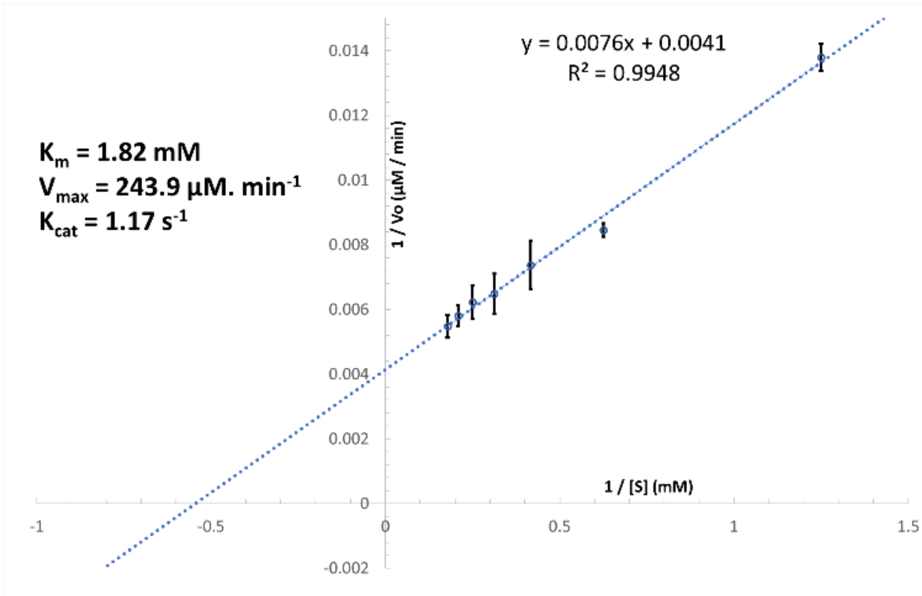

Figure 11: Lineweaver-Burke plot depicting **LSAMS** kinetics under optimized conditions, (n=3).

Assays supplemented with spermidine, spermine or nicotianamine showed no difference to control assays. 1 mM of spermidine or spermine did not affect **LSAMS** activity or product inhibition. Assays containing 0.2 mM nicotianamine did not suggest inhibiting effects; higher concentrations were not investigated due to limited availability and high cost of pure nicotianamine.

1.6. Further analysis of data and LSAMS

LSAMS has been demonstrated in this study as a highly heat/alkali/salt tolerant enzyme. The in vitro activity of many plant SAM-synthetases has not been well established. Structural characterization of plant SAM-synthetases has determined key distinctions from bacterial and other eukaryotic enzymes. SAM-synthetases, many mentioned throughout this paper from *E.* coli, *B. subtilis,* yeasts, etc., are observed as homotetramers or in equilibrium with monomeric and dimeric forms. Tetrameric SAM-synthetase from *E. coli* and human (MAT-II) were shown to both interact with MAT-II β regulatory subunits (LeGros et al., 2000), thus forming a heterohexamer. Plant SAM-synthetases have only been observed as homodimers and lack any regulatory subunit. Sekula, et al. (2020) identified a unique binding site in plant SAM-synthetases which suggests regulation by spermidine, however the activity studies performed here do not suggest regulation by polyamines. Whereas mammalian and bacterial SAM-synthetases are regulated by a protein subunit, the means of regulation among plant SAM-synthetases remains undetermined.

Bacterial SAM-synthetases can be used to infer sites with catalytic or structural importance in plant SAM-synthetases. Critical residues have been identified by *E. coli* SAM-synthetase mutants, improving specific activity 2-fold and reduced substrate inhibition (Ki_{ATP}) 42-fold (Wang et al., 2019). These specific residues in *E. coli* MAT (I303V / I65V / L186V / N104K) and the crystal structure of MAT (Takusagawa et al., 1996) are worth referencing to form a comparison to plant SAM-synthetases. The corresponding residues in giant leucaena SAM-synthetase are (**I**310 / **Y**65 / **I**193 / **A**104) (Fig. 12). Residues I310, I193, and A104 are near the active site and are likely to have a direct role in catalysis or active site accessibility. The significance of Y65 is less clear as it is observed far from the active site (Fig. 12, bottom highlighted residue). Considering the properties of plant SAM-synthetases, Y65 may have indirect effects on activity by enforcing the strict dimerization observed by plant SAM-synthetases.

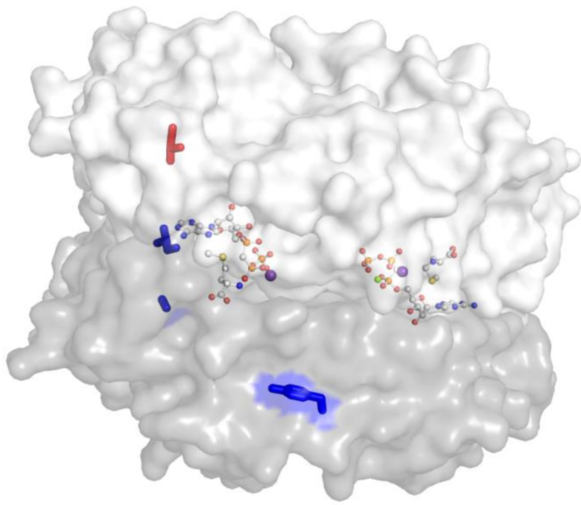

Figure 12: Key residues (I310, Y65, I193, and A104), with suggested importance in ATP inhibition, are highlighted on a 3d-model of giant leucaena SAM-synthetase homodimer. Colored residues indicate positions on either monomer, one of the two active sites are detailed.

Observational analysis of the homotetramer SAM-synthetases, such as those in *E. coli,* suggests that tetramer assembly or dimer-dimer interactions in bacterial SAM-synthetases relies upon this site. Interestingly, tyrosine is strictly conserved at this site *only* in plant SAM-synthetases which are exclusively homodimers. The *Vibrio*, *Paenibacillus*, *Acinetobacter*, *Nitriliruptoraceae*, *Kribella*, and *Soehngenia* sequences reveal a tyrosine residue at this site as well, suggesting a homodimer "plant-like" SAM-synthetase for these oddly-related bacterial genera (see phylogenetic tree, Fig. 7).

Kinetic values determined for **LSAMS** are like those determined by purified native *G. max* SAM-synthetase enzyme ($K_{m\ ATP}$, 1.53 mM, $K_{m\ METHIONINE}$, 1.81 mM) (Kim et al., 1995). Initial efforts in assaying **LSAMS** were focused on determining separate K_m values for ATP and L-methionine, however activity rates did not differ beyond normal experimental error. ATP would be supplied in excess and L-methionine varied (and vice versa) but results were not noticeably different to warrant the extensive assays required for experimentation. Thus, **LSAMS** was treated as a single-substrate enzyme, providing equal concentrations of both ATP and L-methionine in assays. Kamarthapu et al. (2008) characterized the activity of *B. subtilis* SAM-synthetase expressed in *E. coli* BL21(DE3) cells and a pET vector, very similar to this study though Kamarthapu observed slight issues in soluble expression of recombinant enzyme. Peak activity was observed under milder conditions (45 ^{o}C, pH 8.0) and lower K_m values ($K_{m\ ATP}$, 920 µM, $K_{m\ METHIONINE}$, 260 µM) were determined than for **LSAMS**. Recombinant SAM-synthetase from *Streptomyces avermitilis* is far less thermostable (optimal temp = 35 ^{o}C, pH 8.0) and produced even lower constants ($K_{m\ ATP}$, 340 µM, $K_{m\ METHIONINE}$, 110 µM) (Yoon et al., 2006). Compared to the few known characteristics of plant SAM-synthetases, results from this study and some activity observed by bacterial SAM-synthetases, three conclusions may be drawn. 1) Plant SAM-synthetases likely exhibit K_m constants of 1.5 – 2 mM, approximately ten-fold higher than observed by non-plant homologs; 2) Turnover rates of ~ 1 s^{-1} are typical, though can range drastically (~ 0.7 – 17 s^{-1}) (Parungao et al., 2017); 3) s^{-1}; 3) High substrate concentrations did not affect **LSAMS** activity. SAM production stops upon reaching 2.5 mM, compared to stronger feedback inhibition by *E. coli* MAT (complete inhibition at 1.62 mM SAM) (Wang et al., 2019).

Incorporating thermo-stable plant SAM-synthetases may improve stress tolerance, protein production or secondary metabolite production in microbial expression systems. As demonstrated by this study, optimal conditions for enzyme activity must be carefully considered since product degradation can be significant due to high temperature and alkaline pH. Regarding the ionic strength of assay solutions, approximately 15% more SAM (Fig. 9.A) is produced at optimal KCl concentration (200 mM) than at low concentrations (<50 mM) observed in other studies. Greater consideration must be made for the ionic strength of assays when determining optimal conditions for SAM-synthetases. The structure and function relationship of plant SAM-synthetases requires more research, specifically to confirm the extremophilic activity demonstrated by **LSAMS**.

Part II: SAM-synthetase from Acacia koa and mutagenesis experiments

2.1. Characterization and purification of KSAMS and mutant variants

The *A. koa* SAM-synthetase coding sequence (GENBANK ACCESSION No. ON638997) is 1182 bp, producing a 43.2 kDa protein which forms an active homodimer. The amino acid sequence shares a 94.4% similarity to the Arabidopsis SAM-synthetase-1 (AtMAT1) used in modeling. The 3d-model and targeted site for mutagenesis can be observed in Fig. 13 and in the multiple sequence alignment (Fig. 14).

His_6-tagged **KSAMS** and mutant variants were expressed in *E. coli* as soluble protein and eluted from Ni-resin using 500 mM imidazole (Fig. 15). His_6-tag removal by thrombin had no effect on enzyme activity.

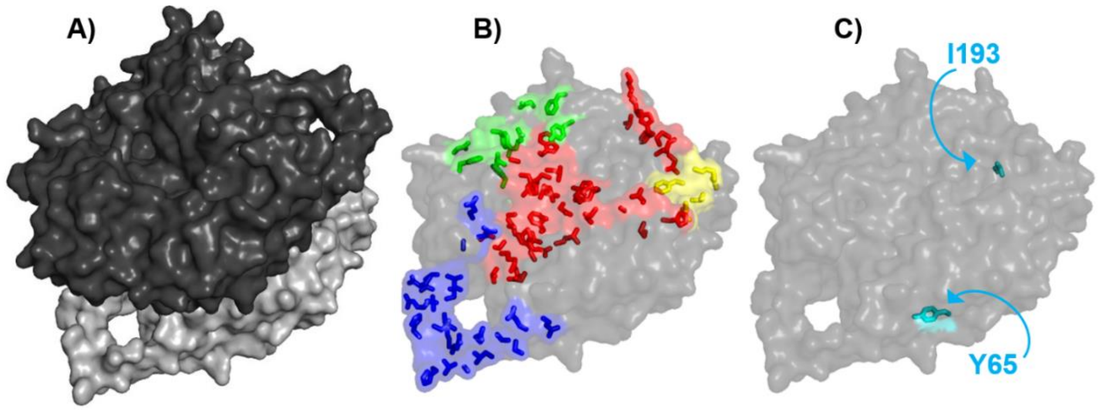

Figure 13: (A) 3d modelling of the *Acacia koa* SAM-synthetase enzyme depicting the native dimeric form. **(B)** Monomeric form displaying highly conserved regions (gate-loop region in blue, ATP binding site in yellow, regulatory site in green, and strictly conserved structural residues in red). **(C)** Select sites and residues for the generation of mutants #1 – 4.

```
                  HOMOLOGY 1 [         .         .         .         .         :         .         .         .         .         .         1 100
1 E.coli               53%   --MAKHLFTSESVSEGHPDKIADQISDAVLDAILEQDPKARVACETYVKTGMVLVGGEITTSAWVDIEEITRNTVREIGYVHSDMGFDANSCAVLSAIGK
2 Giant_leucaena       93%   --METFLFTSESVNEGHPDKLCDQVSDAVLDACLEQDPDSKVACETCTKTNMVMVFGEITTKANVDYEKIVRDTCRNIGFVSDDVGLDADKCKVLVNIEQ
3 Acacia_Koa          100%   --METFLYTSESVNEGHPDKLCDQISDAVLDACLEQDPDSKVACETCTKTNMVMVFGEITTKANVDYEKIVRNTCRNIGFVSDDVGLDADNCKVLVNIEQ
                                                                                               ^ Y65V, M2
                                                                                               ^ Y65A, M3

                         101         .         .         .         .         :         .         .         .         .         2 200
1 E.coli                     QSPDINQGVDR---ADPLEQGAGDQGLMFGYATNETDVLMPAPITYAHRLVQRQAEVRKNGTLPWLRPDAKSQVTFQYDDGK--I--VGIDAVVLSTQHS
2 Giant_leucaena             QSPDIAQGVHGHFTKRPEEVGAGDQGHMFGYATDETPEYMPLSHVLATKLGARLTEVRKNGTCAWLRPDGKTQVTVEYYNDNGAMVPVRVHTVLISTQHD
3 Acacia_Koa                 QSPDIAQGVHGHLTKRPEEIGAGDQGHMFGYATDETPELMPLSHVLATKLGARLTEVRKNGTCPWLRPDGKTQVTVEYYNDKGAMVPIRVHTVLISTQHD
                                                                                                              I193V, M4 ^
                                                                                                              I193A, M5 ^

                          201         .         .         .         .         :         .         .         .         .         3 300
1 E.coli                     EEIDQKSLQEAVMEEIIKPILPAEWLTSATKFFINPTGRFVIGGPMGDCGLTGRKIIVDTYGGMARHGGGAFSGKDPSKVDRSAAYAARYVAKNIVAAGL
2 Giant_leucaena             ETVNNEQIAADLKEHVIKPVIPEKYLDDKTIFHLNPSGRFVIGGPHGDAGLTGRKIIIDTYGGWGAHGGGAFSGKDPTKVDRSGAYVARQAAKSVVANGL
3 Acacia_Koa                 ETVTNDEIAADLKEHVIKPVIPEKYLDEKTIFHLNPSGRFVIGGPHGDAGLTGRKIIIDTYGGWGAHGGGAFSGKDPTKVDRSGAYIVRQAAKSIVANGL

                          301         .         .         .         .         :         .         .         .         .       ] 398
1 E.coli                     ADRCEIQVSYAIGVAEPTSIMVETFGTEKVPSEQLTLLVREFFDLRPYGLIQILDLL---HPIYKETAAYGHFGREH--FPWEKTDKAQLLREAAGLK
2 Giant_leucaena             ARRCLVQVSYAIGVPEPLSVFIDTYGTGKIPEREILQLVKDNFDFRPGMITINLDLKRGGH-RFLKTAAYGHFGREDPDFTWEVVKPLKWEKPQA---
3 Acacia_Koa                 ARRCLVQVSYAIGVPEPLSVFVDSYGTGKIPDKEILKIVKENFDFRPGMISIHLDLKRGGNGRFLKTAAYGHFGREDPDFTWETVKPLKWEKPQA---
```

Figure 14: Multiple sequence alignment showing conserved regions for plant SAM-synthetases and sites of interest. Significant residues/regions are color highlighted (gate-loop region in blue, ATP binding site in yellow, regulatory site in green, and strictly conserved structural residues in red). Protein accession numbers for reference: *E. coli* (MBF5976374), Giant leucaena (UNO31584), *Acacia koa* (UZT04310).

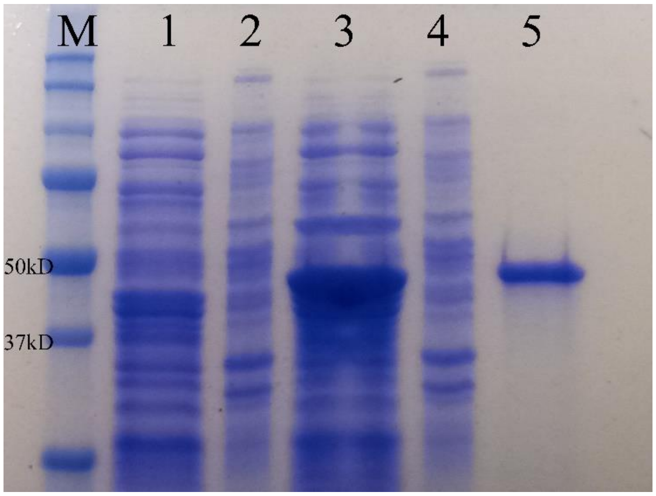

Figure 15: SDS-PAGE analysis of **KSAMS** expression by *E. coli* BL21(DE3). Lane M: BIO-RAD Precision Plus Protein Standard, Lane 1: clarified lysate (uninduced), Lane 2: insoluble protein fraction (uninduced), Lane 3: clarified lysate (induced), Lane 4 insoluble protein fraction (induced), Lane 5: purified **KSAMS** (5 µg).

2.2. Effect of pH, temperature, and salinity on KSAMS

A wide range of pH, temperature and KCl determine optimal conditions to be pH 8.5, temperature 50 °C and 20 mM KCl (Fig. 16). Optimal pH and temperature assays were conducted separately, therefore pH 10.5 appears as optimal in Fig 16.A. Extensive assays performed by Carrillo and Borthakur (2020) demonstrate SAM degradation at high temperatures and high pH. Optimal activity must be precisely defined as the highest measure of *undegraded* SAM, therefor alkaline conditions are not optimal when considering temperature as well.

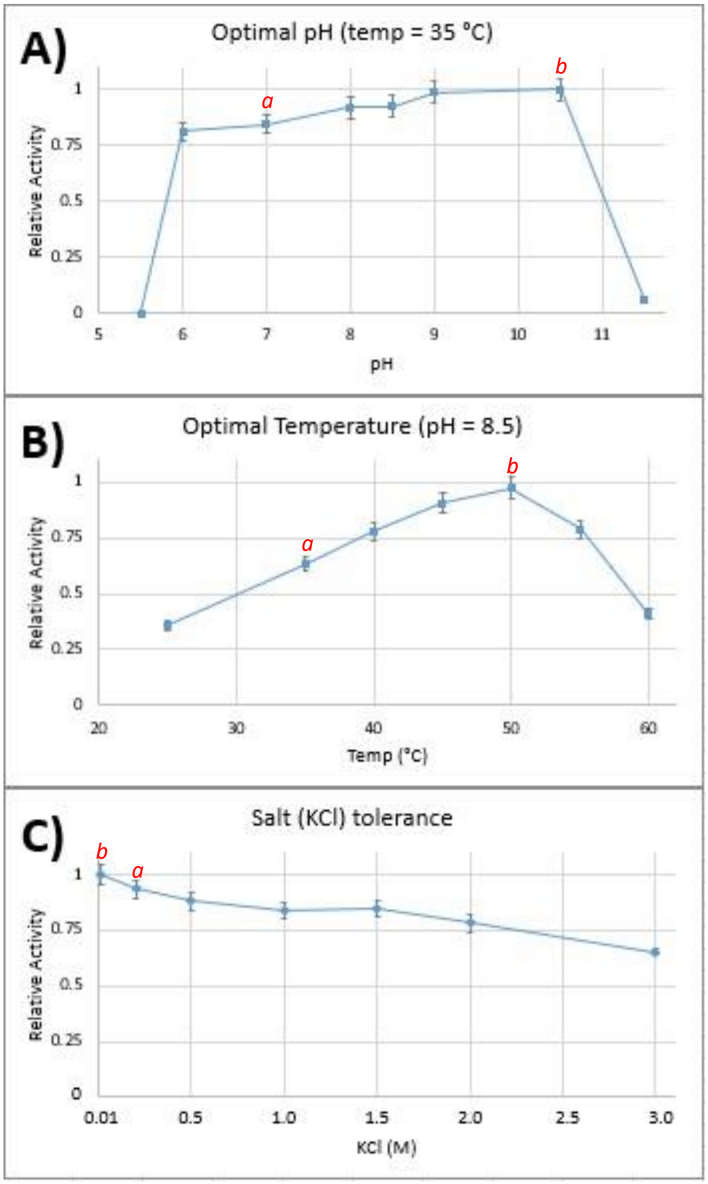

Figure 16: Optimal conditions for **KSAMS**: **(A)** pH, **(B)** temperature and **(C)** KCl tolerance, (n=3). Compared to activity at neutral pH, 35 ˚C or in stronger KCl solutions, **KSAMS** activity is increased significantly ($p < 0.05$).

2.3. Effect of organic solvents on KSAMS

Of the six solvents, only 25% methanol, 25% acetonitrile and 25% dimethylformamide had improved activity (Fig. 17). In each case, SAM accumulation was significantly higher than control assays (0%) at 60 min. Also, the initial reaction rate is slightly improved in 25% methanol and 25% acetonitrile. Select examples from Fig. 17 are included in Table 5.

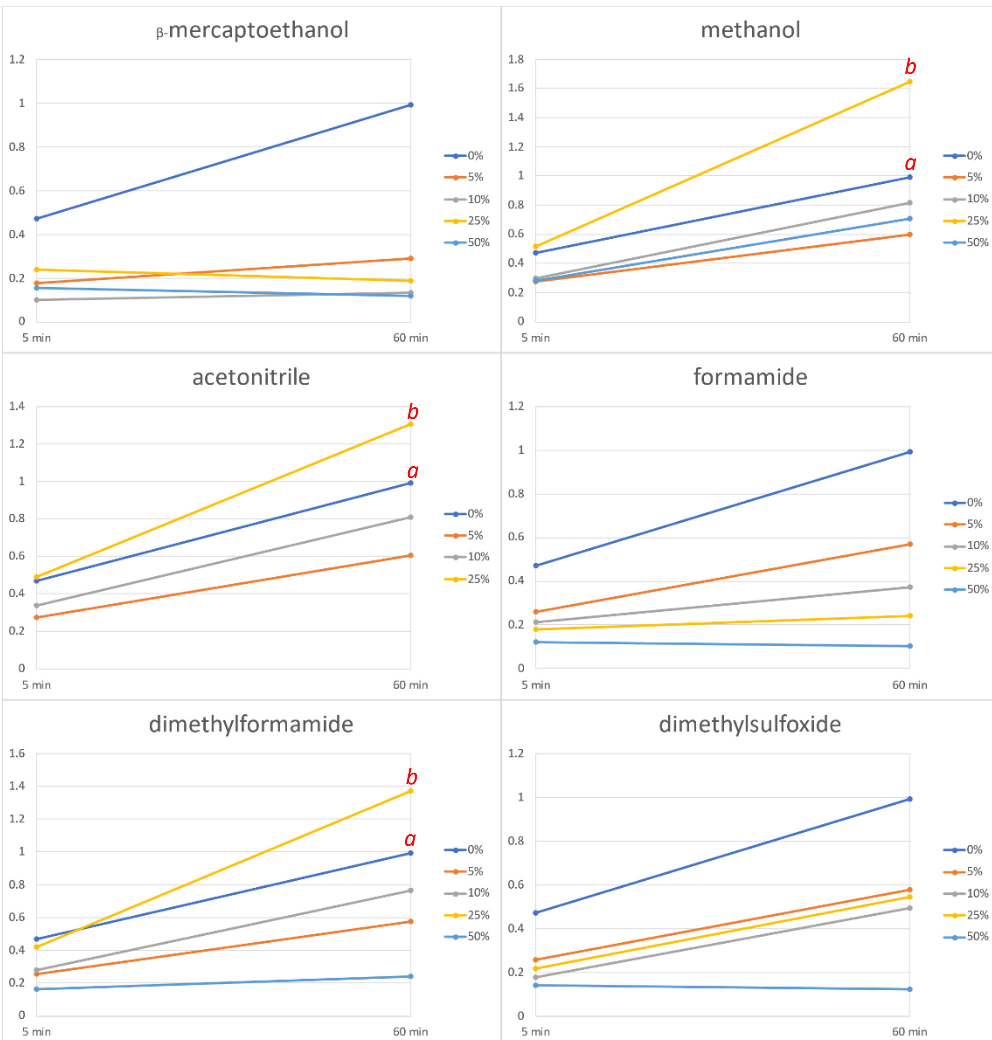

Figure 17: The activity of **KSAMS** in the presence of various organic solvents (n = 3). Error bars excluded for clarity (%-error < 0.05). Compared to the control (0% solvent), **KSAMS** activity is significantly higher ($p < 0.05$).

2.4. Kinetic analyses of KSAMS and mutants Y65V, Y65A, I193V, I193A

Kinetic constants were obtained from the Lineweaver-Burke plot from assays performed at 50 °C and 35 °C (Fig. 18.A.). **KSAMS(Y65V)** exhibited zero activity and **KSAMS(Y65A)** activity was greatly diminished. Mutants from the second mutation site, **KSAMS(I193V)** and **KSAMS(I193A)**, were impaired to a far lesser degree. Interestingly, none of the mutants were active at 50 °C. Only **KSAMS(I193V)** displayed faint activity at 50 °C, otherwise its activity is unchanged at 35 °C. Measurements of SAM production and kinetic values are collected in Table 5.

The effects due to altering these two sites (**Y65** and **I193**) cannot be explained fully, however the essential role of each site is discussed with additional structural analysis.

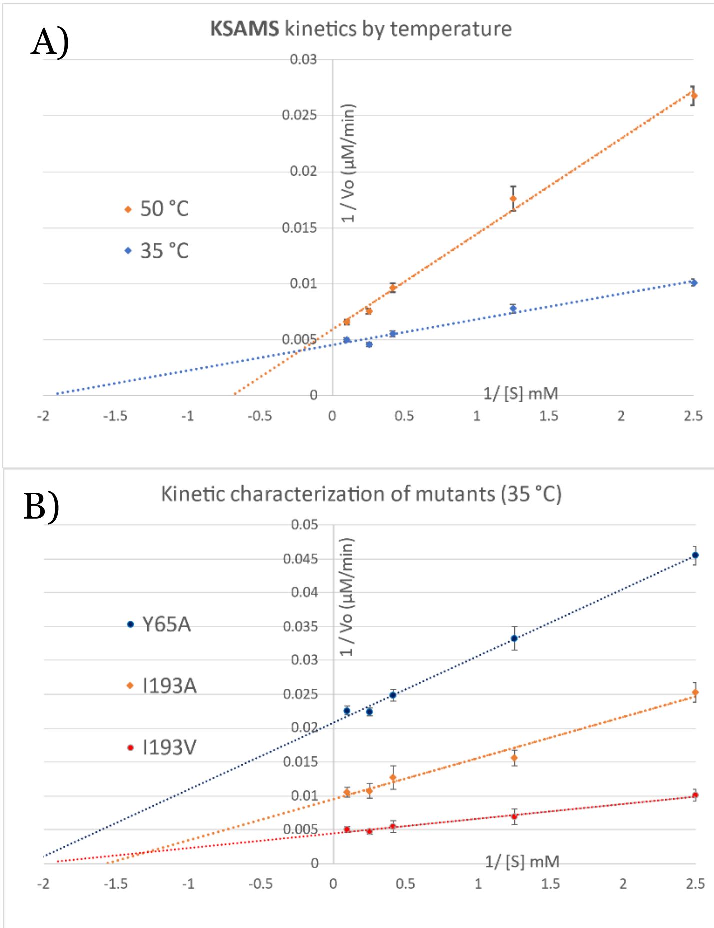

Figure 18: (A) Lineweaver-Burke plot depicting **KSAMS** kinetics at optimal temperature of 50 °C and at moderate temperatures (35 °C) used in reactions containing organic solvent (n=3). **(B)** Kinetic assays of mutants **(Y65A)**, **(I193A)** and **(I193V)** performed at 35 °C, (n=3, R^2 >0.95)

Table 5: Kinetic constants and total SAM production by **KSAMS** and mutant variants. Only organic solvents which enhanced SAM production (25% acetonitrile, methanol or dimethylformamide) are included. The values in red reflect the initial reaction rate in assays with 4 mM substrate (n = 3, %-error < 0.05).

Enzyme	Solvent/Conditions	K_m (mM)	V_{max} (µM. min^{-1})	K_{cat} (sec^{-1})	SAM production (µM at 60 min)
KSAMS	None / 50 °C	1.44	170	1.29	1,358
	None / 35 °C	0.51	222	1.69	1,054
	25% acetonitrile / 35 °C	---	**232**	**1.77**	1,378
	25% methanol / 35 °C	---	**245**	**1.86**	1,735
	25% formamide / 35 °C	---	**198**	**1.51**	1,444
	500 mM urea / 35 °C	---	**162**	**1.23**	639
KSAMS (Y65V)	**(INACTIVE MUTANT)**	----	**(INACTIVE MUTANT)**	----	**(INACTIVE MUTANT)**
KSAMS (Y65A)	**-- INACTIVE at 50 °C --**	----	----	----	----
	None / 35 °C	0.48	48.1	0.36	494
KSAMS (I193V)	**-- INACTIVE at 50 °C --**	----	----	----	----
	None / 35 °C	0.64	105	0.8	989
KSAMS (I193A)	None / 50 °C	----	----	----	196
	None / 35 °C	0.49	215	1.64	910

2.4. Discussion and further analysis of KSAMS

Altering the sites **Y65** and **I193** in this study demonstrates their essential role, whereas these sites in bacteria are less critical. **Y65** appears to be extremely important, yet not essential to activity as **Y65A** exhibits 25% of the original reaction rate. This residue is located at the interface of homotetramer assembly, as it occurs in nonplant SAM-synthetases (Mingorance et al., 1997). Plant SAM-synthetases are structurally distinct and exclusively form homodimers, while bacterial/mammalian homologs form a mixture of active homodimers and homotetramers (Sekula et al., 2020). Wang et al. (2019) reported 50% higher SAM production by a **I165V EcMAT** mutant. In contrast, the activity of **KSAMS(Y65A)** was reduced by 75% and **KSAMS(Y65V)** was completely inactive. The site which contains **Y65** is clearly distinct in plant SAM-synthetases and recent studies have observed interesting effects using nonplant enzymes. Kleiner et al. (2022) demonstrated the significance of **K98** and **E67** in **EcMAT**. Altering these residues disrupted tetramer formation in the absence of substrate but did not affect enzyme activity. In **KSAMS,** the equivalent residues are **E98** and **K67** which flank **Y65** on the enzyme's surface. Gade et al. (2021) showed that for the human SAM-synthetase, the absence of substrate produces a mixture of dimers and monomers. If the mutants produced in this study effected dimer or tetramer formation, could that severely impair activity as observed by **KSAMS(Y65A/V)**? **EcMAT** mutants which remain dimeric do not exhibit any catalytic difference, only differences in enzyme structure, stability and in refolding (Kleiner et al., 2022). Therefore, there is little reason to expect tetrameric and dimeric **KSAMS** to differ. If the flexibility of the "gate-loop" region is affected, this may hinder the activity of **Y65** mutants. In Fig. 19.C., **Y65** can be seen 4.4 Å from **E98** in the open position of the "gate-loop" region. Weak noncovalent forces may be responsible for holding an open position and allowing access to the active site. Closer inspection of this site reveals another interesting feature of plant SAM-synthetases. The surface charge appears to differ from nonplant enzymes, seen as a protruding charged region (Fig. 20, blue regions). **K91**, which appears unique to plant SAM-synthetases, produces a central positive charge which may deter tetramer formation.

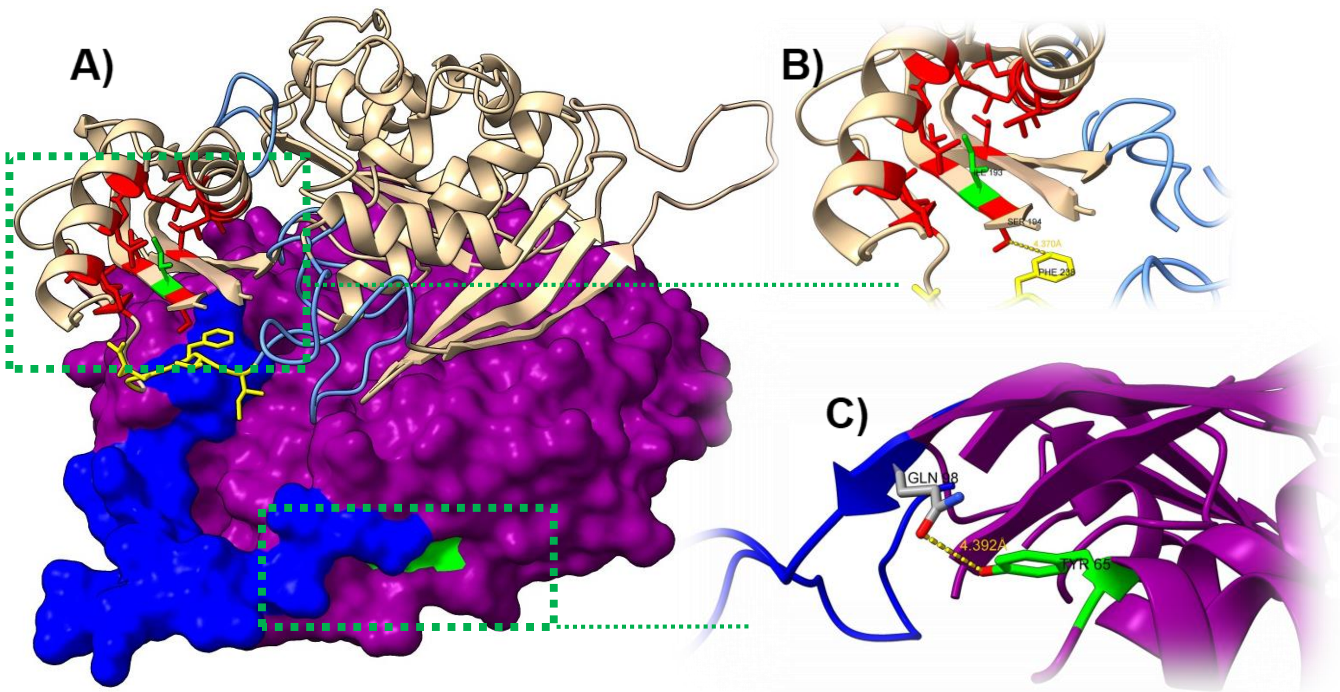

Figure 19: The sites of mutagenesis, relevant residues and distances are shown in **KSAMS**. Residues are colored to indicate key regions (substrate binding (yellow), gate-loop region (blue) and sites of mutagenesis (green). Unstructured flexible lengths of the peptide (light blue) distinguish the region containing **I193**. Hydrophobic residues are colored red and indicate a crowded hydrophobic pocket containing **I193**.

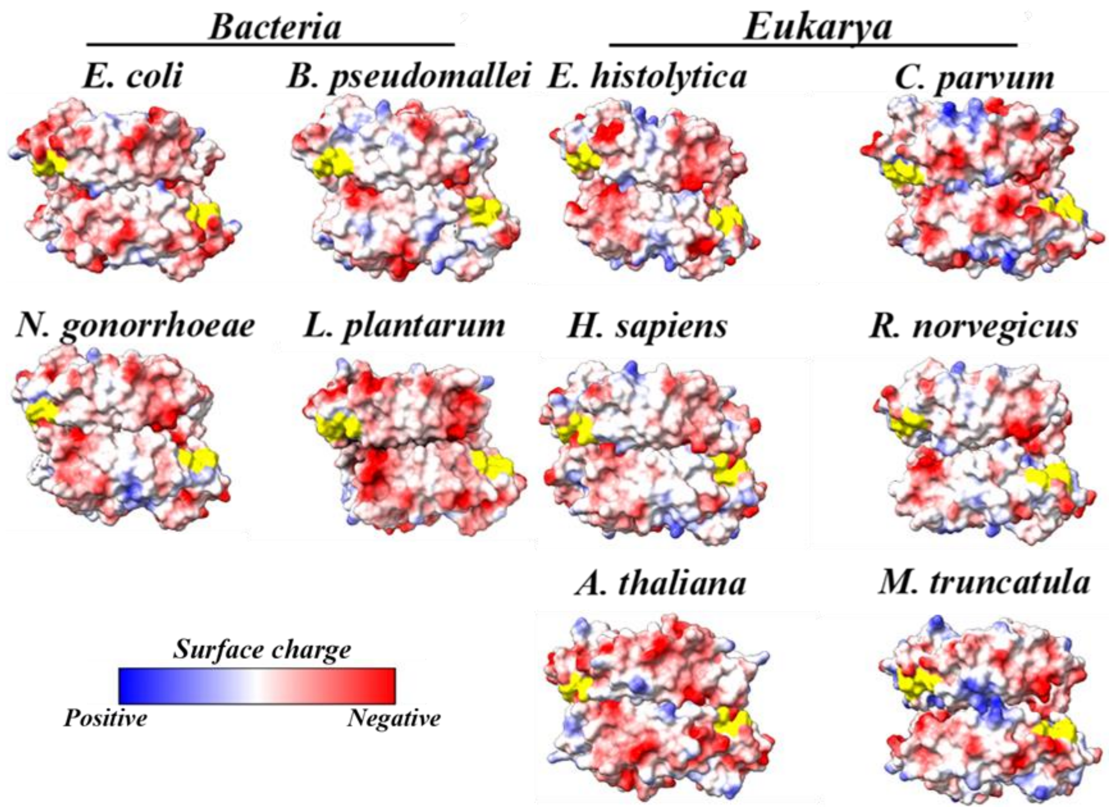

Figure 20: Coulombic electrostatic potential of SAM-synthetases is shown from various species. The face of dimer-dimer interaction is viewed directly with either active site, substrate binding residues in yellow, colored for reference. In the two models of plant SAM-synthetases, note the central positive charge produced by **K91**. PDB ID numbers are listed in "***2.6. Modeling and sequence analysis***".

The quaternary structure of **KSAMS(Y65A/V)** mutants was of interest, however Native-PAGE was inconclusive. Perhaps special conditions may allow Native-PAGE to resolve differences, however aforementioned studies clearly indicate that the presence of substrate has a considerable effect. Native-PAGE is likely not sensitive enough nor can it show the effect of tetramer association/dissociation over time. Recent studies by Gade et al. (2021) and Kleiner et al. (2022) show that size exclusion chromatography is a simple and effective method for discerning quaternary structure of SAM-synthetases.

Despite being nearer the active site, changes at **I193** effected activity less than substitutions at **Y65**. The relative location of **I193** in **KSAMS** is identical to **L186** in **EcMAT**, however identical mutations at this site produced *opposite* effects. Substituting a valine at this site had impaired **KSAMS** activity, whereas in **EcMAT** it nearly doubled SAM production (Wang et al., 2019). The **KSAMS(I193A)** mutant was slightly impaired but a more interesting effect was observed by the **I193V** mutant. At mild temperatures there appears to be little difference between **KSAMS** and **KSAMS(I193V)**, however at 50 °C the mutant is only slightly active. Fig. 17.B. depicts the location of **I193** within a hydrophobic pocket (red) above the ATP binding site (yellow). There are numerous leucine and isoleucine residues which make up this hydrophobic pocket which may serve as hydrophobic "anchors" for this domain. The adjacent residue, **S194,** is shown to interact closely (4.4 Å) with the adenosine binding site **F238** (this same distance measures 4.0 Å in **EcMAT**). Exchanging **I193** for a smaller hydrophobic residue may compromise the stability of this domain, the position of **S194** and ultimately the substrate binding site. Although a very minor change, a **I193V** substitution, could result in shifting the adjacent serine ~ 0.5 Å *further* from the adenosine binding site. Explaining how the *opposite* effect could be produced in **EcMAT** and **KSAMS** mutants is not possible at this time, however this residue appears incredibly sensitive to change. Additional mutants are necessary, perhaps altering other leucine/isoleucine residues in this hydrophobic pocket.

Except for formamide and dimethylsulfoxide increasing concentration of solvent did not consistently affect SAM accumulation (Fig. 17). For example, assays containing

5% or 10% methanol indicate impaired enzyme activity but at 25% solvent the opposite effect is observed. This effect is seen for methanol, acetonitrile and dimethylformamide, therefore each solvent may be producing a similar effect that enables for 30-60% higher SAM production. For methanol and acetonitrile, a slight increase in the initial reaction rate can be observed at the 5 min mark. Even for assays containing 25% dimethylformamide, where the reaction rate is slightly reduced, SAM production is 37% higher after 60 min. Although plant SAM-synthetases are highly resistant to heat and certain organic solvents, **KSAMS** was comparably far more sensitive to urea. **KSAMS** assays containing 500 mM urea were half as productive, whereas the **EcMAT** enzyme remained highly active (80%) in 5 M urea (Park et al., 1996). Plant and nonplant SAM-synthetases exhibit a high tolerance to organic solvents and urea but there are still important questions as to precisely how secondary structure is affected. For example, in assays containing 5 M urea, would **EcMAT** remain as a homotetramer? Or as an active homodimer?

Part III: 5’-methylthioadenosine nucleosidase from giant leucaena

3.1. Characterization of the giant leucaena MTA nucleosidase: sequence analysis and in vitro activity

The giant leucaena MTA-nucleosidase protein shares moderate similarity to homologous enzymes from *L. luteus* (83%), *A. thaliana* (69%), *O. sativa* (70%) and *E. coli* (26%). MTA-nucleosidase activity from these species has been previously characterized, especially from *E. coli*. Optimal pH and temperature of the crude periplasmic extract containing DsbA-**LMTAN** differs significantly from that of other plant MTA-nucleosidases. As observed from studies of other plant and nonplant MTA-nucleosidases, Tris buffer appears to inhibit MTA-nucleosidase activity (Siu et al., 2008; Cornell et al., 1996). Thermophilic properties, like observed by the giant leucaena SAM-synthetase, were apparent (Fig. 21).

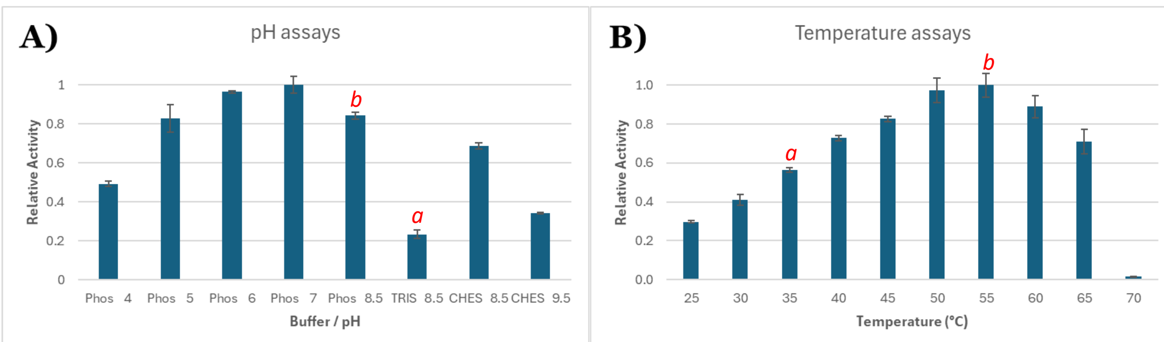

Figure 21: Optimal pH **(A)** and temperature **(B)** for MTA hydrolysis using the periplasmic extract containing DsbA-**LMTAN**, (n = 3). Compared to activity at 35 ˚C, **KSAMS** activity is significantly higher at 55 ˚C ($p < 0.05$). Difference in activity due solely to buffer, indicates that Tris is a potent inhibitor of DsbA-**LMTAN** ($p < 0.05$).

Optimal conditions for the *E. coli* MTA-nucleosidase are 35 - 45 ^{o}C, pH 6.0 (Cornell et al. 1996), while there isn't much evidence of plant MTA-nucleosidase properties. The *L. lupine* MTA-nucleosidase prefers more alkaline conditions, pH 8.0 (Guranowski et al., 1983), however thermophilicity was not considered. It is important to note that upon noting thermophilic activity shown here, the thermostability of MTA was also evaluated in the assay solutions. Degradation of MTA due to heat is only slightly apparent at 70 ^{o}C, with significant degradation taking place at $\geq$ 80 ^{o}C, therefore the thermophilic activity is surely enzyme catalyzed.

The fusion enzyme DsbA-**LMTAN**, although containing an internal histidine tag and a thrombin digestion site, was immune to thrombin digestion and purification efforts. The periplasmic extract of untransformed *E. coli* cultures did not indicate MTA-nucleosidase activity from induced cultures. Selectively concentrating the periplasmic extract ($\geq$ 20 kDal proteins) did not greatly improve the purity of DsbA-**LMTAN**. Most importantly, SAM degradation was not observed using the periplasmic extract and MTA degradation appeared to be highly compatible in a variety of buffers, including the assay solutions used for SAM-synthetase and NA synthase. Therefore, the crude periplasmic extract was considered suitable to incorporate into NA-synthase assays.

MTA was indicated by the specified HPLC method, with a retention time of 5.9 min (Fig. 22).

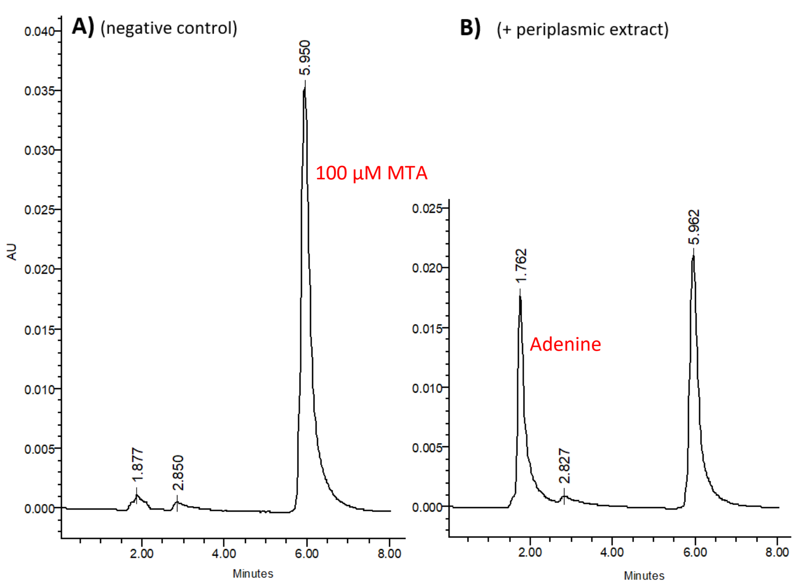

Figure 22: HPLC chromatograms indicating MTA degradation by DsbA-**LMTAN** in the periplasmic extract. **A)** pure MTA (retention time, 5.9 min), **B)** Generic assay showing MTA hydrolysis (Adenine retention time, 1.8 min)

Part IV: nicotianamine synthase from giant leucaena

4.1. Characterization of giant leucaena NA-synthase and improving yield of active enzyme

The giant leucaena NA-synthase transcript (GENBANK ACCESSION No. OL906428), consists of a 5'-untranslated region of 51 bp and an 855 bp coding sequence. The native protein has a calculated molecular weight of 32 kDa and theoretical isoelectric point of 6.51. A rendered model of the leucaena NA-synthase is provided (Fig. 23) with a similarly colored multiple sequence alignment of various NA-synthases (Fig. 24).

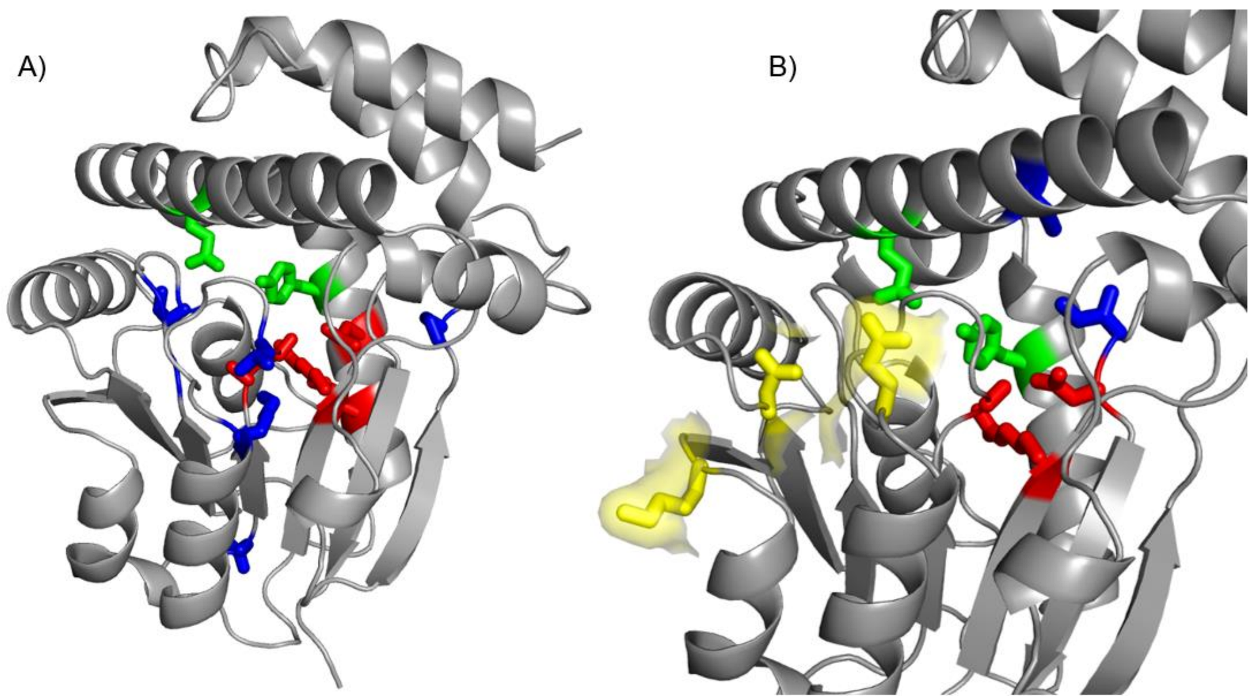

Figure 23: Monomeric giant leucaena nicotianamine synthase, modelled using the determined structure of thermonicotianamine synthase (M. thermoautrophicus).

A) Multiple sequence alignment of plant nicotianamine synthases, non-plant nicotianamine synthases and nicotianamine synthase-like enzymes (CntL) has identified fourteen strictly conserved residues. GREEN (E86, Y112) involved in aminopropyl transfer, RED (L115, A209, A210, R239) stabilize intermediate compounds, BLUE (E119, G138, G140, P143, D204, L211, K219, P268) have unspecified essential roles.

B) Close up of the reaction chamber with colored residues involved in ligand interaction. BLUE (C78, I273), are highly conserved among NA-synthases and may indicate the orientation of azetidine ring. Stabilizing residues, RED (A210, R239, N274), interact with carboxyl groups of intermediate compounds and/or NA. Active site residues GREEN (E86, Y112) and adenosine binding residues YELLOW (D163, K191, E217) indicate the reaction chamber entrance.

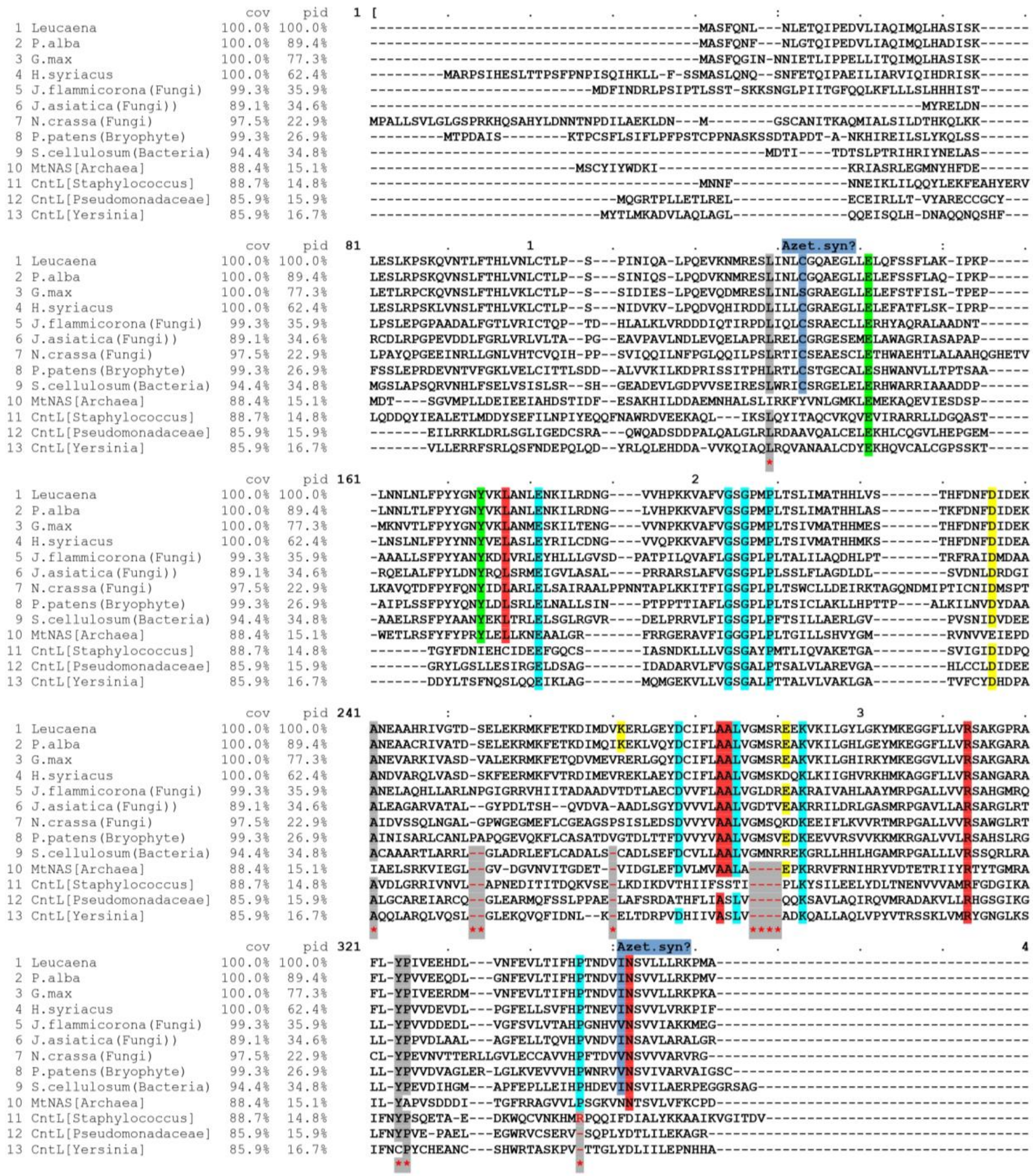

Figure 24: Multiple sequence alignment of plant NA-synthases, nonplant NA-synthases and NA-like-synthase enzymes depicts the conservation of essential residues. These residues and regions are indicated in the text: GREEN = active site, RED = stabilizing effect, BLUE = unspecified, YELLOW = adenosine binding. Other notable regions, appearing highly conserved or absent are indicated by red asterisks. Residues implicated in azetidine synthesis, C78 and I273, are labelled.

The expression of soluble **LNAS** increased with higher NaCl and sorbitol concentrations. Heat-shocking prior to IPTG induction had a beneficial effect on soluble expression, most apparent between “PURE (LB)” and “PURE (LB + HS)” (Fig. 25). Judging by the band intensity and purity of Ni-NTA binding protein fraction, soluble expression of **LNAS** was improved 6-7x higher in supplemented (500 mM NaCl, 500mM sorbitol) cultures and in heat-shocked cell cultures than in control media. As soluble **LNAS** expression increases, preferential binding to Ni-NTA resin results in less copurifying proteins. The purified fractions were not quantified, due to varying amounts of contamination, but it can be roughly estimated that under the ideal expression conditions, soluble **LNAS** produced was < 0.5 mg. L^{-1} cell culture. The purification of **LNAS** under denaturing conditions yielded highly pure recombinant protein (Fig. 26).

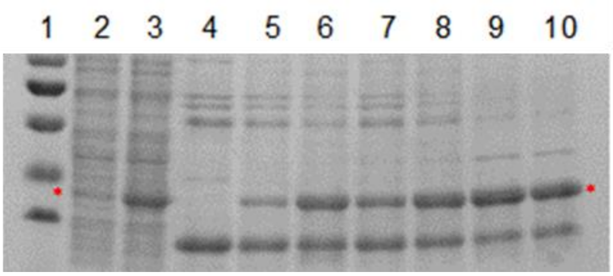

Figure 25: SDS-PAGE analysis of **LNAS** purified from 1 L of various expression media. Expression media and heat shocking (HS) alone account for variance in soluble **LNAS** production. A red asterisk indicates recombinant protein, approximately 35 kDal. (Lane 1: PageRuler Plus Prestained Ladder, Lane 2: E. coli lysate (Negative control), Lane 3: Protein Induction (0.5mM IPTG, Lysate), Lane 4: PURE (Negative control), Lane 5: PURE (LB), Lane 6: PURE (LB +HS), Lane 7: PURE (250mM NaCl/Sorbitol), Lane 8: PURE (250mM NaCl/Sorbitol +HS), Lane 9: PURE (500mM NaCl/Sorbitol), Lane 10: PURE (500mM NaCl/Sorbitol +HS.

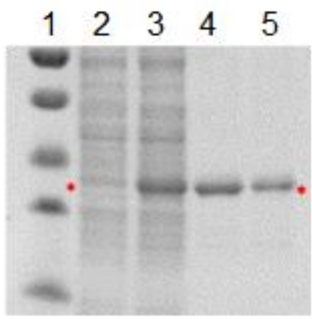

Figure 26: SDS-PAGE analysis of expression, purification and renaturation of **LNAS**. A red asterisk indicates recombinant protein, approximately 35 kDal. Lane 1: PageRuler Plus Prestained Protein Ladder, Lane 2: *E. coli* lysate (Negative control), Lane 3: Protein Induction (0.5 mM IPTG, Lysate), Lane 4: Denatured/PURE NAS (0.5 µg), Lane 5: Renaturation (0.25 µg).

The final yield of purified denatured **LNAS** was 2.5 mg/L bacterial culture (Unsupplemented LB media, standard expression conditions). Various attempts at slow dialysis removal of denaturant proved ineffective and properly refolding **LNAS**. Three conditions were observed to have a beneficial effect on refolding of **LNAS**: high pH (>8.5), reducing conditions (1 mM DTT), and 0.4 M sucrose. The addition of 20 µM SAM slightly improved refolding efficiency (86% recovery of soluble **LNAS**, refolding solution #15), but was omitted from large scale renaturation due to potentially effecting enzyme assays. Refolding solution #15 (50 mM Tris-Cl pH 8.5, 240 mM NaCl, 10 mM KCl, 2 mM $MgCl_2$, 2 mM $CaCl_2$, 0.4 M sucrose, 1 mM DTT) was selected for large scale renaturation of **LNAS** (Fig. 27). A similar recovery of soluble enzyme was recovered by large scale renaturation experiments, yielding a percent recovery of 78% soluble **LNAS**.

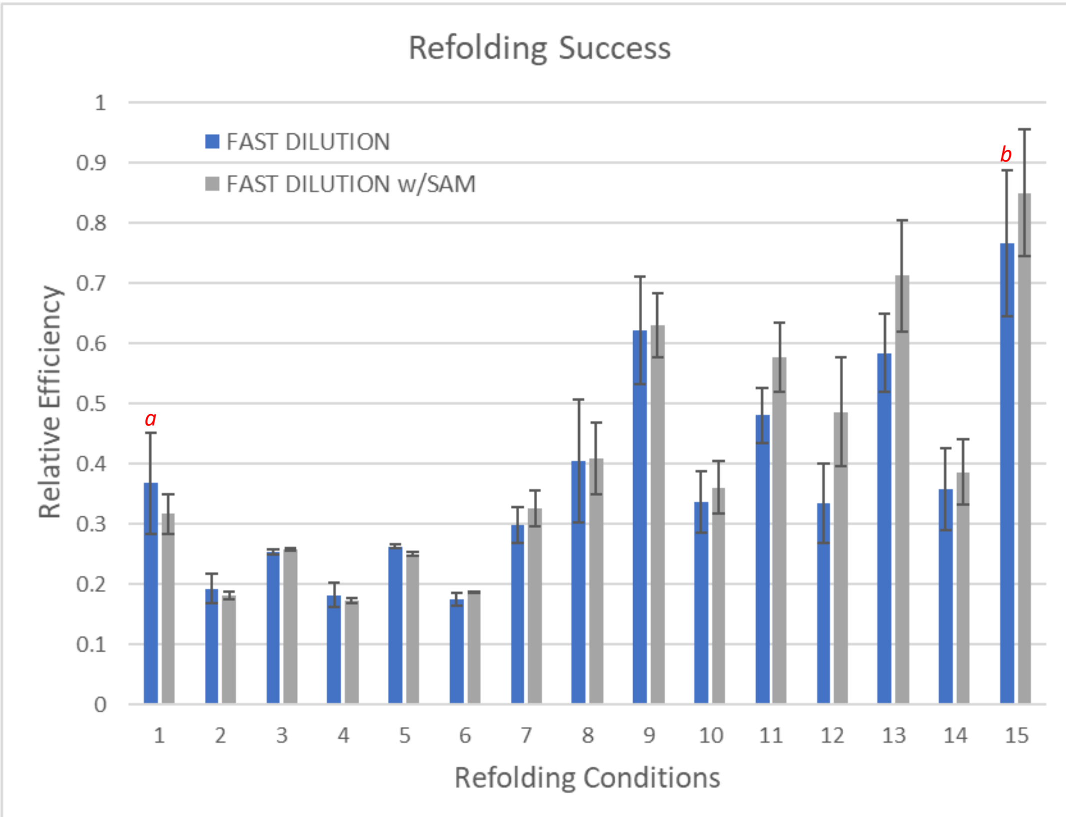

Figure 27: Relative efficiency of 15 solutions in their ability to refold **LNAS** in a soluble form. Improved refolding is observed in alkaline solutions (#8-15) and with reducing agents (odd #). The effect of substrate (20 µM SAM) on **LNAS** refolding indicates a minor benefit, ($n=3$, $p < 0.05$)

4.2. Multi-enzyme assays: Troubleshooting LNAS activity and maximizing NA production

Differences in initial substrate concentration (25 µM in commercial SAM vs. 30 µM in enzymatic SAM) was produced from minor errors in providing precise amounts of L-methionine and ATP in the “activating” solution. The natural degradation of SAM over the 18-hour assay ensured that accurate measurements were made with respect to NA-synthase activity (Fig. 28.A, B.). Thereby, the “true” rate of substrate consumption is conveyed as NA production (Fig. 28.C.) and the initial reaction rate can be roughly judged as: racemic SAM, V_{max} = 0.25 μM. h^{-1}; pure (S,S)-SAM, V_{max} = 1.25 μM. h^{-1}, in terms of NA production.

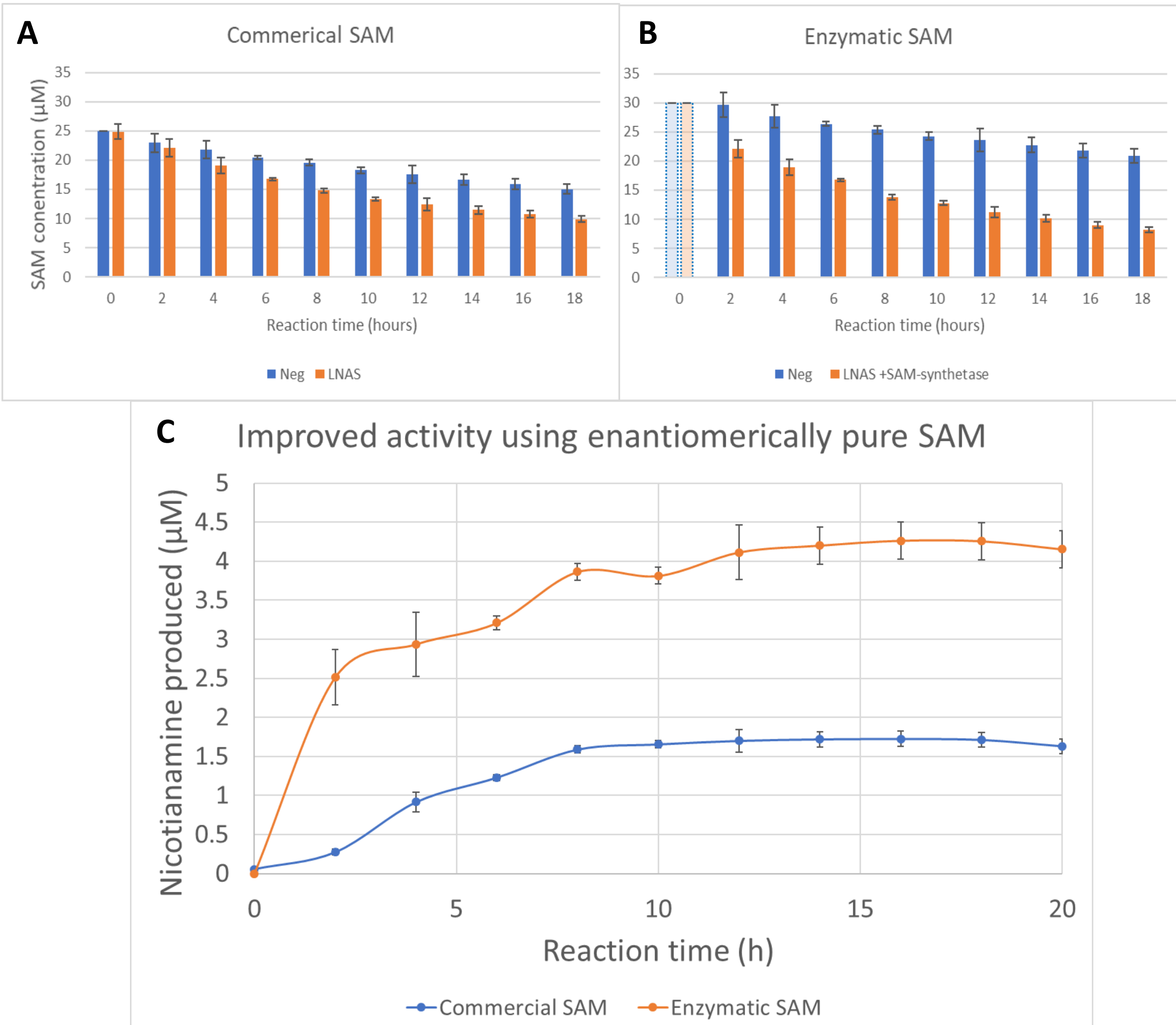

Figure 28: The starting concentration of SAM in (**B**) is approximated (At "0 hour" SAM has yet to be produced enzymatically). The difference in SAM reduction between negative controls and enzyme assays, from **A** and **B**, was reinterpreted to depict nicotianamine production (**C**). The concentration of enzyme present is 0.4 mg. mL^{-1} **LNAS** and 0.4 μg. mL^{-1} **LSAM** (for enzymatic SAM assays), n=3.

Relevant kinetic values and MTA production are summarized in Table 6, extrapolated from the activity measured in Fig. 28.C. Commercial SAM stock solutions were analyzed by HPLC to determine purity, specifically to determine the amount of MTA present. Pure MTA was used as a reference and indicated 2% contamination in stock SAM solutions. Enzyme assays containing 25 µM commercial SAM were therefore presumed to start with an MTA concentration of 0.5 µM (Table 6).

Table 6: The rate of nicotianamine production with respect to inhibitor concentration. Commercial SAM was found to contain 2% MTA. The concentration of enzyme present is 0.4 mg. mL^{-1} **LNAS** and 0.4 µg. mL^{-1} **LSAM** (for enzymatic SAM assays), n=3.

	Commerical SAM		**Enzymatic SAM**	
	NA production rate (µM. h-1)	**MTA conc. (µM)**	**NA production rate, (µM. h-1)**	**MTA conc. (µM)**
0 h	0	0.5	0	0
2 h	0.25*	1.25	1.25*	7.5
8 h	0.21	5	0.25	11.6
16 h	0	5.75	0	12.8
	* or 0.06 picokat. mg-1 **LNAS**		* or 0.28 picokat. mg-1 **LNAS**	

During this window of the assay, from 2 to 8 hours' reaction time, inhibition by MTA can be distinguished by that from (R, S)-SAM. It should be noted that assays containing enzymatic SAM exhibit a much faster reaction rate and cease activity at 12.75 µM MTA, while assays containing commercial SAM cease activity when MTA reaches 5.75 µM. The difference is approximately two-fold and suggests strong inhibitory effects produced by (R, S)-SAM, comparable inhibition to that produced by MTA. The difference in SAM is apparent from comparing the start of each assay, as during this initial phase SAM is being consumed as it is being produced (for enzymatic SAM assays). The rate of SAM depletion, which can be attributed to **LNAS**, ceases at hour 12. Stability tests by Matos et al. (1987) show that the rate of SAM epimerization is less than the rate of degradation and such an assumption may be made given the condition of this assay. Regardless, due to the accumulation of MTA, further **LNAS** activity is not possible.

LNAS activity was not changed with the addition of homoserine or azetidine-2-carboxylic acid. The addition of hydroxylamine, up to 500 µM, did not inhibit **LNAS** activity.

4.3. The effect of MTA-degradation in multi-enzyme LNAS assays

When only two-enzymes are used, either (SAM-synthetase + NA synthase) or (NA synthase + MTA-nucleosidase), in vitro NA production is extremely limited, albeit the latter combination is far more productive. Substrate inhibition by (R, S)-SAM in commercially purified substrate is still apparent, limiting in vitro production to 12 µM NA (Fig. 29). For proper comparison, as shared in the previous section, NA production did not exceed 1.5 µM (**LNAS** only) and 4.3 µM (**LSAMS** + **LNAS**). When all three enzymes are utilized (SAM-synthetase + NA synthase + MTA-nucleosidase) Special considerations were taken to ensure that the periplasmic extract did not catalyze SAM or ATP, which could be incorrectly attributed to **LNAS**.

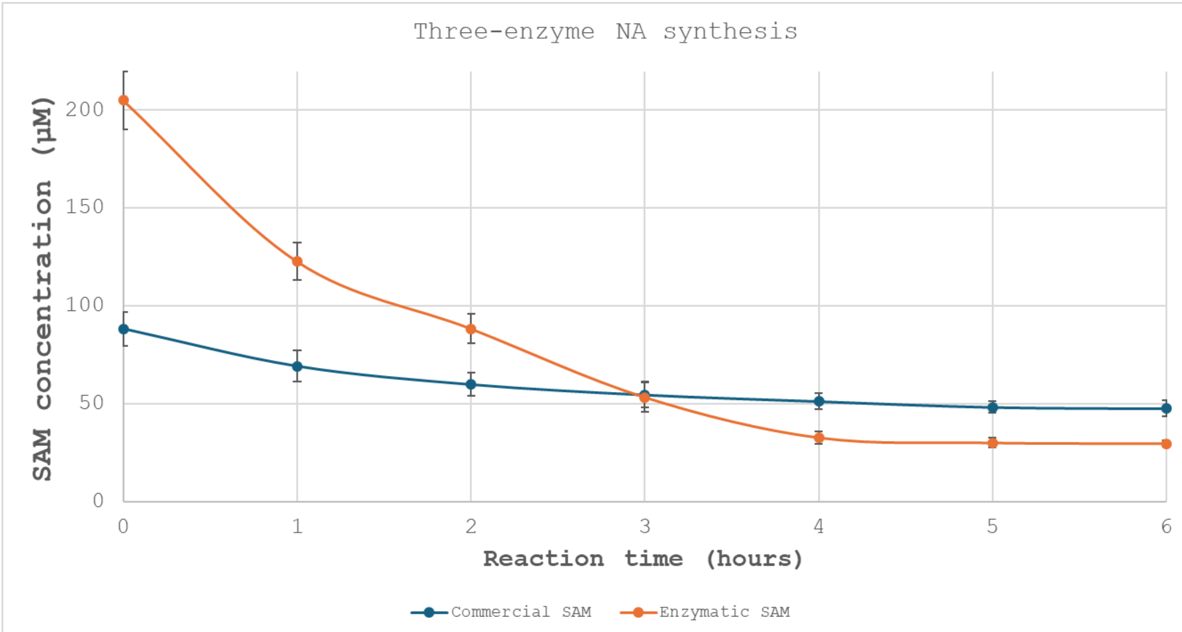

Figure 29: Optimal NA production in three enzyme assays. The final concentration of enzyme present is 0.15 mg. mL^{-1} **LNAS**, 0.1 µg. mL^{-1} DsbA-**LMTAN** and 0.1 µg. mL^{-1} **LSAM** (for enzymatic SAM assays), n=3.

4.4. Strategies to improve in vitro NA-synthase activity

Contamination of commercial SAM preparations was not particularly concerning, at least not due to degradation. No adenine was detected in commercial SAM solutions and a 2% contamination by MTA is not likely the cause for such a slower reaction rate (Table 6). Contamination by (R, S)-SAM, naturally produced by racemization, must be the cause for the inhibition in assays containing commercial SAM. This study shows that the in situ production of SAM must be considered for future in vitro studies. Higuchi et al. (1994) describes the optimum pH as 9.0 for NA-synthase, whereas the optimum pH of bacterial SAM-synthetases range 7-8 (Park et al., 1994; Kamarthapu et al., 2006). Plant SAM-synthetases are less sensitive to inhibition and more tolerant to extreme conditions (pH and temperature) than bacterial SAM-synthetases (Carrillo and Borthakur, 2022), therefore they may be a preferable choice for in vitro applications.

Alternative/unorthodox methods were attempted to improve NA-synthase activity, none of which were effective. As for the *A. koa* SAM-synthetase enzyme assays, the effect of acetonitrile and methanol was evaluated in **LNAS** assays. The addition of organic solvents, up to 25%, relieved feedback inhibition in *Acacia koa* SAM-synthetase assays (Carrillo and Borthakur, 2024) but a similar effect was not apparent in **LNAS** assays. Addressing the hydrophobicity of the substrate binding site is a valid approach, either by changing in vitro conditions or by mutagenesis. Wu et al. (2008) has noted how the hydrophobicity of substrate binding sites may affect MTA inhibition for spermine synthase. Unfortunately, mutagenesis studies have yet to improve the activity of any MTA-sensitive enzyme. The substrate binding site is highly conserved in NA-synthase, though **K191** and **E217** exhibit some variability (multiple sequence alignment, Fig. 24).

Part V: Gene expression analysis following iron fertilization of giant leucaena seedlings

5.1. Real-time PCR

A moderate increase in gene expression, a 2-5 fold increase, can be considered as typical (Fig. 30). Exceptional response to treatment includes NA-synthase (10-30 fold increase), FRO2 (15-fold increase in root only), mimosinase (10-20 fold increase) and glutathione synthase (20-fold increase). In general, upregulation was expected since the selected genes have known functions in iron homeostasis (ferric reduction oxidase-2

(FRO2), IRT2, yellow strip-like (YSL) transporters, NA-synthase) or in oxidative stress management (glutathione pathway, polyamine/ethylene pathway, catalase).

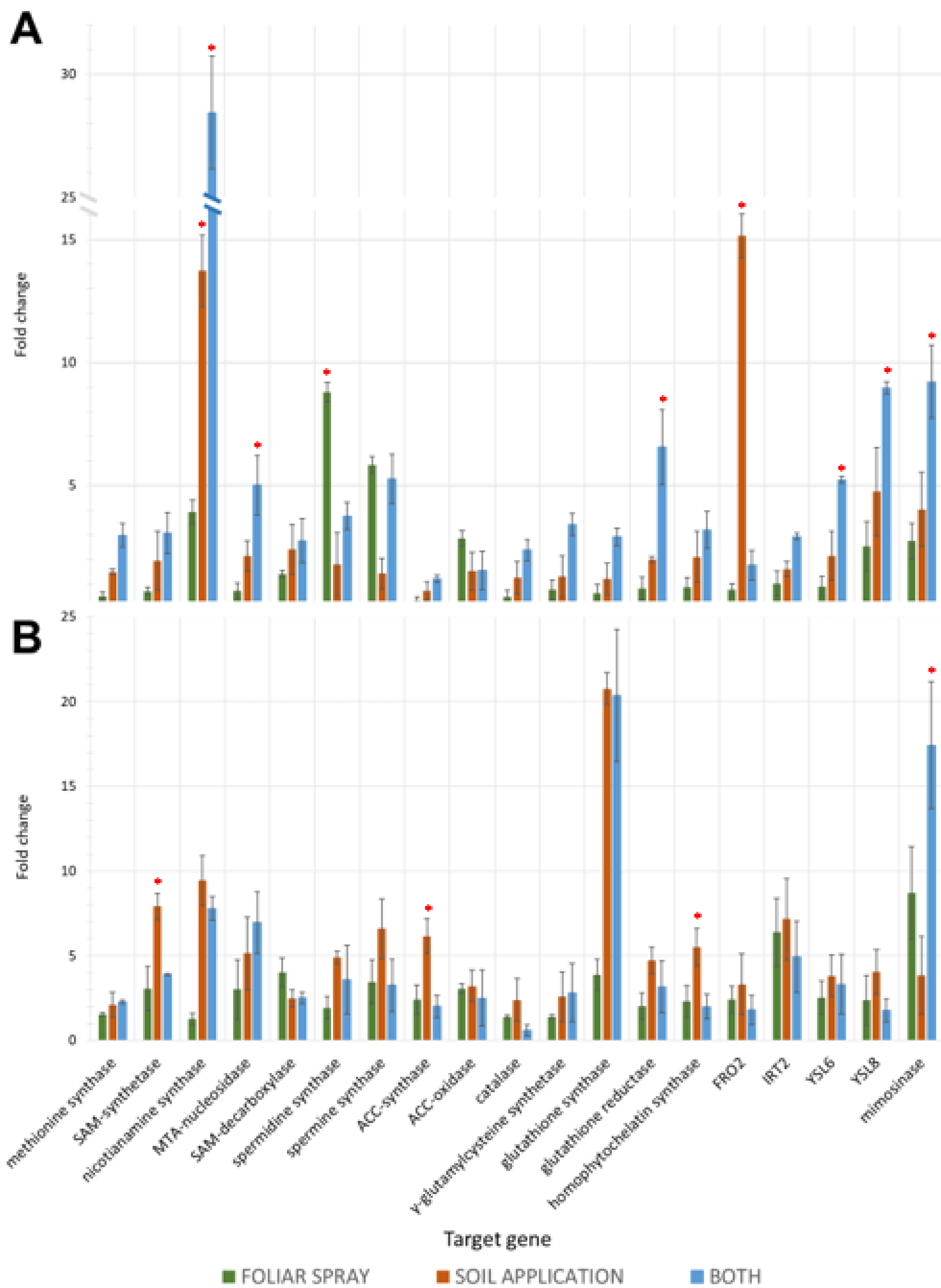

Figure 30: Relative fold change of select genes from root (**A**) and shoot (**B**) tissue following iron treatment, (n = 3). Statistical significance is denoted by red asterisks and is defined by two criteria; a minimum 5 fold-change increase and $p < 0.05$ according to statistical analysis performed using BootstRatio (Clèries et al., 2012).

5.1. *Interpreting qPCR results: direct application vs. internal trafficking of iron*

The gene expression measured in this study agrees with previous qPCR experiments from our lab. Examples include leaf-specific expression of mimosinase and root-specific expression of FRO2 (Honda and Borthakur (2020). The predominant expression of NA-synthase in roots was shown by Ishihara et al., 2016.

The foliar application of iron caused the upregulation of many genes, although to a lesser degree compared to soil application. Metal uptake is clearly a much more efficient process at the root surface however the expression of NA-synthase should be noted. The combined effect of foliar+soil application of iron had a pronounced effect on NA-synthase expression compared to either application alone. Iron acquired through root uptake is quickly distributed by NA throughout the plant body, evident by the upregulation of many genes in foliar tissue (Fig. 30.B.). If iron is also applied to the foliage, then the aerial plant tissues cannot serve as a sink for excess iron. A compounding effect in gene upregulation is evident for NA-synthase, MTA-nucleosidase, YSL6 and glutathione-related gene expression in root tissue (Fig. 30.A.) For example, glutathione reductase expression is nearly tripled in foliar+soil treatments, which suggests that NA production has reached its functional limit. Therefore, as iron concentration becomes toxic, the glutathione-ascorbate cycle must now compensate for greater oxidative stress.

Aside from NA, the importance of glutathione can be noted in both root and leaf tissue. Glutathione synthase was affected most in leaf tissue (20-fold increase), while glutathione reductase was increased 7-fold in the roots. Glutathione and polyamines are often recognized as important metabolites in abiotic stress management. Plant studies can be readily found which demonstrate increased glutathione content and increased stress tolerance (cold/heat stress, salinity/drought, metal toxicity, etc.) due to the exogenous application of spermidine (Li et al., 2015; Nahar et al., 2017; Noctor et al., 2017). Regarding polyamine and ethylene production in the leaf (Fig. 29.B.), the soil application of iron elicited a strong increase in spermine synthase, spermidine synthase and ACC-synthase gene expression. It is unclear why a similar response is not apparent when iron is applied to soil *and* foliage, though this may be due to increased mimosine metabolism. Foliar application of iron appears to strongly induce mimosinase expression, although this is likely a stress response and not an iron-regulated one. This is supported by mimosinase expression in leaf tissue (Fig. 30.B.), which indicates minor upregulation of mimosinase when iron is acquired through root uptake only. Only when iron is applied to the foliage is mimosinase expression effected. This response agrees with a previous study on giant leucaena where stress response compounds, such as ethylene and jasmonic acid, were shown to increase mimosine metabolism (da Silva Rodrigues-Corrêa et al., 2019). Also seen upon foliar application is the upregulation of genes which precede ethylene biosynthesis; SAM-synthetase, SAM-decarboxylase, ACC-synthase. *Why are these stress regulated genes no longer increased in soil+foliage iron treatments?* Mimosine may be relieving iron induced stress, either by chelating free iron or serving as an antioxidant. The product of mimosinase, 3-hydroxy-4-pyridone (3H4P), has enhanced antioxidant properties compared to mimosine (Honda and Borthakur, 2021). Mimosine, or 3H4P, may have interesting applications for the study of metal tolerance in plants and nonplant organisms. More plant studies are needed which consider metal toxicity, stress response and the exogenous application of mimosine or 3H4P. Santos et al. (2016, 2021) has demonstrated that hydroxypyridones are effective at treating iron deficiency and increasing iron content in soybeans, however it is unclear if toxic amounts of iron would produce a similar stress response in the presence of 3H4P.

Spermine synthase, spermidine synthase and ACC-oxidase were upregulated in the root tissue following foliar application of iron, though this may be due to stress hormones produced by the shoot. Jasmonic acid and abiotic stress induced a ten-fold increase in spermidine synthase expression in the root tissue of *Panax ginseng* (Parvin et al., 2010). Although spermidine synthase is active in most tissues, gene expression analyses in Arabidopsis indicate much higher expression levels of spermidine synthase in roots (Hanzawa et al., 2002). Although the iron solution used in this study (5 mM Fe-DTPA, 0.05% Triton X-100 surfactant) did not produce tissue damage, it likely caused significant stress in foliar tissue. In preliminary testing, spraying with > 5 mM Fe-DTPA would result in slight leaf necrosis after 2-3 days. Therefore, it is likely that stress hormones produced in foliage, not iron, are eliciting the stress-response observed in the root (Fig. 30.A.).

~~~~~~~ CONCLUDING STATEMENTS ~~~~~~~

The catalytic differences between plant and nonplant SAM-synthetases remains an interesting subject. Many in vitro properties were demonstrated in this work, using the giant leucaena and *A. koa* SAM-synthetases, however in vivo effect of heterologous expression is entirely unexplored. Plant SAM-synthetases may allow for elevated SAM levels in bacterial hosts as they are unaffected by the host β-regulatory subunits. The growth rate of *pET14b-sams* transformed *E. coli* cell lines was noticeably faster than untransformed *E. coli* (observation only), possibly due to leaky expression. SAM-synthetase activity was shown to greatly affect growth rate in tobacco (Kim et al., 2012) and *E. coli* (Wang et al., 2005). Heterologous expression of plant SAM-synthetases may benefit microbial expression systems by granting higher stress tolerance, improving heterologous expression or improving secondary metabolite production. Overexpression of a bacterial SAM-synthetase in *Monascus ruber* mold increased monacolin-K production 3.3-fold (Lee et al., 2008).

Among higher plant species SAM-synthetase is a conserved enzyme (>85%), whereas a 60 – 70% homology is typical in comparison to nonplant SAM-synthetases. Extremophilic properties may be a general characteristic of all plant SAM-synthetases, however more examples of plant enzymes are required to confirm this. Although *A. koa* is a distinct species of Acacia, one endemic to the Hawaiian Islands, it can be described generally as a woody tropical legume. Giant leucaena is a woody tropical legume species as well, therefore perhaps their activity does not accurately represent all plant SAM-synthetases. In vitro assays of a dissimilar plant SAM-synthetase, such as one from a non-legume species, are required before a general claim can be made.

In addition to the unique in vitro activity of plant SAM-synthetases, SAM-related pathways may be heavily affected in vivo. Plant enzymes can produce interesting effects in nonplant hosts, such as increased salt tolerance in yeast (Dong et al., 2022; Tsai et al., 2022) or SAM-hyperaccumulation (Chan and Appling, 2003). This is likely due to different post-translational regulation strategies for plant and nonplant SAM-synthetases. Regarding the regulatory region proposed by Sekula et al. (2020), there is no known regulatory process for plant SAM-synthetases. This same site in bacterial and mammalian SAM-synthetases interact with a β-regulatory subunit (LeGros et al., 2000), whereas there is no regulatory subunit for plant SAM-synthetases. Suspected regulation by spermidine, spermine and nicotianamine was shown not to be the case for plant SAM-synthetases (Carrillo and Borthakur, 2022). The proposed function of this regulatory region (Fig. 13, 14, green residues) should be studied further by site-directed mutagenesis.

The effect from directly altering SAM production in yeast, e.g. heterologous expression of a plant SAM-synthetase, has not been studied. Distinguishing the in vitro activity of plant SAM-synthetases remains a new area of study, however in vivo type experiments are equally unexplored. The growth rate of *pET14b-sams* transformed *E. coli* cell lines was noticeably faster than untransformed *E. coli* (observation only), possibly due to leaky expression of recombinant enzyme. SAM-synthetase activity was shown to greatly affect growth rate in tobacco (Kim et al., 2012) and *E. coli* (Wang et al., 2005). Heterologous expression of plant SAM-synthetases may benefit microbial expression systems by granting higher stress tolerance, improving heterologous expression or improving secondary metabolite production. In *Monascus ruber* mold expressing a bacterial SAM-synthetase, monacolin-K production increased 3.3-fold (Lee et al., 2008). In vitro activity suggests that plant SAM-synthetases are more productive, therefore they may be preferable to express in microbes.

Regarding the future of research on NA synthase, determining the crystal structure of the enzyme and important residues is required. Dreyfus et al. (2011) has shown, for thermo-NA-synthase, that intermediate compounds can bind similarly to the product. If it is possible to feed intermediate compounds to NA-synthase, thus reducing MTA production, then feedback inhibition may be reduced. This work has demonstrated that homoserine and A2C are not viable substrates, however the intermediate compounds in NA synthesis are not known. The rationale for alternative substrates requires a close examination of the reactions performed by NA-synthase.

1) *What is the first intermediate compound?* It is important to note that there is only one substrate binding site and one entrance to the reaction chamber, thus the first intermediate compound derived from SAM must be retained in the enzyme reaction chamber. The substrate compound SAM is unstable and can non-enzymatically degrade forming homoserine (Sun and Locasale, 2022), therefore the first intermediate compound may resemble homoserine. Radiolabeled homoserine was detected in C14 L-methionine feeding experiments studying NA biosynthesis (Shojima et al., 1990), however Kawai et al. (1994)

indicates that radioactive homoserine is not utilized directly in phytosiderophore biosynthesis. This study suggests that homoserine is not a viable substrate, therefore the binding of SAM may be required to position the aminopropyl group within the enzyme active site.

2) *How are azetidine groups produced in plants?* Other than NA, the only example of azetidine production is that of azetidine-2-carboxylic acid (A2C) (Fig. 31). The "Lily of the Valley" *Convallaria majalis* is notable for its production of high amounts of A2C although lesser amounts have been detected in *Beta vulgaris* (Rubenstein et al., 2006), *Nicotiana tabacum* (Leete, 1975) and *Fagus silvatica* L. (Kristensen and Larsen, 1974). The origin and biosynthesis of A2C is not known however there is reason to suggest that it may resemble NA biosynthesis. Leete et al. (1974) showed deuterium loss at C-2 of A2C, the same hydrogen shift observed by Ma and Nomoto (1994) in NA biosynthesis. Other isotope labelling experiments have indicated that SAM and homoserine were efficient precursors in A2C synthesis (Leete,1975; Leete et al., 1986). The requirement for any cofactors, such as PLP, have not been demonstrated however a bacterial enzyme, VioH from *Cystobacter violaceus*, can synthesize A2C from SAM without any cofactor (Yan and Müller, 2018).

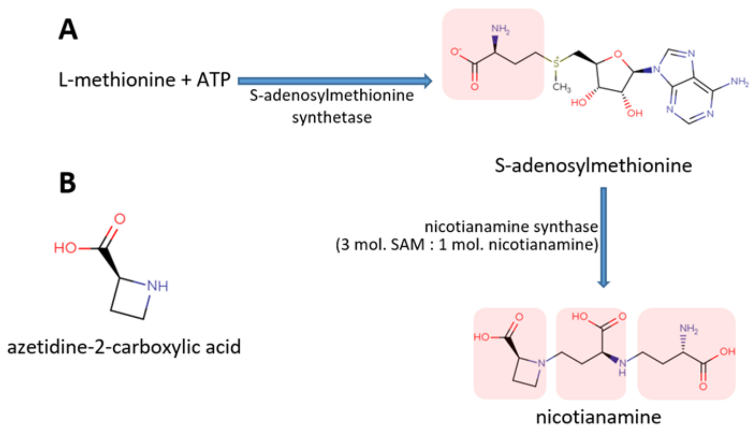

Figure 31: Relevant chemical structures and pathways involving NA. (A) Simplified pathway for nicotianamine biosynthesis. Individual aminopropyl groups are highlighted in red. (B) the chemical structure of A2C.

Some proposed intermediate compounds are shown in Fig. 32, which suggests that azetidine ring cyclization is the final step in NA synthesis. If cyclization was to occur first, it is unclear how intermediates could then be positioned for the proceeding aminopropyl group transfers. Also, since A2C had no effect on **LNAS** activity, cyclization is more likely to be the final step in NA biosynthesis.

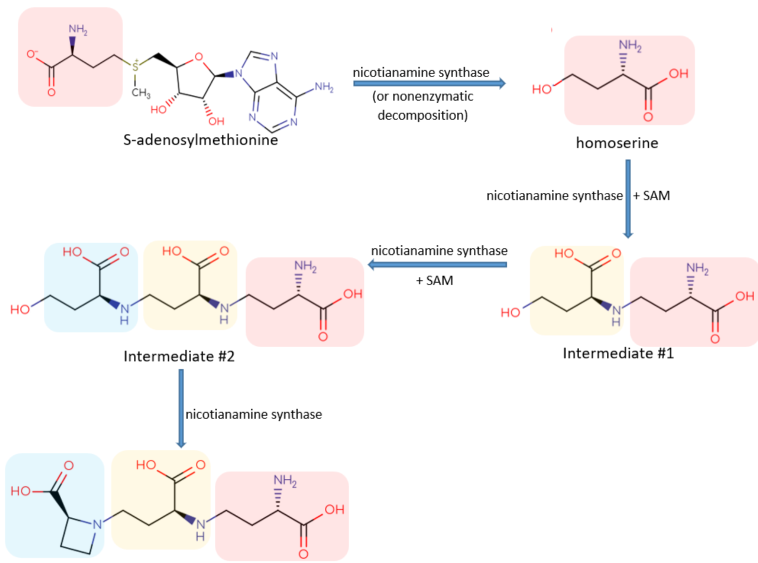

Figure 32: Hypothetical intermediate compounds and order of reactions in NA biosynthesis, starting with homoserine. Individual aminopropyl groups are highlighted.

3) *Do other aminopropyl transferases use covalent catalysis?* There are a few examples of SAM-dependent 3-amino-3-carboxypropyl (ACP) transferases which do not require PLP. BtaA from *Rhodobacter sphaeroides* (Riekhof et al., 2005), the enzyme NAT in nocardicin A biosynthesis (Reeve et al., 1998), TYW2 (Perche-Letuvée et al., 2014) and YfiP (Meyer et al., 2020), which modify bacterial transfer-RNA. These enzymes are quite different from NA-synthase and have not been characterized very well themselves. ACC-synthase shares many similarities to NA-synthase, though it requires a PLP cofactor. Otherwise, both are plant enzymes which perform a cyclization reaction from the ACP group of SAM. Different mechanisms have been proposed for ACC-synthase which suggest one-step cyclization (Ramalingam et al., 1985) or an enzyme bound intermediate (Li et al., 2005). The role of PLP as a cofactor for NA synthesis requires clarification

as it has been claimed to be a cofactor (Herbik et al., 1999) and some evidence suggests a PLP-mediated transamination. Ma and Nomoto (1994) used ^{13}C-, ^{2}H-, and ^{15}N-labeled methionine to reveal the loss of deuterium at the C-2 carbon in NA synthesis, hydrogen rearrangement typical among PLP-dependent enzymes. Unfortunately, Ma and Nomoto (1994) dismiss a PLP cofactor for unclear reasons. A strictly conserved lysine residue is observed in the reaction chamber of every NS-synthase/NS-synthase-like protein sequence, further suggesting a PLP cofactor. However, most in vitro experiments (Higuchi et al., 1999; Schmiedeberg et al., 2003; Shojima et al. 1989a, 1989b; Suzuki et al., 1999) have confirmed NA-synthase activity in the absence of cofactors. Since PLP is clearly not a cofactor for NA-synthase, perhaps an enzyme bound intermediate facilitates the hydrogen shift at C-2 reported by Ma and Nomoto (1994). Unfortunately, such a reaction is unprecedented and no examples can be found.

Renaturation of LNAS was the method of choice for producing active enzyme. In vitro translation was attempted, using E. coli and wheat germ expression systems, however these were not successful and would otherwise produce very little enzyme. Although heat shocking cultures was extremely effective, renaturation was the only method capable of producing large amounts of enzyme. The observed activity of **LNAS**, albeit very poor, aligns with NA-synthase activity reported by Schmiedeberg et al. (2003), Herbik et al. (2009) and Seebach et al. (2023). In general, these in vitro assays required large amounts of NA-synthase and were strongly inhibited by MTA. Soluble expression of a C-terminal His-tagged NA-synthase was reported by Seebach et al. (2023), however the yield of soluble protein was not specified. In our experience, NA-synthase expression in *E. coli* has been problematic when fused with a C-terminal tag, N-terminal tag or with no tag.

Most studies which utilize yeast successfully produce NA in vivo, therefore it is possible that active recombinant NA-synthase could be purified for in vitro purposes. Variable yield of NA was observed by *Saccharomyces pombe*, expressing the *N. crassa* NA-synthase, producing between 60 and 750 µg NA per 120 mL culture (Schmidt et al., 2011). Haydon et al. (2012) improved NA production 1.6-fold in engineered yeast coexpressing the vacuolar Zn-transporter ZIF1. Yeast mutants with elevated SAM content were engineered to express Arabidopsis NA-synthase, accumulating quantities of NA (µg. g-1 dry weight) comparable to soybean (Wada et al., 2006). Despite these achievements using yeast, as with purifying NA from plant tissue, a tremendous amount of effort is required to produce refined NA (Asai et al., 2005). While in vitro methods may benefit the purification process, it is currently limited and not viable. Seebach et al., (2023) has shown by using SAM-synthetase, NA-synthase and MTA-nucleosidase, up to 0.5 mM NA could be produced. Scaling up such a reaction would be too difficult, as approximately 1 mg of recombinant NA-synthase would be required to produce 1 mg of NA. The activity of NA-synthase requires closer examination and in vitro methods must be further improved.

~~~~~~~~~~~~~ REFERENCES ~~~~~~~~~~~~~

1. Ahn, Y.O., Kim, S.H., Lee, J., Kim, H., Lee, H.S., Kwak, S.S., 2012. Three *Brassica rapa* metallothionein genes are differentially regulated under various stress conditions. Molecular Biology Reports 39, 2059–2067.
2. Aisyah, S., Gruppen, H., Madzora, B., Vincken, J.P., 2013. Modulation of isoflavonoid composition of *Rhizopus oryzae* elicited soybean (*Glycine max*) seedlings by light and wounding. Journal of agricultural and food chemistry 61(36), 8657-8667.
3. Al Khateeb, W., Al-Qwasemeh, H., 2014. Cadmium, copper and zinc toxicity effects on growth, proline content and genetic stability of *Solanum nigrum* L., a crop wild relative for tomato; comparative study. Physiology and Molecular Biology of Plants 20, 31–39.
4. Álvarez, L., Mingorance, J., Pajares, M.A., Mato, J.M., 1994. Expression of rat liver S-adenosylmethionine synthetase in *Escherichia coli* results in two active oligomeric forms. Biochemical Journal 301(2), 557-561.
5. Angelova, V.R., Grekov, D.F., Kisyov, V.K., Ivanov, K.I., 2015. Potential of lavender (*Lavandula vera* L.) for phytoremediation of soils contaminated with heavy metals. International Journal of Biological, Food, Veterinary and Agricultural Engineering 9, 465–472.
6. Asai, S., Obata, A., Yamazaki, E., Kinoshita, E., Kikuchi, M., Kikkoman Corp, 2005. Method for preparing nicotianamine or nicotianamine-containing product. U.S. Patent 6,949,263.
7. Bageel, A., Honda, M.D., Carrillo, J.T., Borthakur, D., 2020. Giant leucaena (*Leucaena leucocephala* subsp. glabrata): a versatile tree-legume for sustainable agroforestry. Agroforestry Systems 94(1), 251-268.
8. Bali, S., Jamwal, V.L., Kohli, S.K., Kaur, P., Tejpal, R., Bhalla, V., Ohri, P., Gandhi, S.G., Bhardwaj, R., Al-Huqail, A.A., Siddiqui, M.H., 2019. Jasmonic acid application triggers detoxification of lead (Pb) toxicity in tomato through the modifications of secondary metabolites and gene expression. Chemosphere 235, 734-748.
9. Barbosa, B.C.F., Silva, S.C., de Oliveira, R.R., Chalfun, A., 2017. Zinc supply impacts on the relative expression of a metallothionein-like gene in *Coffea arabica* plants. Plant and Soil 411, 179–191.
10. Barz, W., Mackenbrock, U., 1994. Constitutive and elicitation induced metabolism of isoflavones and pterocarpans in chickpea (*Cicer arietinum*) cell suspension cultures. Plant Cell, Tissue and Organ Culture 38(2), 199-211.
11. Batish, D.R., Lavanya, K., Singh, H.P., Kohli, R.K., 2007. Phenolic allelochemicals released by *Chenopodium murale* affect the growth, nodulation and macromolecule content in chickpea and pea. Plant Growth Regulation 51, 119–128.
12. Beck, A., Lendzian, K., Oven, M., Christmann, A., Grill, E., 2003. Phytochelatin synthase catalyzes key step in turnover of glutathione conjugates. Phytochemistry 62, 423–431.
13. Benatti, M.R., Yookongkaew, N., Meetam, M., Guo, W.J., Punyasuk, N., AbuQamar, S., Goldsbrough, P., 2014. Metallothionein deficiency impacts copper accumulation and redistribution in leaves and seeds of Arabidopsis. New Phytologist 202, 940–951.
14. Blum, R., Beck, A., Korte, A., Stengel, A., Letzel, T., Lendzian, K., Grill, E., 2007. Function of phytochelatin synthase in catabolism of glutathione-conjugates. The Plant Journal 49, 740–749.
15. Borchardt, R.T., Wu, Y.S., 1976. Potential inhibitors of S-adenosylmethionine-dependent methyltransferases. 5. Role of the asymmetric sulfonium pole in the enzymic binding of S-adenosyl-L-methionine. *Journal of medicinal chemistry* 19(9), 1099-1103.
16. Boyd, R.S., 1998. Hyperaccumulation as a plant defensive strategy. In: Brooks, R.R. (Eds.), Plants That Hyperaccumulate Heavy Metals, Centre for Agriculture and Bioscience International, Oxford, pp. 181-201.
17. Buchanan-Wollaston, V., 1994. Isolation of cDNA clones for genes that are expressed during leaf senescence in *Brassica napus* (identification of a gene encoding a senescence-specific metallothionein-like protein). Plant Physiology 105, 839–846.
18. Cabral, A.C.S., Jakovleska, J., Deb, A., Penner-Hahn, J.E., Pecoraro, V.L., Freisinger, E., 2018. Further insights into the metal ion binding abilities and the metalation pathway of a plant metallothionein from *Musa acuminata*. Journal of Biological Inorganic Chemistry 23, 91–107.

19. Callahan, D.L., Kolev, S.D., O'Hair, R.A.J., Salt, D.E., Baker, A.J.M., 2007. Relationships of nicotianamine and other amino acids with nickel, zinc and iron in Thlaspi hyperaccumulators. New Phytologist 176, 836–848.
20. Cao, C., Nie, K., Xu, H., Liu, L., 2023. High-Throughput Screening and Directed Evolution of Methionine Adenosyltransferase from *Escherichia coli*. Applied Biochemistry and Biotechnology, pp.1-14.
21. Carlson, R.E., Dolphin, D.H., 1981. Chromatographic analysis of isoflavonoid accumulation in stressed *Pisum sativum*. Phytochemistry 20(9), 2281-2284.
22. Carrillo, J.T., Borthakur, D., 2021. Methods for metal chelation in plant homeostasis. *Plant Physiology and Biochemistry*163, 95-107.
23. Carrillo, J.T., Borthakur, D., 2022. Heterologous expression and characterization of a thermoalkaliphilic SAM-synthetase from giant leucaena (*Leucaena leucocephala* subsp *glabrata*). *Plant Physiology and Biochemistry* 181, 42-49.
24. Carrillo, J.T., Borthakur, D., 2023. Characterization of a Plant S-Adenosylmethionine Synthetase from *Acacia Koa*. Available at SSRN 4651464.
25. Castillo-González, J., Ojeda-Barrios, D., Hernández-Rodríguez, A., González-Franco, A.C., Robles-Hernández, L., López-Ochoa, G.R., 2018. Zinc Metalloenzymes in Plants. Interciencia 43(4), 242-248.
26. Chan, S.Y., Appling, D.R., 2003. Regulation of S-adenosylmethionine levels in Saccharomyces cerevisiae. Journal of Biological Chemistry 278(44), 43051-43059.
27. Chang, Y.C., Yamamoto, Y., Matsumoto, H., 1999. Accumulation of aluminium in the cell wall pectin in cultured tobacco (*Nicotiana tabacum* L.) cells treated with a combination of aluminium and iron. Plant, Cell & Environment 22, 1009–1017.
28. Che, W.M., Hsieh, H.M., Huang, P.C., 1998. Type 2 rice metallothionein-like gene has two introns. DNA Sequence 8, 223–228.
29. Chen, S.Y., Chi, W.C., Trinh, N.N., Cheng, K.T., Chen, Y.A., Lin, T.C., Lin, Y.C., Huang, L.Y., Huang, H.J., Chiang, T.Y., 2015. Alleviation of allelochemical juglone-induced phytotoxicity in tobacco plants by proline. Journal of Plant Interactions, 10(1), 167-172.
30. Cherest, H., Surdin-Kerjan, Y., 1981. The two methionine adenosyl transferases in Saccharomyces cerevisiae: evidence for the existence of dimeric enzymes. Molecular and General Genetics MGG, 182(1), 65-69.
31. Chobot, V., Hadacek, F., 2009. Milieu-dependent pro-and antioxidant activity of juglone may explain linear and nonlinear effects on seedling development. *Journal of chemical ecology* 35, 383-390.
32. Choi, H.L., Seo, J.W., Hwang, M.H., Yu, C.Y., Seong, E.S., 2022. MsSAMS, a cold stress-responsive gene, provides resistance to environmental stress in T2-generation transgenic plants. *Transgenic Research*, 1-9.
33. Clèries, R., Galvez, J., Espino, M., Ribes, J., Nunes, V., de Heredia, M.L., 2012. BootstRatio: a web-based statistical analysis of fold-change in qPCR and RT-qPCR data using resampling methods. *Computers in biology and medicine*, *42*(4), 438-445.
34. Codon Optimization Tool® program, IDT, Coralville, Iowa, USA. Accessed 17 March, 2022. https://www.idtdna.com/CodonOpt.
35. Coyle, P., Philcox, J.C., Carey, L.C., Rofe, A.M., 2002. Metallothionein: the multipurpose protein. Cellular and Molecular Life Sciences 59, 627–647.
36. da Silva Rodrigues-Corrêa, K.C., Honda, M.D., Borthakur, D., Fett-Neto, A.G., 2019. Mimosine accumulation in *Leucaena leucocephala* in response to stress signaling molecules and acute UV exposure. *Plant Physiology and Biochemistry* 135, 432-440.
37. Dabrowska, G., Mierek-Adamska, A., Goc, A., 2012. Plant metallothineins: putative functions identified by promoter analysis in silico. Acta Biologica Cracoviensia Series Botanica, 54.
38. Dai, Y., Gold, B., Vishwanatha, J.K., Rhode, S.L., 1994. Mimosine inhibits viral DNA synthesis through ribonucleotide reductase. Virology 205, 210–216.
39. De Benedictis, M., Brunetti, C., Brauer, E.K., Andreucci, A., Popescu, S.C., Commisso, M., Guzzo, F., Sofo, A., Ruffini Castiglione, M., Vatamaniuk, O.K., Sanità di Toppi, L., 2018. The *Arabidopsis*

thaliana knockout mutant for phytochelatin synthase1 (cad1-3) is defective in callose deposition, bacterial pathogen defense and auxin content, but shows an increased stem lignification. Frontiers in Plant Science 9, 19.

40. Delalande, O., Desvaux, H., Godat, E., Valleix, A., Junot, C., Labarre, J., Boulard, Y., 2010. Cadmium–glutathione solution structures provide new insights into heavy metal detoxification. The Federation of European Biochemical Societies, 277 (24), 5086-5096.
41. Dereeper, A., Guignon, V., Blanc, G., Audic, S., Buffet, S., Chevenet, F., Dufayard, J.F., Guindon, S., Lefort, V., Lescot, M. ,Claverie, J.M., 2008. Phylogeny. fr: robust phylogenetic analysis for the non-specialist. Nucleic acids research, 36(suppl_2), W465-W469.
42. Desiderio, C., Cavallaro, R.A., De Rossi, A., D'Anselmi, F., Fuso, A., Scarpa, S., 2005. Evaluation of chemical and diastereoisomeric stability of S-adenosylmethionine in aqueous solution by capillary electrophoresis. *Journal of pharmaceutical and biomedical analysis* 38(3), 449-456.
43. Devvret, P.K., Pant, K., Thapliyal, A., Tufchi, N., 2017. Bioinformatics approach toward the Identification of Binding Pockets of Rice Metallothionein and its interaction with the heavy metals. International Journal of Pharmacy Research & Technology 7, 8–14.
44. Dhar, H., Swarnkar, M.K., Gulati, A., Singh, A.K., Kasana, R.C., 2015. Draft genome sequence of a cellulase-producing psychrotrophic Paenibacillus strain, IHB B 3415, isolated from the cold environment of the Western Himalayas, India. Genome announcements 3(1), e01581-14.
45. Ding, C., Chen, T., Yang, Y., Liu, S., Yan, K., Yue, X., Zhang, H., Xiang, Y., An, L., Chen, S., 2015. Molecular cloning and characterization of an S-adenosylmethionine synthetase gene from *Chorispora bungeana*. Gene 572(2), 205-213.
46. Dixon, D.P., Lapthorn, A., Edwards, R., 2002. Plant glutathione transferases. Genome Biology 3, 1–10.
47. Domı´nguez-Solı´s, J.R., Gutiérrez-Alcalá, G., Vega, J.M., Romero, L.C., Gotor, C., 2001. The cytosolic O-acetylserine (thiol) lyase gene is regulated by heavy metals and can function in cadmium tolerance. Journal of Biological Chemistry 276, 9297-9302.
48. Dong, G., Ma, D.P., Li, J., 2008. The histone methyltransferase SDG8 regulates shoot branching in Arabidopsis. Biochemical and biophysical research communications 373(4), 659-664.
49. Dong, Y., Zhang, L., Chang, X., Wang, X., Li, G., Chen, S., Jin, S., 2022. Overexpression of LpCPC from *Lilium pumilum* confers saline-alkali stress (NaHCO3) resistance.Plant Signaling & Behavior17(1), 2057723.
50. Douchkov, D., Gryczka, C., Stephan, U.W., Hell, R., Bäumlein, H., 2005. Ectopic expression of nicotianamine synthase genes results in improved iron accumulation and increased nickel tolerance in transgenic tobacco. Plant, Cell & Environment 28, 365–374.
51. Drakakaki, G., Christou, P., Stöger, E., 2000. Constitutive expression of soybean ferritin cDNA in transgenic wheat and rice results in increased iron levels in vegetative tissues but not in seeds. Transgenic Research 9, 445–452.
52. Dreyfus, C., Larrouy, M., Cavelier, F., Martinez, J., Pignol, D., Arnoux, P., 2011. The crystallographic structure of thermoNicotianamine synthase with a synthetic reaction intermediate highlight the sequential processing mechanism. *Chemical Communications* 47(20), 5825-5827.
53. Dreyfus, C., Lemaire, D., Mari, S., Pignol, D., Arnoux, P., 2009. Crystallographic snapshots of iterative substrate translocations during nicotianamine synthesis in Archaea. *Proceedings of the National Academy of Sciences* 106(38), 16180-16184.
54. Duan, L., Kong, J.J., Wang, T.Q., Sun, Y., 2018. Binding of Cd (II), Pb (II), and Zn (II) to a type 1 metallothionein from maize (*Zea mays*). Biometals 31, 539–550.
55. Ebbs, M.L., Bender, J., 2006. Locus-specific control of DNA methylation by the Arabidopsis SUVH5 histone methyltransferase. The Plant Cell 18(5), 1166-1176.
56. Farago, M.E., Me, F., Wa, M., 1979. Plants which accumulate metals. IV. A possible copper-proline complex from the roots of *Armeria maritima*.
57. Fattahi, B., Arzani, K., Souri, M.K., Barzegar, M., 2019. Effects of cadmium and lead on seed germination, morphological traits, and essential oil composition of sweet basil (*Ocimum basilicum* L.). Industrial Crops and Products 138, 111584.

58. Faulds, C.B., Pérez-Boada, M., Martínez, Á.T., 2011. Influence of organic co-solvents on the activity and substrate specificity of feruloyl esterases. Bioresource technology 102(8), 4962-4967.

59. Fediuc, E., Lips, S.H., Erdei, L., 2005. O-acetylserine (thiol) lyase activity in Phragmites and Typha plants under cadmium and NaCl stress conditions and the involvement of ABA in the stress response. Journal of Plant Physiology 162, 865–872.

60. Fernandez, L.R., Vandenbussche, G., Roosens, N., Govaerts, C., Goormaghtigh, E., Verbruggen, N., 2012. Metal binding properties and structure of a type III metallothionein from the metal hyperaccumulator plant *Noccaea caerulescens*. Biochimica et Biophysica Acta (BBA)-Proteins and Proteomics 1824, 1016–1023.

61. Ferraz, P., Fidalgo, F., Almeida, A., Teixeira, J., 2012. Phytostabilization of nickel by the zinc and cadmium hyperaccumulator *Solanum nigrum* L. Are metallothioneins involved? Plant Physiology and Biochemistry 57, 254–260.

62. Fraser, R.S.S., Creanor, J., 1974. Rapid and selective inhibition of RNA synthesis in yeast by 8-hydroxyquinoline. European Journal of Biochemistry 46, 67–73.

63. Freeman, J.L., Garcia, D., Kim, D., Hopf, A., Salt, D.E., 2005. Constitutively elevated salicylic acid signals glutathione-mediated nickel tolerance in Thlaspi nickel hyperaccumulators. Plant Physiology 137, 1082–1091.

64. Freeman, J.L., Persans, M.W., Nieman, K., Albrecht, C., Peer, W., Pickering, I.J., Salt, D.E., 2004. Increased glutathione biosynthesis plays a role in nickel tolerance in Thlaspi nickel hyperaccumulators. The Plant Cell 16, 2176–2191.

65. Freisinger, E., 2008. Plant MTs—long neglected members of the metallothionein superfamily. Dalton Transactions 6663–6675.

66. Gade, M., Tan, L.L., Damry, A.M., Sandhu, M., Brock, J.S., Delaney, A., Villar-Briones, A., Jackson, C.J. and Laurino, P., 2021. Substrate dynamics contribute to enzymatic specificity in human and bacterial methionine adenosyltransferases. JACS Au 1(12), pp.2349-2360.

67. Gautam, N., Verma, P.K., Verma, S., Tripathi, R.D., Trivedi, P.K., Adhikari, B., Chakrabarty, D., 2012. Genome-wide identification of rice class I metallothionein gene: tissue expression patterns and induction in response to heavy metal stress. Functional & Integrative Genomics 12, 635–647.

68. Gekeler, W., Grill, E., Winnacker, E.L., Zenk, M.H., 1989. Survey of the plant kingdom for the ability to bind heavy metals through phytochelatins. Zeitschrift Für Naturforschung C 44, 361–369.

69. Gericó, T.G., Tavanti, R.F.R., de Lima, J.P., Ribeiro, R.P., dos Santos, L.C.C., da Silva, M.S., dos Reis, A.R., 2020. Cobalt and molybdenum stimulate compounds of primary metabolism, nitrogen forms, and photosynthetic pigments in peanut plants (*Arachis hypogaea* L.). Journal of Plant Nutrition 43(12), 1907-1922.

70. Gilbert, D.M., Neilson, A., Miyazawa, H., DePamphilis, M.L., Burhans, W.C., 1995. Mimosine Arrests DNA Synthesis at Replication Forks by Inhibiting Deoxyribonucleotide Metabolism (∗). *Journal of Biological Chemistry* 270(16), 9597-9606.

71. Goto, F., Yoshihara, T., Shigemoto, N., Toki, S., Takaiwa, F., 1999. Iron fortification of rice seed by the soybean ferritin gene. Nature Biotechnology 17, 282–286.

72. Grill, E., Zenk, M.H., Winnacker, E.L., 1985. Induction of heavy metal-sequestering phytochelatin by cadmium in cell cultures of *Rauvolfia serpentina*. Naturwissenschaften 72, 432–433.

73. Guo, W.J., Bundithya, W., Goldsbrough, P.B., 2003. Characterization of the Arabidopsis metallothionein gene family: tissue-specific expression and induction during senescence and in response to copper. New Phytologist 369–381.

74. Guo, W.J., Meetam, M., Goldsbrough, P.B., 2008. Examining the specific contributions of individual Arabidopsis metallothioneins to copper distribution and metal tolerance. Plant Physiology 146, 1697–1706.

75. Guranowski, A., 1983. Plant 5-methylthioribose kinase: properties of the partially purified enzyme from yellow lupin (*Lupinus luteus* L.) seeds. *Plant Physiology* 71(4), 932-935.

76. Han, Y., Sa, G., Sun, J., Shen, Z., Zhao, R., Ding, M., Deng, S., Lu, Y., Zhang, Y., Shen, X., Chen, S., 2014. Overexpression of *Populus euphratica* xyloglucan endotransglucosylase/hydrolase gene confers enhanced cadmium tolerance by the restriction of root cadmium uptake in transgenic tobacco. Environmental and Experimental Botany 100, 74–83.

77. Hanley-Bowdoin, L., Lane, B.G., 1983. A novel protein programmed by the mRNA conserved in dry wheat embryos: the principal site of cysteine incorporation during early germination. European Journal of Biochemistry 135, 9–15.
78. Hanzawa, Y., Imai, A., Michael, A.J., Komeda, Y., Takahashi, T., 2002. Characterization of the spermidine synthase-related gene family in *Arabidopsis thaliana*. *Febs Letters 527*(1-3), pp.176-180.
79. Harada, E., Sugase, K., Namba, K., Iwashita, T., Murata, Y., 2007. Structural element responsible for the Fe (III)--phytosiderophore specific transport by HvYS1 transporter in barley. Federation of European Biochemical Societies Letters 581, 4298–4302.
80. Hartley-Whitaker, J., Ainsworth, G., Vooijs, R., Ten Bookum, W., Schat, H., Meharg, A.A., 2001. Phytochelatins are involved in differential arsenate tolerance in *Holcus lanatus*. Plant Physiology 126, 299–306.
81. Harun-Ur-Rashid, M., Iwasaki, H., Parveen, S., Oogai, S., Fukuta, M., Hossain, M.A., Anai, T., Oku, H., 2018. Cytosolic cysteine synthase switch cysteine and mimosine production in *Leucaena leucocephala*. Applied biochemistry and biotechnology 186(3), 613-632.
82. Haverkamp, R.G., Marshall, A.T., van Agterveld, D., 2007. Pick your carats: nanoparticles of gold–silver–copper alloy produced in vivo. Journal of Nanoparticle Research 9, 697–700.
83. Haydon, M.J., Kawachi, M., Wirtz, M., Hillmer, S., Hell, R., Krämer, U., 2012. Vacuolar nicotianamine has critical and distinct roles under iron deficiency and for zinc sequestration in Arabidopsis. *The Plant Cell* 24(2), pp.724-737.
84. Heidari, P., Mazloomi, F., Nussbaumer, T., Barcaccia, G., 2020. Insights into the SAM synthetase gene family and its roles in tomato seedlings under abiotic stresses and hormone treatments. Plants 9(5), 586.
85. Herbik, A., Koch, G., Mock, H.P., Dushkov, D., Czihal, A., Thielmann, J., Stephan, U.W., Bäumlein, H., 1999. Isolation, characterization and cDNA cloning of nicotianamine synthase from barley: a key enzyme for iron homeostasis in plants. *European Journal of Biochemistry* 265(1), 231-239.
86. Higuchi, K., Kanazawa, K., Nishizawa, N.K., Chino, M., Mori, S., 1994. Purification and characterization of nicotianamine synthase from Fe-deficient barley roots. *Plant and Soil 165*, 173-179.
87. Higuchi, K., Suzuki, K., Nakanishi, H., Yamaguchi, H., Nishizawa, N.K., Mori, S., 1999. Cloning of nicotianamine synthase genes, novel genes involved in the biosynthesis of phytosiderophores. *Plant physiology* 119(2), 471-480.
88. Honda, M.D., Borthakur, D., 2020. Mimosine facilitates metallic cation uptake by plants through formation of mimosine–cation complexes. *Plant molecular biology*, 102, 431-445.
89. Honda, M.D., Borthakur, D., 2021. Mimosine is a stress-response molecule that serves as both an antioxidant and osmolyte in giant leucaena (*Leucaena leucocephala* subsp. *glabrata*) during environmental stress conditions. *Plant Stress 2*, 100015.
90. Hörger, A.C., Fones, H.N., Preston, G., 2013. The current status of the elemental defense hypothesis in relation to pathogens. Frontiers in Plant Science 4, 395.
91. Hsieh, H.M., Huang, P.C., 1998. Promoter structure and activity of type 1 rice metallothionein-like gene. DNA Sequence 9, 9–18.
92. Huang, G.Y., Wang, Y.S., 2009. Expression analysis of type 2 metallothionein gene in mangrove species (*Bruguiera gymnorrhiza*) under heavy metal stress. Chemosphere 77, 1026–1029.
93. Huang, H., Liu, R., Han, Y., Hao, J., Liu, C. Fan, S., 2021. Effects of exogenous spermidine on polyamine metabolism in lettuce (*Lactuca sativa* l.) under high-temperature stress. Pakistan Journal of Botany 53(5), 1571-1582.
94. Huber, T., Freisinger, E., 2013. Sulfide ions as modulators of metal–thiolate cluster size in a plant metallothionein. Dalton Transactions 42, 8878–8889.
95. Hudspeth, R.L., Hobbs, S.L., Anderson, D.M., Rajasekaran, K., Grula, J.W., 1996. Characterization and expression of metallothionein-like genes in cotton. Plant Molecular Biology 31, 701–705.
96. Ikegami, F., Mizuno, M., Kihara, M., Murakoshi, I., 1990. Enzymatic synthesis of the thyrotoxic amino acid mimosine by cysteine synthase. Phytochemistry 29(11), 3461-3465.

97. Ishihara, K., Lee, E.K., Borthakur, D., 2016a. An improved method for RNA extraction from woody legume species *Acacia koa* A. Gray and *Leucaena leucocephala* (Lam.) de Wit. *Int J Forrstry Wood Sci* 3, 31-35.

98. Ishihara, K., Lee, E.K., Rushanaedy, I., Borthakur, D., 2015. Illumina-based de novo transcriptome analysis and identifications of genes involved in the monolignol biosynthesis pathway in Acacia koa. American Journal of Bioinformatics 4(1), 7.

99. Ishihara, K.L., Honda, M.D., Pham, D.T., Borthakur, D., 2016. Transcriptome analysis of *Leucaena leucocephala* and identification of highly expressed genes in roots and shoots. Transcriptomics 4(135), 2.

100. Ishihara, K.L., Honda, M.D., Pham, D.T., Borthakur, D., 2016b. Transcriptome analysis of *Leucaena leucocephala* and identification of highly expressed genes in roots and shoots. *Transcriptomics* 4(135), 2.

101. Ishimaru, Y., Suzuki, M., Tsukamoto, T., Suzuki, K., Nakazono, M., Kobayashi, T., Wada, Y., Watanabe, S., Matsuhashi, S., Takahashi, M., Nakanishi, H., 2006. Rice plants take up iron as an Fe^{3+}-phytosiderophore and as Fe^{2+}. The Plant Journal 45, 335–346.

102. Iwai, H., Nagayama, T., Nakamura, A., Yamaji, N., Satoh, S., Furukawa, J., 2019. Changes in the distribution of pectin in root border cells under aluminum stress. Frontiers in Plant Science 10, 1216.

103. Jayarambabu, N., Akshaykranth, A., Rao, T.V., Rao, K.V., Kumar, R.R., 2020. Green synthesis of Cu nanoparticles using Curcuma longa extract and their application in antimicrobial activity. Materials Letters 259, 126813.

104. Jones, O.T.G., 1963. The inhibition of bacteriochlorophyll biosynthesis in *Rhodopseudomonas spheroides* by 8-hydroxyquinoline. Biochemical Journal 88, 335–343.

105. Jozefczak, M., Keunen, E., Schat, H., Bliek, M., Hernández, L.E., Carleer, R., Remans, T., Bohler, S., Vangronsveld, J., Cuypers, A., 2014. Differential response of Arabidopsis leaves and roots to cadmium: glutathione-related chelating capacity vs antioxidant capacity. Plant Physiology and Biochemistry 83, 1-9.

106. Kamarthapu, V., Rao, K.V., Srinivas, P.N.B.S., Reddy, G.B., Reddy, V.D., 2008. Structural and kinetic properties of *Bacillus subtilis* S-adenosylmethionine synthetase expressed in *Escherichia coli*. Biochimica et Biophysica Acta (BBA)-Proteins and Proteomics 1784(12), 1949-1958.

107. Kamboh, M.A., Memon, S., Zardari, L.A., Nodeh, H.R., Sherazi, S.T.H., Yilmaz, M., 2018. Removal of toxic metals from canola oil by newly synthesized calixarene-based resin. Turkish Journal of Chemistry 42, 918–928.

108. Kartel, M.T., Kupchik, L.A., Veisov, B.K., 1999. Evaluation of pectin binding of heavy metal ions in aqueous solutions. Chemosphere 38, 2591–2596.

109. Kato, F.H., Carvalho, M.E.A., Gaziola, S.A., Piotto, F.A., Azevedo, R.A., 2020. Lysine metabolism and amino acid profile in maize grains from plants subjected to cadmium exposure. Scientia Agricola 77.

110. Kawai, S., Sasaki, O., Hayasaka, Y., Takagi, S.I., 1994. Biosynthesis of avenic acid A in oat cv. Onward: Studies with 14 C or 15 N labeled compounds. *Plant and soil*, 165, 285-289.

111. Kille, P., Winge, D.R., Harwood, J.L., Kay, J., 1991. A plant metallothionein produced in *E. coli*. Federation of European Biochemical Societies Letters 295, 171–175.

112. Kim, D.G., Park, T.J., Kim, J.Y., Cho, Y.D., 1995. Purification and characterization of S-adenosylmethionine synthetase from soybean (*Glycine max*) axes. BMB Reports 28(2), 100-106.

113. Kim, S., Takahashi, M., Higuchi, K., Tsunoda, K., Nakanishi, H., Yoshimura, E., Mori, S., Nishizawa, N.K., 2005. Increased nicotianamine biosynthesis confers enhanced tolerance of high levels of metals, in particular nickel, to plants. Plant and Cell Physiology 46, 1809–1818.

114. Kim, S.B., Yu, J.G., Lee, G.H., Park, Y.D., 2012. Characterization of *Brassica rapa* S-adenosyl-L-methionine synthetase gene including its roles in biosynthesis pathway. Horticulture, Environment, and Biotechnology 53(1), 57-65.

115. Kimura, T., Oguro, I., Kohroki, J., Takehara, M., Itoh, N., Nakanishi, T., Tanaka, K., 2000. Metallothionein-null mice express altered genes during development. Biochemical and Biophysical Research Communications 270, 458–461.

116. Kisa, D., Öztürk, L., Tekin, Ş., 2016. Gene expression analysis of metallothionein and mineral elements uptake in tomato (*Solanum lycopersicum*) exposed to cadmium. Journal of Plant Research 129, 989–995.
117. Klapheck, S., Chrost, B., Starke, J., Zimmermann, H., 1992. γ-Glutamylcysteinylserine—a new homologue of glutathione in plants of the family Poaceae. Botanica Acta 105, 174–179.
118. Klapheck, S., Fliegner, W., Zimmer, I., 1994. Hydroxymethyl-phytochelatins [([gamma]-glutamylcysteine) n-serine] are metal-induced peptides of the poaceae. Plant Physiology 104, 1325–1332.
119. Klapheck, S., Schlunz, S., Bergmann, L., 1995. Synthesis of phytochelatins and homo-phytochelatins in *Pisum sativum* L. Plant Physiology 107, 515–521.
120. Kleiner, D., Shapiro Tuchman, Z., Shmulevich, F., Shahar, A., Zarivach, R., Kosloff, M. and Bershtein, S., 2022. Evolution of homo-oligomerization of methionine S-adenosyltransferases is replete with structure–function constrains. Protein Science 31(7), p.e4352.
121. Kneer, R., Kutchan, T.M., Hochberger, A., Zenk, M.H., 1992. *Saccharomyces cerevisiae* and *Neurospora crassa* contain heavy metal sequestering phytochelatin. Archives of Microbiology 157, 305–310.
122. Konno, H., Nakashima, S., Katoh, K., 2010. Metal-tolerant moss *Scopelophila cataractae* accumulates copper in the cell wall pectin of the protonema. Journal of Plant Physiology 167, 358–364.
123. Kováčik, J., Babula, P., Hedbavny, J., 2017. Comparison of vascular and non-vascular aquatic plant as indicators of cadmium toxicity. Chemosphere 180, 86–92.
124. Kováčik, J., Klejdus, B., Štork, F., Hedbavny, J., 2011. Nitrate deficiency reduces cadmium and nickel accumulation in chamomile plants. Journal of Agricultural and Food Chemistry 59, 5139–5149.
125. Krämer, U., Cotter-Howells, J.D., Charnock, J.M., Baker, A.J.M., Smith, J.A.C., 1996. Free histidine as a metal chelator in plants that accumulate nickel. Nature 379, 635–638.
126. Krämer, U., Pickering, I.J., Prince, R.C., Raskin, I., Salt, D.E., 2000. Subcellular localization and speciation of nickel in hyperaccumulator and non-accumulator Thlaspi species. Plant Physiology 122, 1343–1354.
127. Kristensen, I.B., Larsen, P.O., 1974. Azetidine-2-carboxylic acid derivatives from seeds of *Fagus silvatica* L. and a revised structure for nicotianamine. Phytochemistry 13(12), 2791-2798.
128. Krupp, E.M., Mestrot, A., Wielgus, J., Meharg, A.A., Feldmann, J., 2009. The molecular form of mercury in biota: identification of novel mercury peptide complexes in plants. Chemical Communications 4257–4259.
129. Krystofova, O., Zitka, O., Krizkova, S., Hynek, D., Shestivska, V., Adam, V., Hubalek, J., Mackova, M., Macek, T., Zehnalek, J., Babula, P., 2012. Accumulation of cadmium by transgenic tobacco plants (*Nicotiana tabacum* L.) carrying yeast metallothionein gene revealed by electrochemistry. International Journal of Electrochemical Science, 7, 886-907.
130. Krzesłowska, M., Lenartowska, M., Mellerowicz, E.J., Samardakiewicz, S., Woźny, A., 2009. Pectinous cell wall thickenings formation—a response of moss protonemata cells to lead. Environmental and Experimental Botany 65, 119–131.
131. Kühnlenz, T., Westphal, L., Schmidt, H., Scheel, D., Clemens, S., 2015. Expression of *Caenorhabditis elegans* PCS in the AtPCS 1-deficient *Arabidopsis thaliana* cad1-3 mutant separates the metal tolerance and non-host resistance functions of phytochelatin synthases. Plant, Cell & Environment 38, 2239–2247.
132. Kumar, G., Kushwaha, H.R., Panjabi-Sabharwal, V., Kumari, S., Joshi, R., Karan, R., Mittal, S., Pareek, S.L.S., Pareek, A., 2012. Clustered metallothionein genes are co-regulated in rice and ectopic expression of OsMT1e-P confers multiple abiotic stress tolerance in tobacco via ROS scavenging. BioMed Central Plant Biology 12, 107.
133. Laffont, C., Arnoux, P., 2020. The ancient roots of nicotianamine: diversity, role, regulation and evolution of nicotianamine-like metallophores. *Metallomics* 12(10), 1480-1493.

134. Le Faucheur, S., Behra, R., Sigg, L., 2005. Phytochelatin induction, cadmium accumulation, and algal sensitivity to free cadmium ion in *Scenedesmus vacuolatus*. Environmental Toxicology and Chemistry: An International Journal 24, 1731–1737.
135. Lee, M.J., Jeong, Y.S. and Chun, G.T., 2008. Enhanced production of monacolin-K through supplement of monacolin-K precursors into production medium and cloning of SAM-synthetase gene (metK). KSBB Journal 23(6), 519-524.
136. Lee, M.J., Jeong, Y.S., Chun, G.T., 2008. Enhanced production of monacolin-K through supplement of monacolin-K precursors into production medium and cloning of SAM synthetase gene (metK). KSBB Journal 23(6), 519-524.
137. Lee, S., Moon, J.S., Ko, T.S., Petros, D., Goldsbrough, P.B., Korban, S.S., 2003. Overexpression of Arabidopsis phytochelatin synthase paradoxically leads to hypersensitivity to cadmium stress. Plant Physiology 131, 656–663.
138. Leete, E., 1975. Biosynthesis of azetidine-2-carboxylic acid from methionine in *Nicotiana tabacum*. *Phytochemistry* 14(9), 1983-1984.
139. Leete, E., Davis, G.E., Hutchinson, C.R., Woo, K.W., Chedekel, M.R., 1974. Biosynthesis of azetidine-2-carboxylic acid in *Convallaria majalis*. *Phytochemistry* 13(2), 427-433.
140. Leete, E., Louters, L.L., Rao, H.P., 1986. Biosynthesis of azetidine-2-carboxylic acid in *Convallaria majalis*: studies with N-15 labelled precursors. *Phytochemistry* 25(12), 2753-2758.
141. LeGros Jr, H.L., Halim, A.B., Geller, A.M., Kotb, M., 2000. Cloning, expression, and functional characterization of the β regulatory subunit of human methionine adenosyltransferase (MAT II). Journal of Biological Chemistry 275(4), 2359-2366.
142. LeGros Jr, H.L., Halim, A.B., Geller, A.M., Kotb, M., 2000. Cloning, expression, and functional characterization of the β regulatory subunit of human methionine adenosyltransferase (MAT II). Journal of Biological Chemistry 275(4), 2359-2366.
143. Leopold, I., Günther, D., Schmidt, J., Neumann, D., 1999. Phytochelatins and heavy metal tolerance. Phytochemistry 50, 1323–1328.
144. Leszczyszyn, O.I., Blindauer, C.A., 2010. Zinc transfer from the embryo-specific metallothionein EC from wheat: a case study. Physical Chemistry Chemical Physics 12, 13408–13418.
145. Leszczyszyn, O.I., White, C.R.J., Blindauer, C.A., 2010. The isolated Cys 2 His 2 site in EC metallothionein mediates metal-specific protein folding. Molecular BioSystems 6, 1592–1603.
146. Li, J., Hu, L., Zhang, L., Pan, X. and Hu, X., 2015. Exogenous spermidine is enhancing tomato tolerance to salinity–alkalinity stress by regulating chloroplast antioxidant system and chlorophyll metabolism. *BMC plant biology* 15(1), 1-17.
147. Li, J.F., Qu, L.H., Li, N., 2005. Tyr152 plays a central role in the catalysis of 1-aminocyclopropane-1-carboxylate synthase. *Journal of experimental botany* 56(418), 2203-2210.
148. Li, X.D., Xia, B., Wang, R., Xu, S., Jiang, Y.M., Yu, F.B., Peng, F., 2013. Molecular cloning and characterization of S-adenosylmethionine synthetase gene from *Lycoris radiata*. Molecular biology reports 40(2), 1255-1263.
149. Liu, Y., Kang, T., Cheng, J., Yi, Y., Han, J., Cheng, H., Li, Q., Tang, N., Liang, M., 2020. Heterologous expression of the metallothionein *PpMT2* gene from *Physcomitrella patens* confers enhanced tolerance to heavy metal stress on transgenic Arabidopsis plants. Plant Growth Regulation 90, 63–72.
150. Liu, Z., Meng, H., Abdulla, H., Zhang, F., Mao, X., 2016. Cloning and characterization of metallothionein gene (*HcMT*) from *Halostachys caspica* and its expression in *E. coli*. Gene 585, 221–227.
151. Livak, K.J., Schmittgen, T.D., 2001. Analysis of relative gene expression data using real-time quantitative PCR and the 2– ΔΔCT method. *Methods*, 25(4), 402-408.
152. Loebus, J., Peroza, E.A., Blüthgen, N., Fox, T., Meyer-Klaucke, W., Zerbe, O., Freisinger, E., 2011. Protein and metal cluster structure of the wheat metallothionein domain γ-E_c-1: the second part of the puzzle. Journal of Biological Inorganic Chemistry 16, 683.
153. Lombi, E., Zhao, F.J., McGrath, S.P., Young, S.D., Sacchi, G.A., 2001. Physiological evidence for a high-affinity cadmium transporter highly expressed in a *Thlaspi caerulescens* ecotype. New Phytologist 149, 53–60.

154. Lozano-Rodriguez, E., Hernandez, L.E., Bonay, P., Carpena-Ruiz, R.O., 1997. Distribution of cadmium in shoot and root tissues of maize and pea plants: physiological disturbances. Journal of Experimental Botany 48, 123–128.
155. Lysenko, E.A., Klaus, A.A., Kartashov, A.V., Kusnetsov, V.V., 2020. Specificity of Cd, Cu, and Fe effects on barley growth, metal contents in leaves and chloroplasts, and activities of photosystem I and photosystem II. Plant Physiology and Biochemistry 147, 191-204.
156. Ma, C., Wang, Y., Gu, D., Nan, J., Chen, S., Li, H., 2017. Overexpression of S-adenosyl-L-methionine synthetase 2 from sugar beet M14 increased Arabidopsis tolerance to salt and oxidative stress. International journal of molecular sciences 18(4), 847.
157. Ma, J.F., Nomoto, K., 1994. Incorporation of Label from 13C-, 2H-, and 15N-Labeled Methionine Molecules during the Biosynthesis of 2 [prime]-Deoxymugineic Acid in Roots of Wheat. *Plant physiology* 105(2), 607-610.
158. Maleki, M., Ghorbanpour, M., Kariman, K., 2017. Physiological and antioxidative responses of medicinal plants exposed to heavy metals stress. Plant Gene 11, 247-254.
159. Malekzadeh, R., Shahpiri, A., 2017. Independent metal-thiolate cluster formation in C-terminal Cys-rich region of a rice type 1 metallothionein isoform. International Journal of Biological Macromolecules 96, 436–441.
160. Marslin, G., Siram, K., Maqbool, Q., Selvakesavan, R.K., Kruszka, D., Kachlicki, P., Franklin, G., 2018. Secondary metabolites in the green synthesis of metallic nanoparticles. Materials 11(6), 940.
161. Martinoia, E., Grill, E., Tommasini, R., Kreuz, K., Amrhein, N., 1993. ATP-dependent glutathione S-conjugate'export'pump in the vacuolar membrane of plants. Nature 364, 247–249.
162. Masuda, H., Suzuki, M., Morikawa, K.C., Kobayashi, T., Nakanishi, H., Takahashi, M., Saigusa, M., Mori, S., Nishizawa, N.K., 2008. Increase in iron and zinc concentrations in rice grains via the introduction of barley genes involved in phytosiderophore synthesis. Rice 1, 100-108.
163. Mathur, M., Sharma, N., Sachar, R.C., 1993. Differential regulation of S-adenosylmethionine synthetase isozymes by gibberellic acid in dwarf pea epicotyls. Biochimica et Biophysica Acta (BBA)-Protein Structure and Molecular Enzymology 1162(3), 283-290.
164. Matos, Jose R., Chi-Huey Wong, 1987. "S-adenosylmethionine: Stability and stabilization." Bioorganic Chemistry 15, 71-80.
165. Mendoza-Cózatl, D.G., Zhai, Z., Jobe, T.O., Akmakjian, G.Z., Song, W.Y., Limbo, O., Russell, M.R., Kozlovskyy, V.I., Martinoia, E., Vatamaniuk, O.K., Russell, P., 2010. Tonoplast-localized Abc2 transporter mediates phytochelatin accumulation in vacuoles and confers cadmium tolerance. Journal of Biological Chemistry 285, 40416–40426.
166. Meyer, B., Immer, C., Kaiser, S., Sharma, S., Yang, J., Watzinger, P., Weiß, L., Kotter, A., Helm, M., Seitz, H.M., Kötter, P., 2020. Identification of the 3-amino-3-carboxypropyl (acp) transferase enzyme responsible for acp3U formation at position 47 in *Escherichia coli* tRNAs. *Nucleic acids research* 48(3), 1435-1450.
167. Mijovilovich, A., Leitenmaier, B., Meyer-Klaucke, W., Kroneck, P.M.H., Götz, B., Küpper, H., 2009. Complexation and toxicity of copper in higher plants. II. Different mechanisms for copper versus cadmium detoxification in the copper-sensitive cadmium/zinc hyperaccumulator *Thlaspi caerulescens* (Ganges ecotype). Plant Physiology 151, 715–731.
168. Mingorance, J., Alvarez, L., Pajares, M.A., Mato, J., 1997. Recombinant rat liver S-adenosyl-L-methionine synthetase tetramers and dimers are in equilibrium. The international journal of biochemistry & cell biology 29(3), 485-491.
169. Mir, G., Domènech, J., Huguet, G., Guo, W.-J., Goldsbrough, P., Atrian, S., Molinas, M., 2004. A plant type 2 metallothionein (MT) from cork tissue responds to oxidative stress. Journal of Experimental Botany 55, 2483–2493.
170. Moghrovyan, A., Sahakyan, N., Babayan, A., Chichoyan, N., Petrosyan, M., Trchounian, A., 2019. Essential oil and ethanol extract of oregano (*Origanum vulgare* L.) from Armenian flora as a natural source of terpenes, flavonoids and other phytochemicals with antiradical, antioxidant, metal chelating, tyrosinase inhibitory and antibacterial activity. Current Pharmaceutical Design 25(16), 1809-1816.

171. Moisyadi, S., Stiles, J.I., 1995. A cDNA encoding a metallothionein I-like protein from coffee leaves (*Coffea arabica*). Plant Physiology 107, 295.

172. Mottaghipisheh, J., Iriti, M., 2020. Sephadex® LH-20, Isolation, and Purification of Flavonoids from Plant Species: A Comprehensive Review. Molecules 25(18), 4146.

173. Mudalkar, S., Golla, R., Sengupta, D., Ghatty, S., Reddy, A.R., 2014. Molecular cloning and characterisation of metallothionein type 2a gene from *Jatropha curcas* L., a promising biofuel plant. Molecular Biology Reports 41, 113–124.

174. Murata, Y., Ma, J.F., Yamaji, N., Ueno, D., Nomoto, K., Iwashita, T., 2006. A specific transporter for iron (III)–phytosiderophore in barley roots. The Plant Journal 46, 563–572.

175. Murphy, A., Zhou, J., Goldsbrough, P.B., Taiz, L., 1997. Purification and immunological identification of metallothioneins 1 and 2 from *Arabidopsis thaliana*. Plant Physiology 113, 1293–1301.

176. Nahar, K., Hasanuzzaman, M., Suzuki, T. and Fujita, M., 2017. Polyamines-induced aluminum tolerance in mung bean: A study on antioxidant defense and methylglyoxal detoxification systems. *Ecotoxicology 26*, 58-73.

177. Negi, V.S., Bingham, J.P., Li, Q.X., Borthakur, D., 2013. midD-encoded 'rhizomimosinase' from *Rhizobium* sp. strain TAL1145 is a C–N lyase that catabolizes L-mimosine into 3-hydroxy-4-pyridone, pyruvate and ammonia. *Amino acids*(44), 1537-1547.

178. Negi, V.S., Bingham, J.P., Li, Q.X., Borthakur, D., 2014. A carbon-nitrogen lyase from *Leucaena leucocephala* catalyzes the first step of mimosine degradation. *Plant Physiology* 164(2), 922-934.

179. Nezhad, R.M., Shahpiri, A., Mirlohi, A., 2013. Heterologous expression and metal-binding characterization of a type 1 metallothionein isoform (OsMTI-1b) from rice (*Oryza sativa*). The Protein Journal 32, 131–137.

180. Nikiforova, V.J., Bielecka, M., Gakiere, B., Krueger, S., Rinder, J., Kempa, S., Morcuende, R., Scheible, W.R., Hesse, H., Hoefgen, R., 2006. Effect of sulfur availability on the integrity of amino acid biosynthesis in plants. Amino Acids 30, 173–183.

181. Nishanthi, R., Malathi, S., Palani, P., 2019. Green synthesis and characterization of bioinspired silver, gold and platinum nanoparticles and evaluation of their synergistic antibacterial activity after combining with different classes of antibiotics. Materials Science and Engineering: C 96, 693-707.

182. Noctor, G., Mhamdi, A., Chaouch, S., Han, Y.I., Neukermans, J., Marquez-Garcia, B.E.L.E.N., Queval, G. and Foyer, C.H., 2012. Glutathione in plants: an integrated overview. Plant, cell & environment 35(2), 454-484.

183. Oganesyan, N., Ankoudinova, I., Kim, S.H., Kim, R., 2007. Effect of osmotic stress and heat shock in recombinant protein overexpression and crystallization. *Protein expression and purification* 52(2), 280-285.

184. Pagani, M.A., Tomas, M., Carrillo, J., Bofill, R., Capdevila, M., Atrian, S., Andreo, C.S., 2012. The response of the different soybean metallothionein isoforms to cadmium intoxication. Journal of Inorganic Biochemistry 117, 306–315.

185. Pan, Yu, Pan, Yanglu, Zhai, J., Xiong, Y., Li, J., Du, X., Su, C., Zhang, X., 2016. Cucumber metallothionein-like 2 (CsMTL2) exhibits metal-binding properties. Genes 7, 106.

186. Park, E.Y., Choi, W.S., Oh, S.I., Kim, K.N., Shin, J.S., Song, H.K., 2009. Biochemical and structural characterization of 5′-methylthioadenosine nucleosidases from *Arabidopsis thaliana*. *Biochemical and biophysical research communications* 381(4), 619-624.

187. Park, J., Tai, J., Roessner, C.A., Scott, A.I., 1995. Overcoming product inhibition of S-Adenosyl-L-methionine (SAM) synthetase: Preparation of SAM on the 30 mM scale. Bioorganic & Medicinal Chemistry Letters 5(19), 2203-2206.

188. Park, J., Tai, J., Roessner, C.A., Scott, A.I., 1996. Enzymatic synthesis of S-adenosyl-L-methionine on the preparative scale. *Bioorganic & Medicinal Chemistry* 4(12), 2179-2185.

189. Parungao, G.G., Zhao, M., Wang, Q., Zano, S.P., Viola, R.E., Blumenthal, R.M., 2017. Complementation of a metK-deficient *E. coli* strain with heterologous AdoMet synthetase genes. Microbiology 163(12), 1812.

190. Parvin, S., Kim, Y.J., Pulla, R.K., Sathiyamoorthy, S., Miah, M.G., Kim, Y.J., Wasnik, N.G., Yang, D.C., 2010. Identification and characterization of spermidine synthase gene from *Panax ginseng*. *Molecular biology reports* 37, 923-932.
191. Pence, N.S., Larsen, P.B., Ebbs, S.D., Letham, D.L.D., Lasat, M.M., Garvin, D.F., Eide, D., Kochian, L.V., 2000. The molecular physiology of heavy metal transport in the Zn/Cd hyperaccumulator *Thlaspi caerulescens*. Proceedings of the National Academy of Sciences 97, 4956–4960.
192. Peng, J.S., Ding, G., Meng, S., Yi, H.Y., Gong, J.M., 2017. Enhanced metal tolerance correlates with heterotypic variation in SpMTL, a metallothionein-like protein from the hyperaccumulator *Sedum plumbizincicola*. Plant, Cell & Environment 40, 1368–1378.
193. Perche-Letuvée, P., Molle, T., Forouhar, F., Mulliez, E., Atta, M., 2014. Wybutosine biosynthesis: structural and mechanistic overview. *RNA biology* 11(12), 1508-1518.
194. Persans, M.W., Yan, X., Patnoe, J.M.M.L., Krämer, U., Salt, D.E., 1999. Molecular dissection of the role of histidine in nickel hyperaccumulation in *Thlaspi goesingense* (Hálácsy). Plant Physiology 121, 1117–1126.
195. Petraglia, A., De Benedictis, M., Degola, F., Pastore, G., Calcagno, M., Ruotolo, R., Mengoni, A., di Toppi, L., 2014. The capability to synthesize phytochelatins and the presence of constitutive and functional phytochelatin synthases are ancestral (plesiomorphic) characters for basal land plants. Journal of Experimental Botany 65, 1153–1163.
196. Pettersen, E.F., Goddard, T.D., Huang, C.C., Meng, E.C., Couch, G.S., Croll, T.I., Morris, J.H., Ferrin, T.E., 2021. UCSF ChimeraX: Structure visualization for researchers, educators, and developers. Protein Science 30(1), pp.70-82.
197. Pianelli, K., Mari, S., Marquès, L., Lebrun, M., Czernic, P., 2005. Nicotianamine over-accumulation confers resistance to nickel in *Arabidopsis thaliana*. Transgenic Research 14, 739–748.
198. Planchais, S., Glab, N., Inzé, D., Bergounioux, C., 2000. Chemical inhibitors: a tool for plant cell cycle studies. Federation of European Biochemical Societies Letters 476, 78–83.
199. Porollo, A., Meller, J., 2007. Versatile annotation and publication quality visualization of protein complexes using POLYVIEW-3D. *BMC bioinformatics* 8(1), 1-8.
200. Qi, Y.C., Wang, F.F., Zhang, H., Liu, W.Q., 2010. Overexpression of *Suadea salsa* S-adenosylmethionine synthetase gene promotes salt tolerance in transgenic tobacco. Acta physiologiae plantarum 32(2), 263-269.
201. Qin, F.J., Sun, Q.W., Huang, L.M., Chen, X.S., Zhou, D.X., 2010. Rice SUVH histone methyltransferase genes display specific functions in chromatin modification and retrotransposon repression. Molecular plant 3(4), 773-782.
202. Ramalingam, K., Lee, K.M., Woodard, R.W., Bleecker, A.B., Kende, H., 1985. Stereochemical course of the reaction catalyzed by the pyridoxal phosphate-dependent enzyme 1-aminocyclopropane-1-carboxylate synthase. *Proceedings of the National Academy of Sciences* 82(23), 7820-7824.
203. Redjala, T., Zelko, I., Sterckeman, T., Legué, V., Lux, A., 2011. Relationship between root structure and root cadmium uptake in maize. Environmental and Experimental Botany 71, 241–248.
204. Reeve, A.M., Breazeale, S.D., Townsend, C.A., 1998. Purification, characterization, and cloning of an S-adenosylmethionine-dependent 3-amino-3-carboxypropyltransferase in nocardicin biosynthesis. *Journal of Biological Chemistry* 273(46), 30695-30703.
205. Rellán-Álvarez, R., Abadía, J., Álvarez-Fernández, A., 2008. Formation of metal-nicotianamine complexes as affected by pH, ligand exchange with citrate and metal exchange. A study by electrospray ionization time-of-flight mass spectrometry. *Rapid Communications in Mass Spectrometry: An International Journal Devoted to the Rapid Dissemination of Up-to-the-Minute Research in Mass Spectrometry* 22(10), 1553-1562.
206. Rensing, S.A., Lang, D., Zimmer, A.D., Terry, A., Salamov, A., Shapiro, H., Nishiyama, T., Perroud, P.F., Lindquist, E.A., Kamisugi, Y., Tanahashi, T., 2008. The *Physcomitrella* genome reveals evolutionary insights into the conquest of land by plants. *Science* 319(5859), 64-69.
207. Ribeiro, V.E., Pereira, M.P., de Castro, E.M., Corrêa, F.F., das Graças Cardoso, M., Pereira, F.J., 2019. Enhanced essential oil and leaf anatomy of *Schinus molle* plants under lead contamination. Industrial Crops and Products 132, 92-98.

208. Riekhof, W.R., Andre, C., Benning, C., 2005. Two enzymes, BtaA and BtaB, are sufficient for betaine lipid biosynthesis in bacteria. *Archives of Biochemistry and Biophysics* 441(1), 96-105.
209. Roeder, S., Dreschler, K., Wirtz, M., Cristescu, S.M., van Harren, F.J., Hell, R., Piechulla, B., 2009. SAM levels, gene expression of SAM synthetase, methionine synthase and ACC oxidase, and ethylene emission from *N. suaveolens* flowers. Plant molecular biology 70(5), 535-546.
210. Rubenstein, E., Zhou, H., Krasinska, K.M., Chien, A., Becker, C.H., 2006. Azetidine-2-carboxylic acid in garden beets (*Beta vulgaris*). Phytochemistry 67(9), 898-903.
211. Rüegsegger, A., Brunold, C., 1992. Effect of cadmium on γ-glutamylcysteine synthesis in maize seedlings. Plant Physiology 99, 428–433.
212. Rüegsegger, A., Schmutz, D., Brunold, C., 1990. Regulation of glutathione synthesis by cadmium in *Pisum sativum* L. Plant Physiology 93, 1579–1584.
213. Rzewuski, G., Cornell, K.A., Rooney, L., Bürstenbinder, K., Wirtz, M., Hell, R., Sauter, M., 2007. OsMTN encodes a 5′-methylthioadenosine nucleosidase that is up-regulated during submergence-induced ethylene synthesis in rice (*Oryza sativa* L.). *Journal of experimental botany* 58(6), 1505-1514.
214. Sá, Raquel A, Sá, Renata A, Alberton, O., Gazim, Z.C., Laverde Jr, A., Caetano, J., Amorin, A.C., Dragunski, D.C., 2015. Phytoaccumulation and effect of lead on yield and chemical composition of *Mentha crispa* essential oil. Desalination and Water Treatment 53, 3007–3017.
215. Salt, D.E., Thurman, D.A., Tomsett, A.B., Sewell, A.K., 1989. Copper phytochelatins of *Mimulus guttatus*. Proceedings of the Royal Society of London B, Biological Sciences 236, 79–89.
216. Santos, C.S., Carvalho, S.M., Leite, A., Moniz, T., Roriz, M., Rangel, A.O., Rangel, M., Vasconcelos, M.W., 2016. Effect of tris (3-hydroxy-4-pyridinonate) iron (III) complexes on iron uptake and storage in soybean (*Glycine max* L.). *Plant Physiology and Biochemistry* 106, 91-100.
217. Santos, C.S., Rodrigues, E., Ferreira, S., Moniz, T., Leite, A., Carvalho, S.M., Vasconcelos, M.W., Rangel, M., 2021. Foliar application of 3-hydroxy-4-pyridinone Fe-chelate [Fe (mpp) 3] induces responses at the root level amending iron deficiency chlorosis in soybean. *Physiologia Plantarum* 173(1), 235-245.
218. Schat, H., Sharma, S.S., Vooijs, R., 1997. Heavy metal-induced accumulation of free proline in a metal-tolerant and a nontolerant ecotype of *Silene vulgaris*. Physiologia Plantarum 101, 477–482.
219. Schmidt, H., Böttcher, C., Trampczynska, A., Clemens, S., 2011. Use of recombinantly produced 15 N 3-labelled nicotianamine for fast and sensitive stable isotope dilution ultra-performance liquid chromatography/electrospray ionization time-of-flight mass spectrometry. *Analytical and bioanalytical chemistry* 399(3), 1355-1361.
220. Schmiedeberg, L., Krüger, C., Stephan, U.W., Bäumlein, H., Hell, R., 2003. Synthesis and proof-of-function of a [14C]-labelled form of the plant iron chelator nicotianamine using recombinant nicotianamine synthase from barley. *Physiologia Plantarum* 118(3), 430-438.
221. Seebach, H., Radow, G., Brunek, M., Schulz, F., Piotrowski, M., Krämer, U., 2023. Arabidopsis nicotianamine synthases comprise a common core-NAS domain fused to a variable autoinhibitory C terminus. *Journal of Biological Chemistry*, 299(6).
222. Sekula, B., Ruszkowski, M., Dauter, Z., 2020. S-adenosylmethionine synthases in plants: Structural characterization of type I and II isoenzymes from *Arabidopsis thaliana* and *Medicago truncatula*. International journal of biological macromolecules 151, 554-565.
223. Shafiei, M., Ziaee, A.A., Amoozegar, M.A., 2012. Purification and characterization of a halophilic α-amylase with increased activity in the presence of organic solvents from the moderately halophilic Nesterenkonia sp. strain F. Extremophiles 16(4), 627-635.
224. Shah, K., Dubey, R.S., 1997. Effect of cadmium on proline accumulation and ribonuclease activity in rice seedlings: role of proline as a possible enzyme protectant. Biologia Plantarum 40, 121–130.
225. Shahpiri, A., Deljoonia, R., 2018. Enhancement of catalase and superoxide dismutase activities in transgenic *Escherichia coli* expressing rice metallothionein isoforms. Journal of BioScience and Biotechnology 7(1), 5-10.
226. Shahpiri, A., Mohammadzadeh, A., 2018. Mercury removal by engineered *Escherichia coli* cells expressing different rice metallothionein isoforms. Annals of Microbiology 68, 145–152.

227. Sharma, S.S., Dietz, K.J., 2006. The significance of amino acids and amino acid-derived molecules in plant responses and adaptation to heavy metal stress. Journal of Experimental Botany 57, 711–726.
228. Sharma, S.S., Schat, H., Vooijs, R., 1998. In vitro alleviation of heavy metal-induced enzyme inhibition by proline. Phytochemistry 49, 1531–1535.
229. Shcolnick, S., Keren, N., 2006. Metal homeostasis in cyanobacteria and chloroplasts. Balancing benefits and risks to the photosynthetic apparatus. Plant physiology 141(3), 805-810.
230. Shenker, M., Fan, T.M., Crowley, D.E., 2001. Phytosiderophores influence on cadmium mobilization and uptake by wheat and barley plants. Journal of Environmental Quality 30, 2091–2098.
231. Shojima, S., Nishizawa, N.K., Fushiya, S., Nozoe, S., Irifune, T., Mori, S., 1990. Biosynthesis of phytosiderophores: in vitro biosynthesis of 2′-deoxymugineic acid from L-methionine and nicotianamine. *Plant Physiology* 93(4), 1497-1503.
232. Shojima, S., Nishizawa, N.K., Fushiya, S., Nozoe, S., Kumashiro, T., Nagata, T., Ohata, T., Mori, S., 1989a. Biosynthesis of nicotianamine in the suspension-cultured cells of tobacco (*Nicotiana megalosiphon*). *Biology of Metals* 2(3), 142-145.
233. Shojima, S., Nishizawa, N.K., Mori, S., 1989b. Establishment of a cell-free system for the biosynthesis of nicotianamine. *Plant and cell physiology* 30(5), 673-677.
234. Sievers, F., Wilm, A., Dineen, D., Gibson, T.J., Karplus, K., Li, W., Lopez, R., McWilliam, H., Remmert, M., Söding, J., Thompson, J.D., 2011. Fast, scalable generation of high-quality protein multiple sequence alignments using Clustal Omega. *Molecular systems biology 7*(1), 539.
235. Singh, G., Tripathi, S., Shanker, K., Sharma, A., 2019. Cadmium-induced conformational changes in type 2 metallothionein of medicinal plant *Coptis japonica*: insights from molecular dynamics studies of apo, partially and fully metalated forms. Journal of Biomolecular Structure and Dynamics, 37(6), 1520-1533.
236. Singh, S.P., Keller, B., Gruissem, W., Bhullar, N.K., 2017. Rice NICOTIANAMINE SYNTHASE 2 expression improves dietary iron and zinc levels in wheat. Theoretical and Applied Genetics 130, 283–292.
237. Singh, V., Bhatt, I., Aggarwal, A., Tripathi, B.N., Munjal, A.K., Sharma, V., 2010. Proline improves copper tolerance in chickpea (*Cicer arietinum*). Protoplasma 245, 173–181.
238. Siu, K.K., Lee, J.E., Sufrin, J.R., Moffatt, B.A., McMillan, M., Cornell, K.A., Isom, C., Howell, P.L., 2008. Molecular determinants of substrate specificity in plant 5′-methylthioadenosine nucleosidases. *Journal of molecular biology* 378(1), 112-128.
239. Smitha, S.L., Philip, D., Gopchandran, K.G., 2009. Green synthesis of gold nanoparticles using *Cinnamomum zeylanicum* leaf broth. Spectrochimica Acta Part A: Molecular and Biomolecular Spectroscopy 74, 735–739.
240. Sneller, F.E.C., Van Heerwaarden, L.M., Kraaijeveld-Smit, F.J.L., Ten Bookum, W.M., Koevoets, P.L.M., Schat, H., Verkleij, J.A.C., 1999. Toxicity of arsenate in *Silene vulgaris*, accumulation and degradation of arsenate-induced phytochelatins. New Phytologist 144, 223–232.
241. Sobrino-Plata, J., Barón-Sola, Á., Ortega-Villasante, C., Ortega-Campayo, V., González-Berrocal, C., Conesa-Quintana, C., Carrasco-Gil, S., Muñoz-Pinilla, M., Abadia, J., Alvarez-Fernandez, A., Hernandez, L.E., 2020. Sulphur and biothiol metabolism determine toxicity responses and fate of mercury in Arabidopsis. Environmental and Experimental Botany 182, 104302.
242. Soda, N., Sharan, A., Gupta, B.K., Singla-Pareek, S.L., Pareek, A., 2016. Evidence for nuclear interaction of a cytoskeleton protein (OsIFL) with metallothionein and its role in salinity stress tolerance. Scientific Reports 6, 34762.
243. Soedarjo, M., Borthakur, D., 1998. Mimosine, a toxin produced by the tree-legume Leucaena provides a nodulation competition advantage to mimosine-degrading Rhizobium strains. Soil Biology and Biochemistry 30, 1605–1613.
244. Solti, Á., Sárvári, É., Tóth, B., Mészáros, I., Fodor, F., 2016. Incorporation of iron into chloroplasts triggers the restoration of cadmium induced inhibition of photosynthesis. Journal of plant physiology 202, 97-106.

245. Song, X.Q., Liu, L.F., Jiang, Y.J., Zhang, B.C., Gao, Y.P., Liu, X.L., Lin, Q.S., Ling, H.Q., Zhou, Y.H., 2013. Disruption of secondary wall cellulose biosynthesis alters cadmium translocation and tolerance in rice plants. Molecular Plant 6, 768–780.

246. Sorokin, D.Y., van Pelt, S., Tourova, T.P., Evtushenko, L.I., 2009. *Nitriliruptor alkaliphilus* gen. nov., sp. nov., a deep-lineage haloalkaliphilic actinobacterium from soda lakes capable of growth on aliphatic nitriles, and proposal of *Nitriliruptoraceae* fam. nov. and *Nitriliruptorales* ord. nov. International journal of systematic and evolutionary microbiology 59(2), 248-253.

247. Sugiura, Y., Nomoto, K., 1984. Phytosiderophores structures and properties of mugineic acids and their metal complexes, In: Siderophores from Microorganisms and Plants. Springer, Heidelberg, pp. 107–135.

248. Sun, X.M., Lu, B., Huang, S.Q., Mehta, S.K., Xu, L.L., Yang, Z.M., 2007. Coordinated expression of sulfate transporters and its relation with sulfur metabolites in *Brassica napus* exposed to cadmium. Botanical Studies 48, 43–54.

249. Sun, Y., Locasale, J.W., 2022. Rethinking the bioavailability and cellular transport properties of S-adenosylmethionine. *Cell Stress* 6(1), 1.

250. Suzuki, K., Higuchi, K., Nakanishi, H., Nishizawa, N.K., Mori, S., 1999. Cloning of nicotianamine synthase genes from *Arabidopsis thaliana*. *Soil science and plant nutrition* 45(4), 993-1002.

251. Suzuki, K., Sffimada, K., Nozoe, S., Tanzawa, K., Ogita, T., 1996. Isolation of nicotianamine as a gelatinase inhibitor. *The Journal of antibiotics* 49(12), 1284-1285.

252. Suzuki, M., Nozoye, T., Nagasaka, S., Nakanishi, H., Nishizawa, N.K., Mori, S., 2016. The detection of endogenous 2'-deoxymugineic acid in olives (*Olea europaea* L.) indicates the biosynthesis of mugineic acid family phytosiderophores in non-graminaceous plants. Soil Science and Plant Nutrition 62, 481–488.

253. Tadaiesky, L.B., da Silva, B.R., Batista, B.L. and Lobato, A.K.D.S., 2020. Brassinosteroids trigger tolerance to iron toxicity in rice. Physiologia Plantarum. Accepted 8 October 2020 (Preprint).

254. Takagi, S., 1976. Naturally occurring iron-chelating compounds in oat-and rice-root washings: I. Activity measurement and preliminary characterization. Soil Science and Plant Nutrition 22, 423–433.

255. Takusagawa, F., Kamitori, S., Markham, G.D., 1996. Structure and function of S-adenosylmethionine synthetase: crystal structures of S-adenosylmethionine synthetase with ADP, BrADP, and PPi at 2.8 Å resolution. Biochemistry 35(8), 2586-2596.

256. Tharayil, N., 2009. To survive or to slay: Resource-foraging role of metabolites implicated in allelopathy. Plant Signaling & Behavior 4, 580–583.

257. Tharayil, N., Bhowmik, P., Alpert, P., Walker, E., Amarasiriwardena, D., Xing, B., 2009. Dual purpose secondary compounds: phytotoxin of *Centaurea diffusa* also facilitates nutrient uptake. New Phytologist 181, 424–434.

258. Tharayil, N., Bhowmik, P., Alpert, P., Walker, E., Amarasiriwardena, D., Xing, B., 2009. Dual purpose secondary compounds: phytotoxin of *Centaurea diffusa* also facilitates nutrient uptake. *New Phytologist* 181(2), 424-434.

259. Tomas, M., Tinti, A., Bofill, R., Capdevila, M., Atrian, S., Torreggiani, A., 2016. Comparative Raman study of four plant metallothionein isoforms: insights into their Zn (II) clusters and protein conformations. Journal of Inorganic Biochemistry 156, 55–63.

260. Trampczynska, A., Böttcher, C., Clemens, S., 2006. The transition metal chelator nicotianamine is synthesized by filamentous fungi. *FEBS letters* 580(13), 3173-3178.

261. Tsai, H.C., Hsieh, C.H., Hsu, C.W., Hsu, Y.H., Chien, L.F., 2022. Cloning and Organelle Expression of Bamboo Mitochondrial Complex I Subunits Nad1, Nad2, Nad4, and Nad5 in the Yeast Saccharomyces cerevisiae. International journal of molecular sciences 23(7), 4054.

262. Tsednee, M., Yang, S.C., Lee, D.C., Yeh, K.C., 2014. Root-secreted nicotianamine from *Arabidopsis halleri* facilitates zinc hypertolerance by regulating zinc bioavailability. Plant Physiology 166, 839–852.

263. Tsuji, N., Hirayanagi, N., Iwabe, O., Namba, T., Tagawa, M., Miyamoto, S., Miyasaka, H., Takagi, M., Hirata, K., Miyamoto, K., 2003. Regulation of phytochelatin synthesis by zinc and cadmium in marine green alga, *Dunaliella tertiolecta*. Phytochemistry 62, 453–459.

264. Tsyganov, V.E., Tsyganova, A. V, Gorshkov, A.P., Seliverstova, E. V, Kim, V.E., Chizhevskaya, E.P., Belimov, A.A., Serova, T.A., Ivanova, K.A., Kulaeva, O.A., Kusakin, P.G., 2020. Efficacy of a Plant-Microbe System: *Pisum sativum* (L.) Cadmium-Tolerant Mutant and *Rhizobium leguminosarum* Strains, Expressing Pea Metallothionein Genes *PsMT1* and *PsMT2*, for Cadmium Phytoremediation. Frontiers in Microbiology 11, 15.
265. Ueno, D., Rombola, A.D., Iwashita, T., Nomoto, K., Ma, J.F., 2007. Identification of two novel phytosiderophores secreted by perennial grasses. New Phytologist 174, 304–310.
266. Ulusu, Y., Öztürk, L., Elmastaş, M., 2017. Antioxidant capacity and cadmium accumulation in parsley seedlings exposed to cadmium stress. Russian journal of plant physiology 64(6), 883-888.
267. Van de Poel, B., Bulens, I., Oppermann, Y., Hertog, M.L., Nicolai, B.M., Sauter, M., Geeraerd, A.H., 2013. S-adenosyl-l-methionine usage during climacteric ripening of tomato in relation to ethylene and polyamine biosynthesis and transmethylation capacity. Physiologia plantarum 148(2), 176-188.
268. Vatamaniuk, O.K., Bucher, E.A., Ward, J.T., Rea, P.A., 2001. A New Pathway for Heavy Metal Detoxification in Animals PHYTOCHELATIN SYNTHASE IS REQUIRED FOR CADMIUM TOLERANCE IN *CAENORHABDITIS ELEGANS*. Journal of Biological Chemistry 276, 20817–20820.
269. von Wirén, N., Khodr, H., Hider, R.C., 2000. Hydroxylated phytosiderophore species possess an enhanced chelate stability and affinity for iron (III). Plant Physiology 124, 1149–1158.
270. von Wirén, N., Klair, S., Bansal, S., Briat, J.F., Khodr, H., Shioiri, T., Leigh, R.A., Hider, R.C., 1999. Nicotianamine chelates both FeIII and FeII. Implications for metal transport in plants. Plant Physiology 119, 1107–1114.
271. Wada, Y., Kobayashi, T., Takahashi, M., Nakanishi, H., Mori, S., Nishizawa, N.K., 2006. Metabolic engineering of Saccharomyces cerevisiae producing nicotianamine: potential for industrial biosynthesis of a novel antihypertensive substrate. Bioscience, biotechnology, and biochemistry 70(6), 1408-1415.
272. Wang, C., Na, G., Bermejo, E.S., Chen, Y., Banks, J.A., Salt, D.E., Zhao, F.J., 2018. Dissecting the components controlling root-to-shoot arsenic translocation in Arabidopsis thaliana. New Phytologist 217(1), 206-218.
273. Wang, Q., Yang, Z., Wang, L., Ma, M., Xu, B., 2007a. Molecular hydrogel-immobilized enzymes exhibit superactivity and high stability in organic solvents. Chemical communications 10, 1032-1034.
274. Wang, S., Arends, S.R., Weiss, D.S., Newman, E.B., 2005. A deficiency in S-adenosylmethionine synthetase interrupts assembly of the septal ring in *Escherichia coli* K-12. Molecular microbiology 58(3), 791-799.
275. Wang, X., Jiang, Y., Wu, M., Zhu, L., Yang, L., Lin, J., 2019. Semi-rationally engineered variants of S-adenosylmethionine synthetase from *Escherichia coli* with reduced product inhibition and improved catalytic activity. Enzyme and microbial technology 129, 109355.
276. Wang, Y., Boghigian, B.A., Pfeifer, B.A., 2007b. Improving heterologous polyketide production in Escherichia coli by overexpression of an S-adenosylmethionine synthetase gene. Applied microbiology and biotechnology 77(2), 367-373.
277. Waterhouse, A., Bertoni, M., Bienert, S., Studer, G., Tauriello, G., Gumienny, R., Heer, F.T., de Beer, T.A.P., Rempfer, C., Bordoli, L., Lepore, R., Schwede, T., 2008. SWISS-MODEL: homology modelling of protein structures and complexes. Nucleic Acids Res. 46, W296-W303.
278. Weber, M., Harada, E., Vess, C., Roepenack-Lahaye, E. v, Clemens, S., 2004. Comparative microarray analysis of *Arabidopsis thaliana* and *Arabidopsis halleri* roots identifies nicotianamine synthase, a ZIP transporter and other genes as potential metal hyperaccumulation factors. The Plant Journal 37, 269–281.
279. Webster, E.A., Gadd, G.M., 1996. Cadmium replaces calcium in the cell wall of *Ulva lactuca*. BioMetals 9, 241–244.
280. Wirth, J., Poletti, S., Aeschlimann, B., Yakandawala, N., Drosse, B., Osorio, S., Tohge, T., Fernie, A.R., Günther, D., Gruissem, W., Sautter, C., 2009. Rice endosperm iron biofortification by targeted and synergistic action of nicotianamine synthase and ferritin. Plant Biotechnology Journal 7, 631–644.

281. Wu, F.B., Chen, F., Wei, K., Zhang, G.P., 2004. Effect of cadmium on free amino acid, glutathione and ascorbic acid concentrations in two barley genotypes (*Hordeum vulgare* L.) differing in cadmium tolerance. Chemosphere 57, 447–454.
282. Wu, H., Min, J., Zeng, H., McCloskey, D.E., Ikeguchi, Y., Loppnau, P., Michael, A.J., Pegg, A.E., Plotnikov, A.N., 2008. Crystal Structure of Human Spermine Synthase: IMPLICATIONS OF SUBSTRATE BINDING AND CATALYTIC MECHANISM*♦. *Journal of Biological Chemistry* 283(23), 16135-16146.
283. Xia, Y., Lv, Y., Yuan, Y., Wang, G., Chen, Y., Zhang, H., Shen, Z., 2012. Cloning and characterization of a type 1 metallothionein gene from the copper-tolerant plant *Elsholtzia haichowensis*. Acta Physiologiae Plantarum 34, 1819–1826.
284. Xue Mei, S.U.N., Bo, L., Si Qi Huang, S.K.M., Lai Lang, X.U., 2007. Coordinated expression of sulfate transporters and its relation with sulfur metabolites in *Brassica napus* exposed to cadmium. Botanical Studies, 48, 43-54.
285. Yan, F., Müller, R., 2018. Class I methyltransferase VioH catalyzes unusual S-adenosyl-l-methionine cyclization leading to 4-methylazetidinecarboxylic acid formation during vioprolide biosynthesis. *ACS Chemical Biology* 14(1), 99-105.
286. Yang, J.L., Zhu, X.F., Peng, Y.X., Zheng, C., Li, G.X., Liu, Y., Shi, Y.Z., Zheng, S.J., 2011. Cell wall hemicellulose contributes significantly to aluminum adsorption and root growth in Arabidopsis. Plant Physiology 155, 1885–1892.
287. Yang, M., Zhang, F., Wang, F., Dong, Z., Cao, Q., Chen, M., 2015. Characterization of a type 1 metallothionein gene from the stresses-tolerant plant *Ziziphus jujuba*. International Journal of Molecular Sciences 16, 16750–16762.
288. Yoon, G.S., Ko, K.H., Kang, H.W., Suh, J.W., Kim, Y.S., Ryu, Y.W., 2006. Characterization of S-adenosylmethionine synthetase from *Streptomyces avermitilis* NRRL8165 and its effect on antibiotic production. Enzyme and microbial technology 39(3), 466-473.
289. Yoon, S., Lee, W., Kim, M., Kim, T.D., Ryu, Y., 2012. Structural and functional characterization of S-adenosylmethionine (SAM) synthetase from *Pichia ciferrii*. Bioprocess and biosystems engineering 35(1), 173-181.
290. Yoshihara, T., Ooyama, A., Goto, F., Takaiwa, F., 2005. Iron accumulation does not parallel the high expression level of ferritin in transgenic rice seeds. Planta 222, 225–233.
291. Zemanová, V., Pavlík, M., Pavlíková, D., Tlustoš, P., 2014. The significance of methionine, histidine and tryptophan in plant responses and adaptation to cadmium stress. Plant, Soil and Environment 60, 426–432.
292. Zhang, B., Zhang, C., Liu, C., Jing, Y., Wang, Y., Jin, L., Yang, L., Fu, A., Shi, J., Zhao, F., Lan, W., 2018. Inner envelope CHLOROPLAST MANGANESE TRANSPORTER 1 supports manganese homeostasis and phototrophic growth in Arabidopsis. Molecular plant 11(7), 943-954.
293. Zhang, F.S., Römheld, V., Marschner, H., 1991. Diurnal rhythm of release of phytosiderophores and uptake rate of zinc in iron-deficient wheat. Soil Science and Plant Nutrition 37, 671–678.
294. Zhang, H., Lv, S., Xu, H., Hou, D., Li, Y., Wang, F., 2017. H2O2 is involved in the metallothionein-mediated rice tolerance to copper and cadmium toxicity. International Journal of Molecular Sciences 18, 2083.
295. Zhang, J., Klinman, J.P., 2015. High-performance liquid chromatography separation of the (S, S)- and (R, S)-forms of S-adenosyl-L-methionine. *Analytical biochemistry* 476, 81-83.
296. Zhang, Z., Gao, X., Qiu, B., 2008. Detection of phytochelatins in the hyperaccumulator *Sedum alfredii* exposed to cadmium and lead. Phytochemistry 69, 911–918.
297. Zheng, L., Yamaji, N., Yokosho, K., Ma, J.F., 2012. YSL16 is a phloem-localized transporter of the copper-nicotianamine complex that is responsible for copper distribution in rice. The Plant Cell 24, 3767–3782.
298. Zhou, J., Chu, J., Wang, Y.H., Zhang, S.L., Zhuang, Y.P., Yuan, Z.Y., 2008. Purification and properties of *Saccharomyces cerevisiae* S-adenosylmethionine synthetase expressed in recombinant *Pichia pastoris*. World Journal of Microbiology and Biotechnology 24(6), 789-796.

299. Zimeri, A.M., Dhankher, O.P., McCaig, B., Meagher, R.B., 2005. The plant MT1 metallothioneins are stabilized by binding cadmiums and are required for cadmium tolerance and accumulation. Plant Molecular Biology 58, 839–855.